Spring 2010

Integration and test of a refrigerant-based cold-gas propulsion system for small satellites

Ryan Alan Pahl

Department:

INTEGRATION AND TEST OF A REFRIGERANT-BASED COLD-GAS PROPULSION SYSTEM FOR SMALL SATELLITES

by

RYAN ALAN PAHL

A THESIS

Presented to the Faculty of the Graduate School of the

MISSOURI UNIVERSITY OF SCIENCE AND TECHNOLOGY

In Partial Fulfillment of the Requirements for the Degree

MASTER OF SCIENCE IN AEROSPACE ENGINEERING

2010

Approved by:

Dr. Henry J. Pernicka, Advisor
Dr. David W. Riggins
Dr. Joshua L. Rovey

ABSTRACT

Due to the launch safety constraints placed on university-built small satellites, designing a low-cost propulsion system to meet mission requirements presents a significant challenge to aspiring student engineers. The Missouri University of Science and Technology is currently developing a low-cost, two-phase propulsion system using the refrigerant R-134a as the propellant that can be stored at low pressures while still providing sufficient performance to meet mission goals. The purpose of this study is to present the testing results of a refrigerant-based cold gas system utilizing R-134a as a saturated liquid propellant and the ability to design this system to be portable to host buses at other universities. This work completed a preliminary design using R-134a and conducted parametric and endurance testing to validate R-134a as a safe and affordable propellant for university-class satellites. Based on these results, other universities can calculate the performance properties required by their propulsion system and use this information to size and construct a low-cost system capable of meeting their goals using commercial off-the-shelf (COTS) hardware.

ACKNOWLEDGMENTS

First, I would like to express my sincere thanks to my advisor, Dr. Henry Pernicka, for his outstanding tutelage and guidance these past years. He fueled my deep desire to work with spacecraft and guided me in the development and execution of this project. I thank him for his time and effort.

I would also like to thank my committee for their time and advice as I prepared this thesis. Dr. David Riggins opened my eyes to the beauty of propulsion and led me to the point where I am today. Dr. Joshua Rovey channeled my love of spacecraft propulsion into the field of electric propulsion and helped me apply it. I look forward to working with him in the future.

I would also like to thank the staff of Missouri S&T for their help and guidance. George Green, in particular, helped me whenever I needed it, whether to make a last minute addition to get the vacuum chamber up and running or to accompany the Miners In Space team to Houston. The shop technicians, Joe Boze and Bob Hribar were there every time I needed a part designed and fabricated. Without these individuals, this thesis could not have been completed.

Finally, I want to thank my family who has always been there when life was difficult. They have always supported me, making sure that I applied myself and became the best person I could be. I thank them for all the love they have shown me these past 22 years. No matter what happens, I know that I am always welcome. Finally, I would like to thank all my friends, but two in particular: Kimberly Stratton has been there during the good and the bad, always bringing a smile to my face. Krystina Tacchi has always pushed me to apply myself and to continue reaching for my dreams.

TABLE OF CONTENTS

Page

LIST OF ILLUSTRATIONS

LIST OF TABLES

NOMENCLATURE

Symbol	Description
A^*	Nozzle Throat Area
a_0	Speed of Sound
A_d	Distributor Cross-Sectional Area
A_e	Nozzle Exit Area
AR	Area Ratio
$\bar{B}$	Magnetic Field Vector
c^*	Characteristic Velocity
γ	Ratio of Specific Heat
d	Diameter
d_0	Outer Diameter
d_i	Inner Diameter
ΔV	Change in Velocity
E	Elastic Modulus
$\bar{E}$	Electric Field Vector
e	Elongation
F	Force
$\bar{F}$	Force Vector
F_n	Force Per Bolt
ζ_d	Discharge Correction Factor
ζ_F	Force Correction Factor
ζ_p	Propulsive Capability Correction Factor
ζ_v	Velocity Correction Factor
g_0	Gravitational Constant
I	Moment of Inertia
I_{sp}	Specific Impulse
kl	Boundary Condition Parameter
L	Length of Bolt
l	Length of Beam

l_d	Length of Distributor
$\dot{m}$	Mass Flow Rate
m_0	Initial Mass
m_f	Mass of Liquid Propellant
m_g	Mass of Gaseous Propellant
m_p	Mass of Propellant
μ	Mass Per Unit Length
N	Number of Bolts
ν	Specific Volume of Propellant Mixture
ν_f	Specific Volume of Liquid Propellant
ν_g	Specific Volume of Gaseous Propellant
P	Pressure
P_c	Chamber Pressure
P_e	Exit Pressure
PR	Pressure Ratio
q	Particle Charge
R	Gas Constant
ρ	Density
T	Temperature
V	Volume
$\bar{V}$	Velocity Vector
V_e	Exhaust Velocity
w_d	Width of Distributor
ω	Natural Frequency
x	Fluid Quality

1. INTRODUCTION

1.1. HISTORY OF SPACE PROPULSION

When the world awoke on the morning of October 4, 1957, it was greeted by the "beep-beep" of Iskustvennyi Sputnik Zemli ("fellow traveler of the Earth"), better known as Sputnik I. The world's first artificial satellite, it represented a flexing of Russian technological strength in an emerging technology race with the United States. In their quest to best the United States, the Russians had designed Sputnik I (Figure 1.1 taken from [3]) to carry little more than a radio transmitter and a silver-zinc battery, a simplicity that minimized the time from design to launch [1]. Weighing in at 83.6 kg and measuring 58 cm in diameter, Sputnik I looked more like a beach ball than a technological breakthrough. It sported four antennas (two eight foot long and two ten foot long) so that it could broadcast its now-famous signal back to Earth as it tumbled uncontrolled around the globe. However, due to a low orbit of only 588 km altitude and without a means of altering its orbit, Sputnik I's historic flight ended after just 92 days, at which point it re-entered Earth's atmosphere on January 4, 1958 [2].

Figure 1.1. Technician Working on Sputnik I

After the initial success of Sputnik I, both Russia and the United States focused on developing more sophisticated satellites capable of unlocking more of the universe's secrets. On November 3, 1957, Sputnik II (Figure 1.2 taken from [4]) carried the dog known as Laika into orbit, making it the first creature from Earth to circle the globe [4].

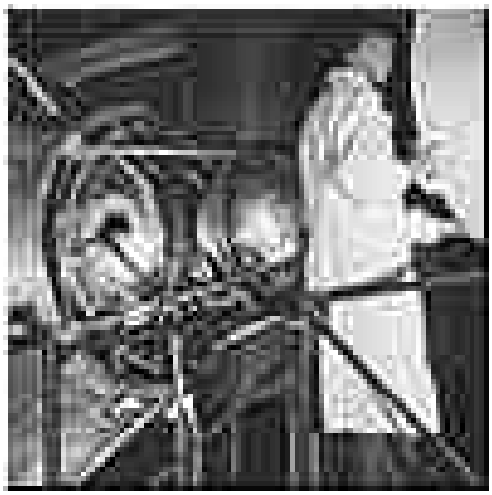

Figure 1.2. Sputnik II During Final Integration

Riding on the heels of Sputnik II was the United States' first successful mission, Explorer I. After taking a back seat to the Russians for almost three months, the United States finally joined Russia in space on February 1, 1958. Explorer I (Figure 1.3 taken from [5]) sought to reach out in space beyond the orbit of the Sputnik satellites. Its mission led to the discovery of a radiation belt that circles the planet; later named the Van Allen Radiation Belt after the principle investigator of the mission. The Jet Propulsion Laboratory (JPL) team led by German scientist Wernher Von Braun designed Explorer I in only three short months so that the United States would not fall any farther behind in the space race [4], [5].

Figure 1.3. Explorer I Presented by JPL Team

The U.S. Navy's Vanguard project was one of the most controversial endeavors of the day. Many believed that the United States would have been first to place an artificial satellite into space had they backed the Army's Wernher von Braun and Explorer I rather than the Naval Research Laboratory's (NRL) Vanguard project [7]. However, the early failures of the Vanguard project led to launch of Explorer I before Vanguard. Nonetheless, the Vanguard project finally succeeded with the placement of the Vanguard 1 (Figure 1.4 taken from [8]) satellite into orbit on March 17, 1958. The Vanguard I was designed to have an orbital life of 1,000 years; however, unexpected solar radiation pressure due to unusually high solar activity caused an increase in solar drag, reducing the satellite's lifetime to an estimated 240 years. As of today, Vanguard 1 is the oldest artificial satellite still in orbit. One of the major successes of the Vanguard 1 mission was the first use of solar arrays to actively charge the batteries of the satellite and thus decrease the mission duration. The Vanguard 1 satellite transmitter failed in June 1958 when the batteries finally ran down, but the mission of approximately three months was the longest of any satellite up until that time [8].

Figure 1.4. Vanguard I Spacecraft

The launch of a US spacecraft brought about yet another first for spaceflight. The Pioneer I satellite carried an 11 kg solid propellant-rocket for orbital insertion, along with eight small, low-thrust, solid-rocket motors for velocity adjustment, making it the first satellite to have an on-board propulsion system for use after separation to maintain and correct the orbital trajectory. The goal of Pioneer I (Figure 1.5 taken from [9]) was to gather images of the Moon, measure the ambient radiation, detect micrometeorites, measure magnetic fields as low as five-micro gauss, and measure the internal change in temperature. Unfortunately, due to an error in burnout velocity calculated from a faulty accelerometer, Pioneer I took a ballistic trajectory and re-entered Earth's atmosphere only 43 short hours later [9].

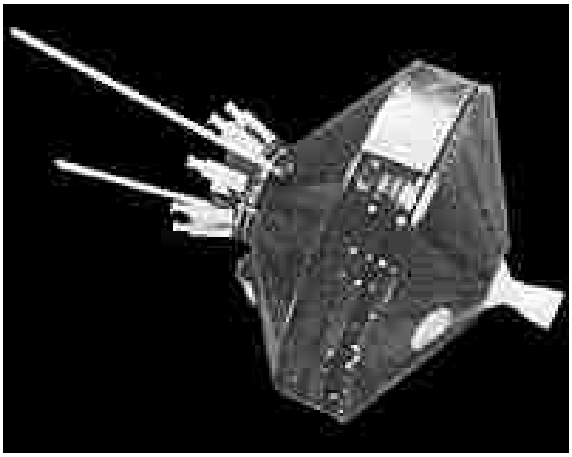

Figure 1.5. Pioneer I Spacecraft

1.2. TYPES OF SPACECRAFT PROPULSION

Since the days of the Pioneer space program, various types of propulsion systems have been successfully used on missions ranging from long-range space probes to geosynchronous communication satellites. These propulsion systems have enabled scientists and engineers to create more complex satellites with longer mission lives and broader capabilities, expanding mankind's knowledge of the universe. They can be split into three main categories: chemical, electric, and cold gas. Each method of propulsion has unique characteristics from which satellite designers can choose depending on the required lifespan of the mission, necessary thrust, etc. Table 1.1 summarizes the requirements for specific impulse (a measure of how efficiently an engine uses its propellant), and thrust (the amount of force generated to propel the spacecraft [10]).

Table 1.1. Performance Characteristics of Various Forms of Propulsion Systems

Type	I_{sp} (sec)	Thrust (N)
Cold Gas	50 - 75	0.05 - 200
Chemical		
Solid	280 - 300	10 - 10^6
Liquid		
Monopropellant	150 - 225	50 - $5x10^6$
Bipropellant	330 - 450	3 - $5x10^6$
Hybrid	225	225 - $3.5x10^6$
Electrical		
Electrothermal		
Resistojet	150 - 700	0.005 - 0.5
Arcjet	450 - 1,500	0.05 - 5
Electrostatic		
Ion	2,000 - 6,000	$5x10^{-6}$ - 0.5
Colloid	1,200	$5x10^{-6}$ - 0.05
Hall Effect Thruster	1,500 - 2,500	$5x10^{-6}$ - 0.1
Electromagnetic		
Magnetoplasmadynamic	2,000	25 - 200
Pulsed Plasma	1,500	$5x10^{-6}$ - 0.005
Pulse Inductive	2,500 - 4,000	2 - 200

1.2.1. Chemical Propulsion Systems. Chemical rockets currently provide the only means to access to space due to their high-thrust capabilities at the cost of low efficiency. One major disadvantage of chemical rockets is their weight of propellant. The vast majority of a launch vehicle's mass is fuel/oxidizer mass and only a small percentage is actual payload; thus, large and expensive rockets are necessary to haul only a small amount of useful cargo. This reality presents a significant challenge for mankind's effort to reach beyond Earth.

A more detailed analysis of chemical propulsion systems can be found in Appendix A [10].

1.2.2. Electric Propulsion Systems. With today's current technology, most electric propulsion systems use of power generated from photovoltaic solar arrays that

convert sunlight to electricity. This presents a problem for many electrical systems because greater thrust and efficiency generally requires more power. Figure 1.6 demonstrates that as the thrust of a propulsion system increases, the efficiency of that system decreases, and vice versa. Electric propulsion systems have the advantage of extremely high efficiency, but at the cost of reduced thrust. To increase the thrust of these systems, future systems will require levels of power typical of modern nuclear reactors [10]. The power level required for a specific thrust and specific impulse is given by

$$P = \frac{T I_{sp}\, g}{2\eta} \qquad [1.1]$$

where P is power, T is thrust, I_{sp} is specific impulse, g is the gravitational of Earth, and η is the system efficiency. The results are shown graphically in Figure 1.6.

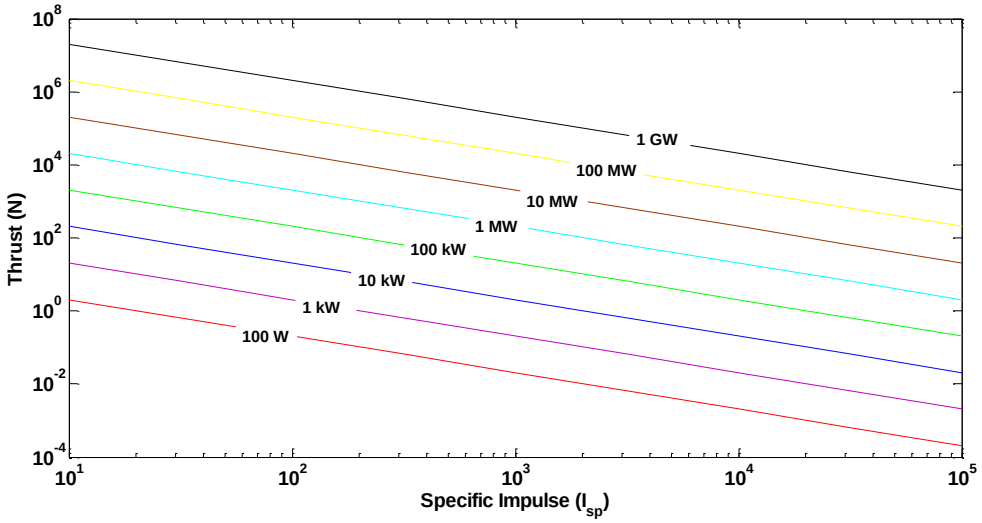

Figure 1.6. Dependence of Thrust and Specific Impulse on Power

More information on various forms of electric propulsion systems can be found in Appendix A [10]-[15].

1.2.3. Cold-Gas Propulsion. The expulsion of pressurized gas through a diverging nozzle is the simplest form of spacecraft propulsion currently being employed today. Most often, cold-gas systems are used when simplicity or reliability represent the primary concern on a mission [10]. The benefit of a cold-gas system is its ability to provide low thrust for precise orbital maneuvers with lower power consumption than other types of propulsion systems. Due to the size limitations of satellites, potential solar cell coverage is minimal, precluding the use of electric systems that consume a great deal of power. The need for low thrust rules out most chemical systems, making cold-gas systems the most likely candidate. However, because of they require heavy tubing, a propellant tank, and hardware to regulate pressure, cold-gas systems have a higher weight-to-performance ratio than other propulsion systems.

1.2.3.1 Single-phase cold-gas propellant. Typical cold-gas systems use large storage containers or pressure vessels in which a propellant is placed under high pressure so that fuel sufficient to complete the mission can be contained in the specified volume. Typically, the pressures in these containers are well over 1000 psi, depending on the propellant selection and storage volume. Common choices for a single-phase propellant include nitrogen, freon, and helium [10]. Freon, however, is being phased out of use due to concerns about ozone depletion and safety.

The performance characteristics, summarized in Table 1.1 of single-phase cold-gas systems are relatively low. Although these systems are less than optimal, however, they do have some advantages. Their primary advantage is that they require only a few pieces of additional hardware to create a fully functional propulsion system. In most cases, the high-pressure reservoir is reduced from a high pressure to a relatively low pressure, and the flow of propellant is controlled by inhibitor valves that can be opened on command. The lack of complicated hardware has two primary benefits: First, the simplicity of the system makes it one of the least expensive on the market; second, cold-gas systems are safer than systems that rely on traditional propellants such as hydrazine or other toxic or explosive chemicals.

1.2.3.2 Two-phase cold gas propellant. To reduce the high pressures typically associated with a cold-gas system, two-phase systems have been introduced that use propellants with low saturation pressures that can be stored in the propulsion tank as a saturated liquid. By definition, a saturated liquid consists of both the liquid and gaseous phases of a substance, and a quantity known as the "quality" is used to determine how much of each substance is present at a given temperature and pressure using thermodynamic tables [16] and the following relationships:

$$v = \frac{V}{m} \quad [1.2]$$

$$v = xv_g + (1 - x)v_f \quad [1.3]$$

$$x = \frac{m_g}{m_{total}} = \frac{m_g}{m_g + m_f} \quad [1.4]$$

Equation 1.2 is used to determine the specific volume of the propellant by dividing the total internal volume of the tank by the total mass of propellant. Once the specific volume is determined, Eq. 1.3 is applied to calculate the quality, x, of the fluid. This value can then be substituted into Eq. 1.4 to determine the mass of each phase. R-134a property tables are easily used to find the specific volume of the gaseous phase (v_g) and the liquid phase (v_l). Table 1.2 shows the fluid properties of some two-phase propellant options [17].

Table 1.2. Saturated Liquid Properties of Candidate Two-Phase Propellants

Liquid	Vapor Pressure (at 21°C)	Liquid Density (kg/m^3)	Critical Temperature (°C)
Acetone C_3H_6O	0.3 bar (4.5 psi)	790	172.0
Ammonia NH_3	8.8 bar (127 psi)	682	132.4
Carbon Dioxide CO_2	62.0 bar (900 psi)	763	31.0
Iso-Butane C_4H_{10}	2.6 bar (38 psi)	556	134.9
Nitrous Oxide N_2O	50.0 bar (725 psi)	1223	36.4
R-134a CH_2FCF_3	5.8 bar (84 psi)	1150	100.9
Sulfur Hexafluoride SF_6	21.7 bar (315 psi)	1880	45.5
Xenon Xe	53.5 bar (773 psi)	3057	16.5

Table 1.2 indicates that xenon has the greatest liquid density of all propellants. Due to its low critical temperature, however, it remains in the liquid state only under high pressure and poses a safety hazard to the ground crew, launch vehicle, and payload.

Acetone offers a lower pressure option, but it provides only a small amount of thrust due to its low saturation pressure. To optimize the propulsion system, a propellant is required that meets the needs of the mission without posing additional safety concerns.

Nitrous oxide and carbon dioxide both have moderate storage potential, but both suffer from the same problem as xenon. The high vapor pressure in the tank would require additional safety procedures and a reinforced propulsion tank capable of withstanding the increased pressure, adding more mass to the satellite. Additionally, if the temperature of the mixture increased, the low critical temperature would cause all the

propellant to enter the gaseous phase, thus raising the pressure and increasing the chance that the tank would rupture.

At first glance, sulfur hexafluoride appears to be a good candidate due to its high storage density (second greatest of all propellants investigated) and a saturation pressure less than half that of comparable fuels. Sulfur hexafluoride, however, has a moderately low critical temperature, making that the propulsion system susceptible to overheating and leaks or rupture. Nonetheless, its saturation pressure is higher than appropriate for the inlet pressure to a nozzle; therefore, some type of regulation system is necessary if small impulse bits are desired, increasing system mass and complexity. Additionally, due to its high density, sulfur hexafluoride poses a potential suffocation hazard because it will displace oxygen in the surrounding area. Currently, the Canadian Advanced Nanospace Experiment (CanX) plans to use sulfur hexafluoride on their CanX-2 satellite as a scaled test bed for larger future missions, CanX-4 and CanX-5 [16].

Candidates for a two-phase system include R-134a (1-1-1-2 tetrafluoroethane, CH_2FCF_3) and ammonia because both have moderate liquid storage density and high critical temperatures. Both systems have saturation pressures that could be used without regulation resulting in higher than desired thrust. The flow can be regulated if desired at the cost of added complexity and weight. However, the hazardous nature of ammonia would require additional safety precautions and raise the cost of development, testing, and integration. R-134a is a common refrigerant used in most automotive and household air conditioners; it replaced older chlorofluorocarbons that depleted the ozone. In most states, R-134a can be purchased in small quantities without a license, but due to the moderately high potential for global warming, some states and foreign countries have begun limiting the amount of R-134a that can be purchased without a license.

One of the most common choices for two-phase systems is butane because its vapor pressure is high enough to overcome internal inertial forces due to friction in the tubes, but low enough to ensure that the thrust remains small so that the satellite can be controlled precisely without added regulation. These properties make it an ideal candidate. Some well-known successful implementations of butane propellant have been achieved by researchers at the Surrey Space Centre; these are addressed later in this paper.

1.3. HISTORY OF SMALL SATELLITE PROPULSION SYSTEMS

Two trends are currently apparent in the satellite community: First, the on-orbit masses of communication satellites typically range from 1,000 to over 4,000 kg and researchers hope to expand this range up to between 8,000 to 12,000 kg; Second, the focus has turned to smaller satellites, with a particular emphasis on reducing development time and costs [18]. In the 1960s, after the successful launches of Earth's first artificial satellites, the mass of spacecraft quickly exceeded the limits of the microsatellite class as engineers tried to reach farther and do more with each generation of satellites. Not until the 1990s did the trend toward microsatellites reemerge due to increased interest on the part of the Defense Advanced Research Projects Agency (DARPA) and the Surrey Space Centre. And not until the launch of four Amateur Satellite Corporation (AMSAT) satellites in 1990 did nanosatellites gain momentum with the launch of SNAP-1, the most advanced nanosatellite yet designed [19]. Table 1.3 shows a breakdown of satellite classes by mass [18].

Table 1.3. Satellite Classification by Size

Satellite Class	Mass Range (kg)
Large	>1000
Medium	500 - 1000
Mini	100 - 500
Micro	10 - 100
Nano	1 - 10
Pico	0.1 - 1
Femto	< 0.1

A small satellite is defined as any satellite that falls in the mini-class or lower, or simply any satellite less than 500 kg.

1.3.1. Small-Satellite Propulsion Systems. The first Surrey Nanosatellite Application Platform (SNAP-1) was launched on June 28th, 2000, with 32.6 grams of butane, which provided the 6.5 kg satellite with just under 3.5 m/s of ΔV [20]. To provide sufficient propellant, SNAP-1 (Figure 1.7) required a method of storing the fuel in a very limited space. To reduce the time and cost of developing a custom tank for the mission, Surrey scientists used coiled titanium tubing, shown in Figure 1.7, that was bent into a triangular shape that would allow the propulsion system to be successfully integrated into the satellite [20].

Figure 1.7. SNAP-1 Two-Phase Butane Propulsion System

The SNAP-1 mission encountered a problem when the propellant was ingested by the propellant line and liquid butane was expelled. This ingestion resulted in a higher mass flow rate and reduced the specific impulse from a theoretical value of 70 seconds to 43 seconds. This difficulty highlights the need to provide a better means of controlling the phase of the propellant during ejection, whether passively or through active heating.

An additional success of the Surrey Space Centre was the launch of the Disaster Monitoring Constellation (DMC), which passes over every part of the globe on a daily basis and relays data back to Earth. This constellation made use of the knowledge gained from the SNAP-1 mission and scaled up to a much larger satellite (100 kg). For this mission, 2.3 kg of saturated liquid butane provides the DMC satellites with enough ΔV for constellation formation, station keeping and drag compensation for the duration of the mission [21].

1.3.2. Typical Mission Goals of Small Satellites. With a growing trend toward smaller, more versatile satellites, the demand is growing for more space-efficient and capable systems able to alter their orbit. A typical mission for such a system would include [20]:

- a remote service vehicle capable of inspecting the host spacecraft, maneuvering around it, and rendezvousing for refueling and recharging [22]
- constellation flights requiring that satellites alter their positions to maneuver into a formation dictated by the mission requirements
- de-orbiting (i.e., rendezvous and docking with an obsolete satellite or debris) and orbit changing.

Additionally, a typical mission for a small satellite requires approximately 20 m/s of ΔV unless a de-orbit burn is required, in which case that number is much higher [21].

1.3.3. University Satellites. Because of the continued increase in the use of commercial off-the-shelf (COTS) components due to their low cost, many universities have begun to design small satellites with the hope of securing a launch as a secondary payload on launch vehicle. Many universities have adopted the CubeSat standard set forth by the joint effort of Stanford University and California Polytechnic State University San Luis Obispo in which the scope of the satellite was reduced to a special envelope of 3,000 cm^3 and 3 kg, classifying it as a nanosat. Since 2000, over 23 schools have joined in the effort to design these more responsive systems, and increase from the 21 teams over the past 20 years [22]. Unfortunately, many such schools lack the time and expertise to add a propulsion system to their satellites, creating a need for a portable

propulsion system that can be easily adapted and incorporated into a host satellite. For example, in the Nanosat 6 competition sponsored by the Air Force Research Laboratory (AFRL), eleven universities are participating in a two-year competition to design, build, and test a fully functional satellite. The winner of the competition will receive assistance from AFRL in securing a launch opportunity. Of the eleven schools participating in this program, only three of the schools are currently pursuing the use of a propulsion system. MIT is developing an ion thruster capable of up a ΔV of 1 km/s, the Missouri University of Science and Technology (S&T) and Saint Louis University are working on refrigerant-based two-phase cold-gas systems using R-134a stored as a saturated liquid. With the development of a portable propulsion system for satellites ranging from nano- to micro-class, other universities will be able to design enhanced missions that would not have been possible without active orbit and attitude control.

1.4. PURPOSE

The purpose of this study was to test a refrigerant-based cold-gas system using R-134a as a saturated liquid propellant and to design a system portable to host buses at other universities. This will grant these schools the ability to design more advanced missions, thereby increasing the learning potential from each satellite successfully launched into orbit. The testing conducted by the author in this thesis confirmed the viability of R-134a as a propellant for small university spacecraft and demonstrated the performance characteristics of the system. The nonvolatile, nontoxic nature of the propellant makes it a strong candidate for university-level satellites since no extra safety measures are necessary to protect students, ground crew, or the launch vehicle.

1.5. THESIS ORGANIZATION

The introductory section of this thesis is followed by five additional sections:

2. Background – Covers the University Nanosat Program and the Missouri Satellite Team. It also discusses preliminary calculations in a previous study [28] based on the Nanosat 4 propulsion system and later compared these values to test results.

3. Parametric Study – Several combinations of fluid temperature and pressure were analyzed by the author to determine their effects on the thrust of the MR SAT propulsion system. Additionally, it offers a qualitative discussion of losses for R-134a-based systems. This discussion rests on correction factors determined based on the theoretical data presented in Section 2.

4. Endurance Test – Describes an endurance test completed by the author for which various masses of R-134a were placed in the MR SAT propulsion tank and then ejected the propellant from a nozzle into a vacuum environment. This test determined the dependence of exhaust duration on initial fluid mass and quality.

5. Integration into Nanosat 6 Design – Enhancements to the Nanosat 4 design are discussed in detail and a new thruster layout overseen by the author is presented to maximize the performance of the MR SAT propulsion system.

6. Conclusion – Reviews the lessons learned during the course of this research and explains how this knowledge can be applied to small and university-class satellite propulsion systems in general. Additionally, this section discusses how the information presented here can be used by others to construct an R-134a-based cold-gas propulsion system.

2. BACKGROUND

2.1. UNIVERSITY NANOSATELLITE PROGRAM

One of the single greatest challenges posed to university satellite teams is acquiring a means of launching their payload into space. At a cost of approximately $10,000 per kilogram [23], a small spacecraft or nanosatellite can reduce overall costs by minimizing the cost of the launch through its low size and mass. Student satellites face additional challenges because they are typically launched as a secondary payload, meaning they are manifested on the launch vehicle after the primary payload. In an attempt to prevent the cost from deterring low-funded research, the Department of Defense (DoD) created the Space Test Program (STP) aimed at providing free launches to satellites with DoD-relevant missions. The STP program was established in 1966, and by early 2000 had already recorded launches of 410 payloads on 150 missions [24]. One consequence of the push to launch these satellites was the creation of the AFRL University Nanosatellite Program (UNP). It a joint venture between AFRL's Space Vehicles Directorate (SPD), the Air Force Office of Scientific Research (AFOSR), and the American Institute of Aeronautics and Astronautics (AIAA) [25]. The UNP program seeks to advance the level of training of the future workforce through a national satellite design and fabrication experiment conducted at the university level. At the time of this writing, the Nanosat 6 competition is underway, with eleven universities participating in the two-year program. Each university must undergo several design reviews similar to those faced by professionals. At the conclusion of the program, a joint committee selects a winner based on DoD relevance, overall completeness, and a K-12 outreach program. The winning team then receives assistance in their attempt to pass the Space Experiments Review Board (SERB) and secure a flight on a future DoD launch [24].

A detailed description of the Missouri Satellite Team (M-SAT) mission and hardware can be found in Appendix B [25], [26], [28] – [32]. The equipment used in the testing outlined in this thesis was M-SAT hardware unless noted otherwise.

2.2. PREVIOUS RESEARCH

Reference [28] documents the first-generation design and analysis of the MR SAT propulsion system. Since its publication, many design upgrades have been made, requiring a review and update of the analyses performed in [28] using the most current specifications. For the first-generation Nanosat 4 design, the inlet design conditions used for the analysis are shown in Table 2.1.

Table 2.1. Nanosat 4 Inlet Conditions for Propulsion Performance Calculations

Propellant Mass (grams)	m_P	60.52
Temperature (°C)	T_C	20
Pressure [kPa (psia)]	P_C	137.9 (20)
Specific Heat Ratio	γ	1.127
Nozzle Exit Diameter (m)	D_e	5×10^{-3}
Nozzle Exit Area (m^2)	A_e	1.9635×10^{-5}
Spacecraft Mass (kg)	m_o	25

This analysis is governed by the rocket equation and nozzle flow calculations as shown below in Eqns. 2.3-2.9. Additionally, the following assumptions are made:

- Flow in the nozzle is isentropic.
- Tank and propellant lines contain isothermal fluid.
- Propellant is in gaseous state and obeys ideal gas laws.
- No shocks or discontinuities present in the nozzle.
- Flow is quasi-one-dimensional in the axial direction.
- Nozzle boundary layers are disregarded.
- Propellant flow is constant with no open/close transient effects.

- Ambient pressure is zero in space.

For more information on the governing equations, refer to [28], [33], and [34].

Sonic velocity:

$$a_0 = \sqrt{\gamma R T_0} \quad [2.1]$$

Characteristic Velocity:

$$c^* = \frac{a_0}{\gamma\left(\frac{2}{\gamma+1}\right)^{\frac{\gamma+1}{2(\gamma-1)}}} \quad [2.2]$$

Pressure ratio from area ratio relationship:

$$\frac{A_e}{A^*} = AR = \sqrt{\frac{\left(\frac{\gamma-1}{2}\right)\left(\frac{2}{\gamma+1}\right)^{\frac{\gamma+1}{\gamma-1}}}{PR^{\left(\frac{2}{\gamma}\right)}\left[1-PR^{\frac{\gamma-1}{\gamma}}\right]}} \quad [2.3]$$

Mass flow rate:

$$\dot{m} = \frac{A^* P_C}{c^*} \quad [2.4]$$

Specific Impulse:

$$I_{sp} = \frac{c^*\gamma}{g_0}\sqrt{\left(\frac{2}{\gamma-1}\right)\left(\frac{2}{\gamma+1}\right)^{\frac{\gamma+1}{\gamma-1}}\left[1-PR^{\frac{\gamma-1}{\gamma}}\right]} \quad [2.5]$$

Velocity change:

$$\Delta V = g_0 I_{SP} ln\left(\frac{m_0}{m_0 - m_P}\right) \quad [2.6]$$

Thrust:

$$F = A^* P_C \gamma \sqrt{\left(\frac{2}{\gamma-1}\right)\left(\frac{2}{\gamma+1}\right)^{\frac{\gamma+1}{\gamma-1}}\left[1 - PR^{\frac{\gamma-1}{\gamma}}\right]} + P_e A_e \qquad [2.7]$$

From these equations, the performance characteristics of a thruster design can be determined over a range of inlet conditions and nozzle geometries. Previous work [28] varied the area ratio over a large range and found that an area ratio of 100 provided adequate performance in terms of thrust, I_{sp} and ΔV. Tables 2.2and 2.3 show both the ideal performance characteristics assuming an isentropic nozzle and conservative values based on a colder inlet gas temperature of 15 °C (288 Kelvin) and factoring in loss coefficients due to friction, tube length, and other factors. Refer to Seubert [28] for detailed loss coefficient calculations.

Table 2.2. Nanosat 4 Predicted Performance Characteristics

Table 2.3. Nanosat 4 Under Various Tank Pressures Predicted Performance Characteristics

	Ideal Conditions		Conservative Conditions	
Max Tank Pressure at 100 °C [kPa (psia)]	ΔV (m/s)	Total Thrust Exhaust Duration (mins)	ΔV (m/s)	Total Thrust Exhaust Duration (mins)
689.48 (100)	0.943	7.10	0.935	11.34
1378.96 (200)	2.041	15.34	2.024	24.52
2068.44 (300)	3.374	25.31	3.345	40.46

As mentioned above, however, at the time of this initial analysis, the hardware selection was still in progress, and some of the initial values were based on estimates. For example, a regulated pressure of 137.9 kPa (20 psia) was assumed until selection of the Swagelok regulator, which is specified to provide a pressure of 170.3 kPa (24.7 psia). However, the actual pressure given by Swagelok and confirmed by laboratory testing indicated that the regulated pressure will fluctuate based on the system's flow rate. The regulated pressure will vary from approximately 25.7 psia (11 psig) to 21.7 (7 psig) as the flow rate increases from zero to five std. L/min, as illustrated in Figure 2.1 [35].

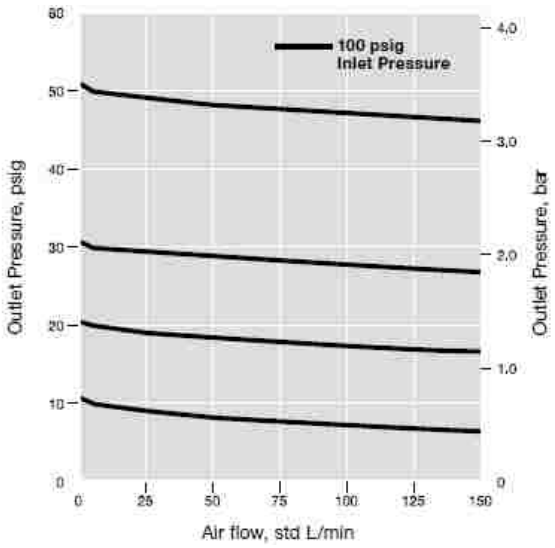

Figure 2.1. Regulated Pressure of HFS3B Series Regulator vs. Flow Rate of Air

Values obtained from laboratory testing of the MR SAT propulsion system have been used here to update previous analyses and generate theoretical performance characteristics for the Nanosat 6 design. Although the previous analysis included a conservative value based on estimated lost coefficients, Table 2.4 shows both the theoretical (using Eqns. 2.3 – 2.9) and actual performance values based on laboratory testing in a vacuum chamber, discussed in greater detail in Section 3.

Table 2.4. Nanosat 6 Theoretical and Actual Performance Characteristics

Inlet Pressure (psia)		24.7
Inlet Temperature (°C)		20
Initial Mass (kg)		26
	Ideal Conditions	Actual Conditions
I_{sp} (sec)	48.97	20.92
Thrust (mN)	69.9	24.13
ΔV (m/s)	1.117	0.477

Based on the actual performance of the MR SAT propulsion system measured in vacuum, the loss coefficients were determined for the entire system. Rather than isolating the efficiency of individual components, the entire system was analyzed as a whole. However, future research should focus on minimizing the losses associated with the system to maximize efficiency. Based on this analysis, a thrust correction factor, ζ_F, was calculated to be 0.383 where

$$F_{ACTUAL} = \zeta_F F_{IDEAL}. \quad [2.8]$$

Similarly, velocity (I_{sp}) and discharge ($\dot{m}$) correction factors were determined to be 0.401 and 1.0, respectfully:

$$I_{sp_{ACTUAL}} = \zeta_v I_{sp_{IDEAL}} \quad [2.9]$$

$$\dot{m}_{ACTUAL} = \zeta_d \dot{m}_{IDEAL}. \quad [2.10]$$

Because of the difficulty of measuring the system's mass flow rate under various conditions, a reliable measurement could not be obtained. Therefore, the actual mass flow rate is assumed to be the same as the theoretical rate. Since ΔV is a function of I_{sp}, any losses in the later will directly affect the amount of ΔV that the system is capable of producing, resulting in a propulsive capability (ΔV) correction factor of 0.401:

$$\Delta V_{ACTUAL} = \zeta_p \Delta V_{IDEAL}. \quad [2.11]$$

Initial calculations did not include a propulsive capability correction factor [28]; however, such a factor was added in this analysis to permit direct correlation of the theoretical ΔV with that required to complete the mission objectives. These correction factors are listed in Table 2.5.

Table 2.5. Correction Factors for MR SAT Propulsion System

	Symbol	Correction Factor Range	Predicted Correction Factor	Actual Correction Factor	Percent Error
Discharge (m)	ζ_d	1.00 - 1.15	1.08	1.00	-
Velocity (Isp)	ζ_v	-	0.900	0.401	124.49
Propulsive Capability (ΔV)	ζ_p	-	-	0.401	-
Force (Thrust)	ζ_F	0.92-1.00	0.972	0.383	153.85

The correction factors were estimated based on ranges provided by analysis of current propulsion systems. Based on these ranges, a conservative value was selected assuming a worst-case design; however, the M-SAT propulsion system clearly suffers

from inefficiencies far greater than those of traditional systems. Because of the limited budget of the M-SAT mission, the system could be optimized only to the extent that cost would allow. With sufficient time and funding, a nozzle designed using the method of characteristics may eliminate some of the losses due to the conical nozzle geometry. Section 3.5 provides additional information on the experimental setup and sources of error.

3. PARAMETRIC STUDY

3.1. THEORETICAL PREDICTIONS

One goal of this research is to determine the effect of thruster inlet conditions on performance characteristics. Because various propulsion system configurations are possible, the characteristics of the propellant as it enters the nozzle of an arbitrary system will likely vary from the inlet conditions presented for the MR SAT propulsion system. The result of a parametric study will permit end users to determine the performance characteristics needed for a mission and determine what nozzle inlet conditions are necessary to achieve those characteristics. Using the equations presented in Section 2.4, this work used MATLAB code written to determine the performance characteristics of a system given a range of inlet nozzle temperatures and pressures; the results are shown in Figures 3.1 through 3.3. To validate the numerical results, a physical experiment was constructed and tested in a vacuum environment, and the results are presented in this section.

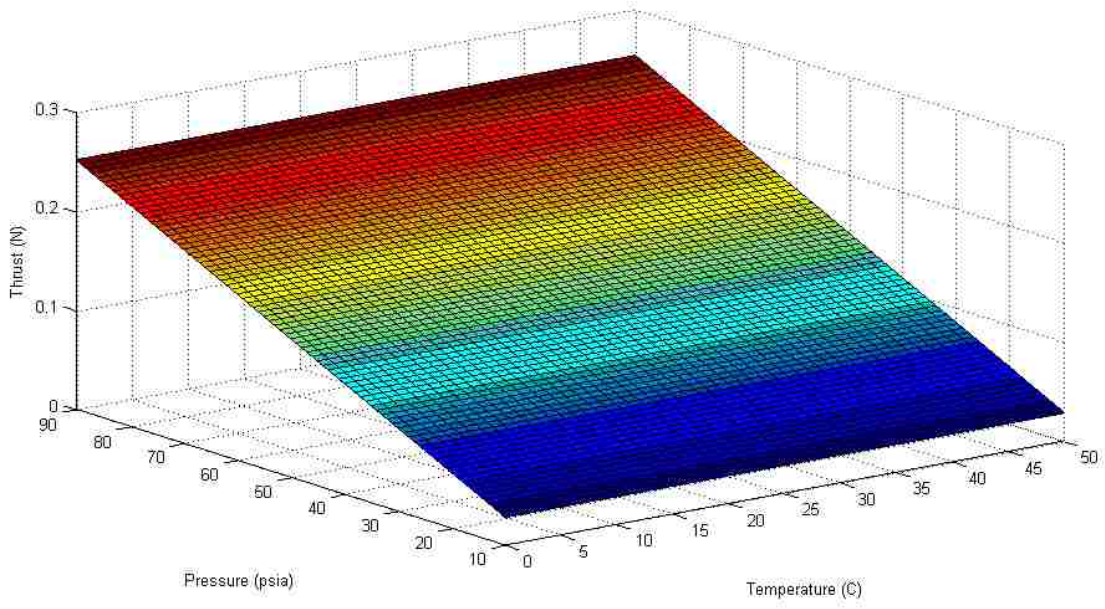

Figure 3.1. Ideal Thrust as a Function of Temperature and Pressure of R-134a

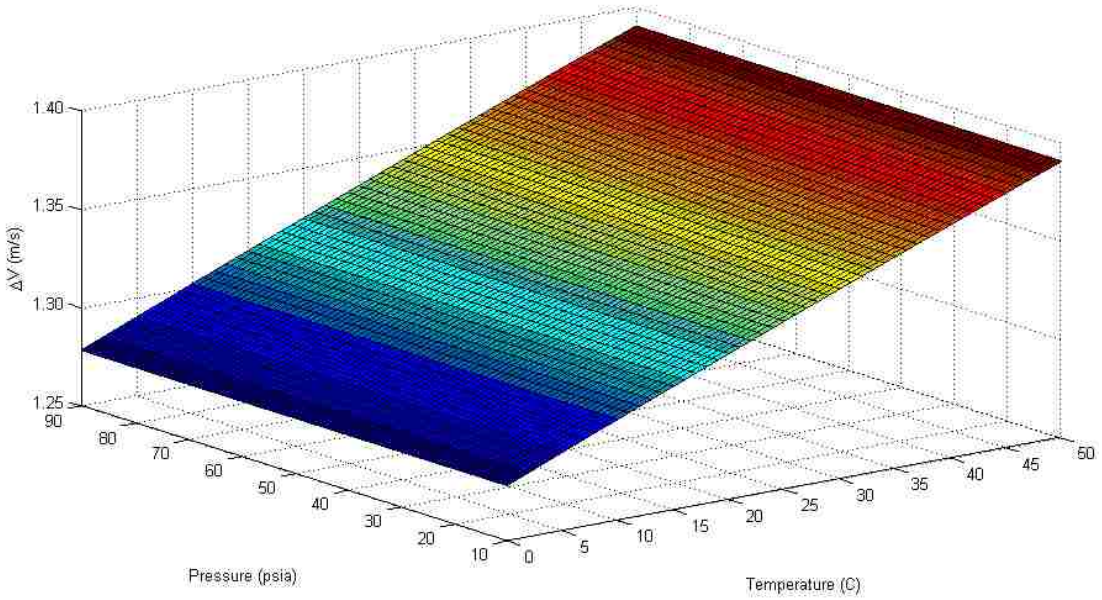

Figure 3.2. Ideal ΔV as a Function of Temperature and Pressure of R-134a

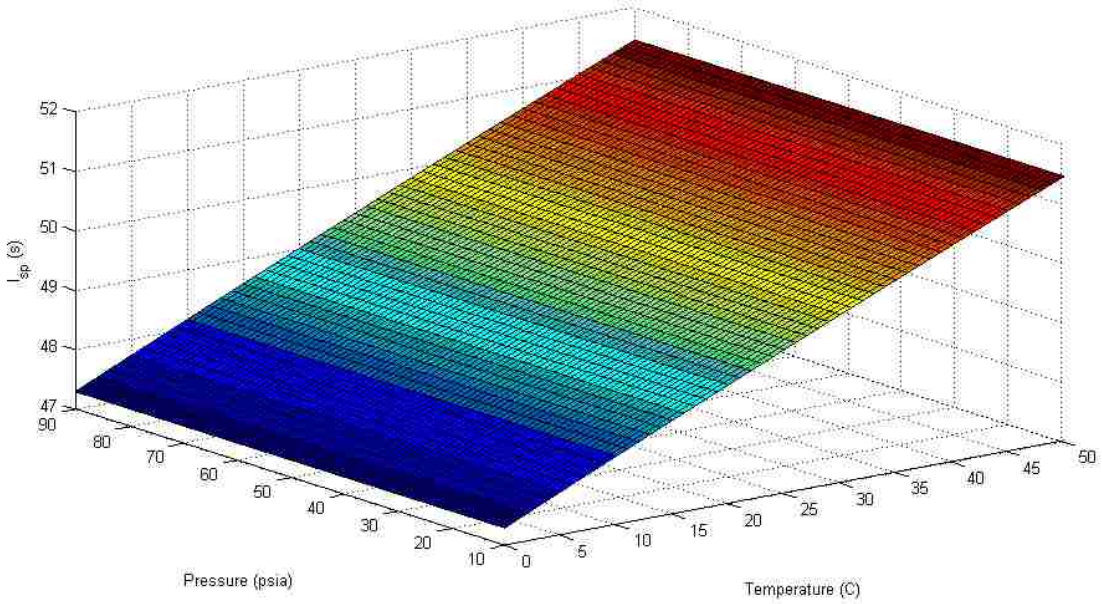

Figure 3.3. Ideal I_{sp} as a Function of Temperature and Pressure of R-134a

Figure 3.1 indicates that the thrust is independent of the inlet temperature of the nozzle, whereas Figures 3.2 and 3.3 show that pressure is independent of both ΔV and I_{sp}. These results, however, assume ideal conditions and a ground test is required to validate the theoretical analysis and obtain more realistic results.

3.2. TESTING SETUP

To test the propulsion system, an environment was simulated similar to that experienced by thrusters in orbit. A bell jar vacuum chamber 24" diameter by 27" long (Figure 3.4) provided by the Missouri S&T Aerospace Plasma Laboratory under the direction of Dr. Joshua Rovey was used to create a near-space environment of approximately 30 mTorr. The chamber is capable of pressures of 10^{-6} to 10^{-7} Torr with the use of a turbo pump; however, the additional time needed to achieve these pressures did not justify the small increase in accuracy that could be obtained.

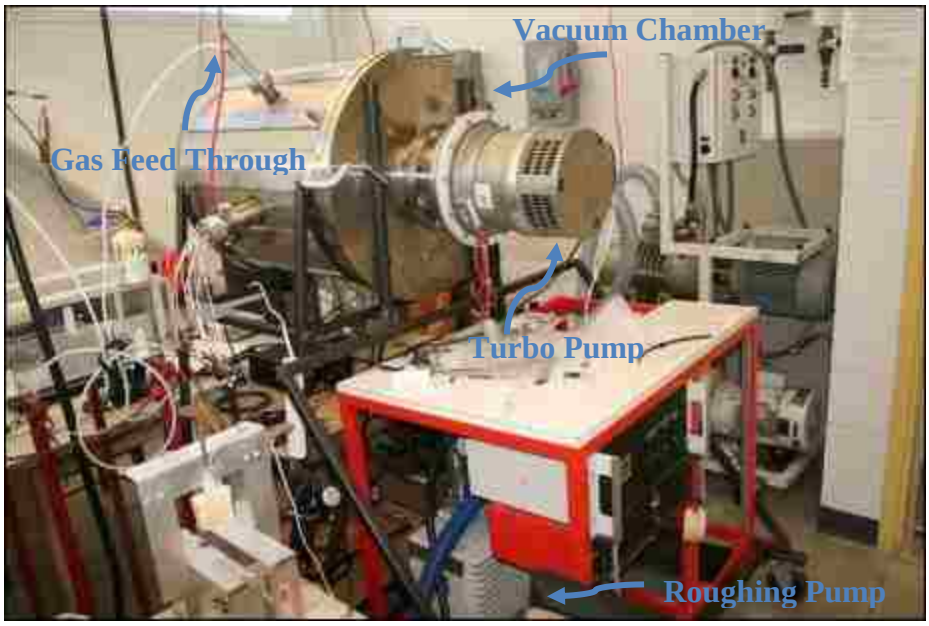

Figure 3.4. Aerospace Plasma Laboratory Bell Jar Vacuum Chamber

A consultation with David Gibbon of Surrey Satellite Technology led the team to conclude that a simple mass balance could accurately measure the thrust being produced by the M-SAT thrusters. A mass balance able to withstand vacuum environment without damage, however, was not readily available. The team consulted again with Mr. Gibbon, who recommended the "My Weight iBalance 1200," which he has used successfully in the past. To ensure that the thruster remained perpendicularly to the scale, a small thruster test stand was constructed to secure and align the thruster, as shown in Figure 3.5.

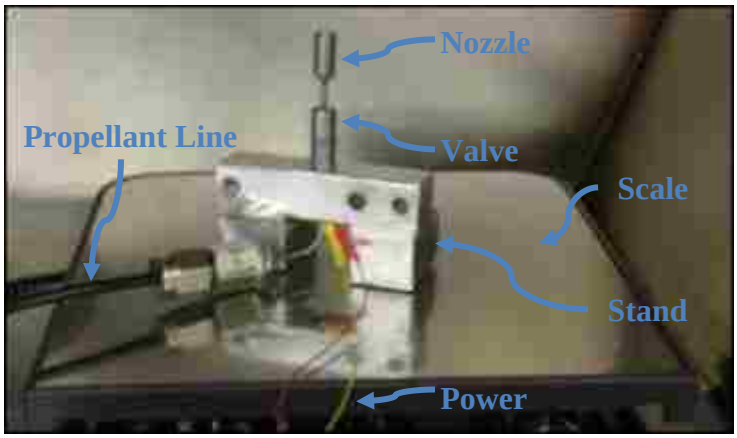

Figure 3.5. Thruster Test Stand

Additionally, because of the increased amount of tubing needed to deliver the propellant into the vacuum chamber, the downstream pressure transducer was relocated inside the vacuum chamber to shorten the length of tubing needed to attach the thruster to the transducer. By reducing the tubing length, the losses were minimized and the pressure more accurately determined as it entered the thruster as shown in Figure 3.6.

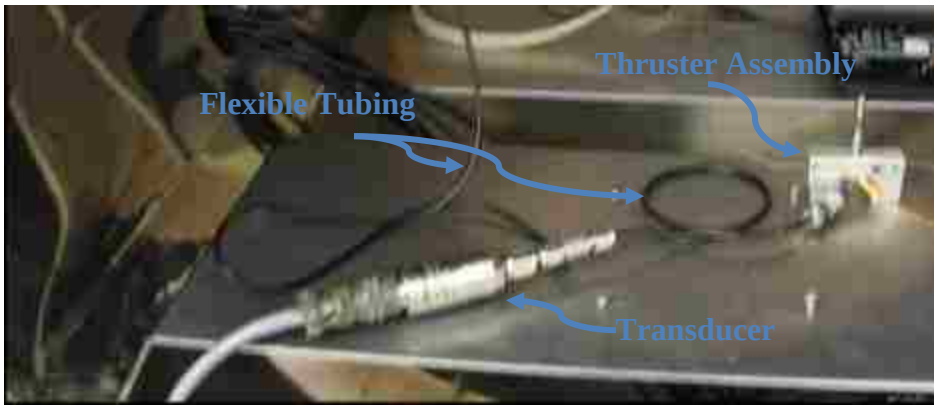

Figure 3.6. Downstream Pressure Transducer Inside Vacuum Chamber

The heaters used here have only two settings, on and off. To maintain control of the propellant temperature, therefore, additional measures were necessary. To prevent damage to the primary propulsion tank, small, off-the-shelf cans of R-134a were used, and these were immersed in a hot water bath to heat the propellant during a test firing, maintaining a constant temperature environment. Immediately connected to the can of R-134a was a regulator from Swagelok that was capable of accepting inlet pressures up to 1,000 psia and maintaining the outlet pressure between 0-100 psia. Because of the limited amount of propellant available in a small satellite propulsion system, a regulated pressure of 100 psia would have depleted the reservoir of propellant too quickly. Furthermore, higher pressures would extract more energy from the system than the heaters could restore, reducing the pressures over time. Located downstream of the regulator was a Swagelok 0.5 micron stainless steel filter designed to prevent propellant contamination, which could damage the thruster. The first pressure transducer was located just past the filter as so that any losses through the filter and regulator would not affect the resulting data. Finally, the R-134a was piped into the vacuum chamber, then into the second pressure transducer, and from there directly to the thruster. With no hardware between the transducers, the pressure differential associated with line losses could be measured and used to predict losses for similar small satellite propulsion systems.

The number of electrical pass-throughs on the vacuum chamber presented a challenge. The bell jar had eleven pass-throughs (nine BNC connections and two high voltage), whereas the experimental setup required nineteen (seventeen BNC and two high voltage). The difficulty arose from the mass balance used in the experiment. Although the balance could withstand a vacuum environment, the LCD screen had to remain outside the chamber, requiring thirteen pass-throughs on its own. To resolve this situation, a custom flange (Figure 3.7) was constructed from 3/8" Plexiglas and copper wire. First, a stainless steel flange was used as a template to machine Plexiglas to the proper size and ensure that the bolt hole pattern and gasket aligned with the vacuum chamber. Next, thirteen holes were added to the custom flange; they were kept within the limits of the gasket to ensure that the system sealed properly. Finally, copper wires were then epoxied in place and two DB-9 connectors were added (one with six pins and the other with seven) to either end of the flange to permit integration of the scale or any other equipment that might be added later.

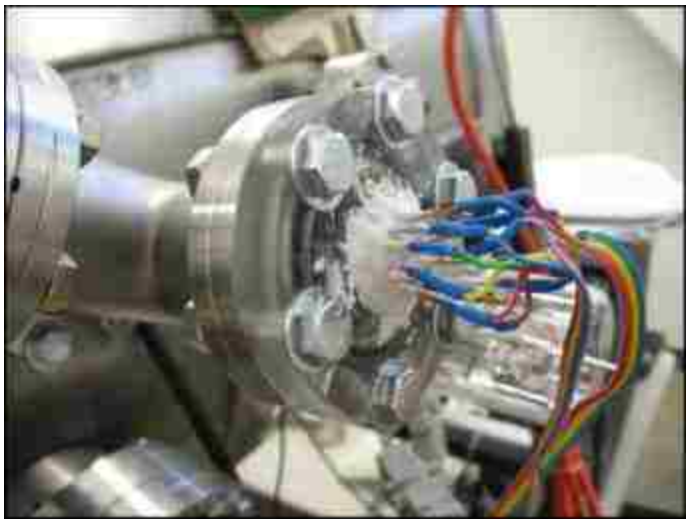

Figure 3.7. Thirteen-Pin Custom Flange

Once the flange was installed, the scale was disassembled and the LCD panel was relocated to the front of the vacuum chamber door so that it could be read more easily during the experiment while the power for the scale was run through the high-voltage pass-throughs. Next, the transducer and thruster were wired through the nine BNC pass-throughs to a LabVIEW workstation capable of recording data from both pressure transducers and controlling the firing of the thruster. Only the temperature and thrust measurements were not automatically recorded; they were recorded manually and transcribed into Excel for analysis. A complete system schematic can be seen in Figure 3.8.

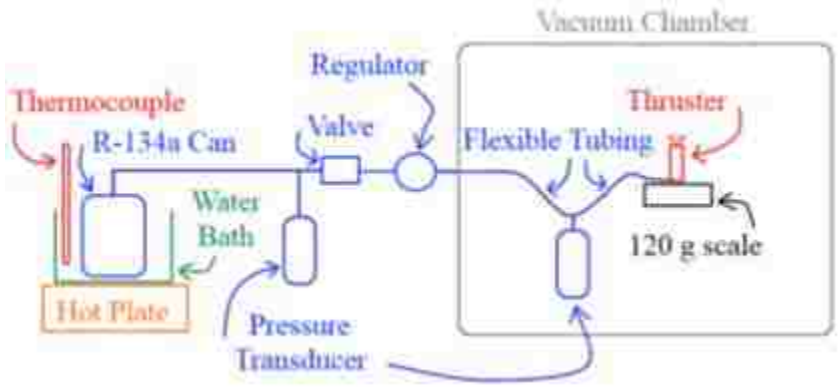

Figure 3.8. Parametric Study System Schematic

3.3. PROCEDURE

The temperature range for this study was varied from 0-40 °C in increments of 10 °C, and pressure ranged from 10-100 psia in 10 psia increments. At lower temperatures, however, the saturation pressure of the propellant was lower than 100 psia and thus the range only went as high as the saturation pressure. Because the temperature was the most challenging of the variables to regulate, requiring several minutes to reach equilibrium after each increase or decrease, the temperature was held constant throughout the test

while the pressure was varied. Additionally, to ensure that the propellant was at precisely the desired temperature, a simple program was written in MATLAB (Appendix C) to determine the time needed for the can of R-134a to reach equilibrium. This time was determined to be about ten seconds, therefore, once the thermocouple used to monitor the temperature of the water bath reached the desired temperature and sustained it for ten seconds, it was assumed that all propellant within the can had reached the target temperature.

A methodical testing procedure was implemented to ensure consistent data. First, all valves were closed, the regulator set to zero, and the vacuum chamber door sealed. Next, the propellant was set to the target temperature either by adding ice to the water bath or by turning on the hot plate. Once the propellant had reached the desired temperature, the vacuum chamber was pumped down to approximately 30 mTorr. The valve on the can of R-134a was then opened and the regulator adjusted to the appropriate pressure. Because of the difference between the dynamic and static regulated pressures of the regulator, the thruster was briefly fired so that a dynamic pressure could be obtained and the regulator appropriately adjusted to ensure an accurate pressure. Finally, when the vacuum chamber expelled the propellant from the test firing and returned to base pressure, and when the propellant had reached a constant temperature, the thruster was fired and the data recorded by the LabVIEW workstation. Because of the time required to transition fully to the dynamic pressure and due to the timing delay of the mass balance, the thruster was fired continually for several seconds so that the thrust reading could reach equilibrium. Each pair of temperature and pressure was tested a minimum of five times to ensure accuracy, each time waiting for the vacuum chamber and temperature to re-equilibrate. After completing a data set, the pressure was increased to the next point and the test was performed again. When the pressure either reached 100 psia or could no longer be increased due to saturated pressure limits, the test for the specified temperature was concluded, and regulator and valves were returned to their off positions.

3.4. RESULTS

The results for the various thrust tests confirm the theoretical predictions that show the independence of thrust from the temperature of the propellant and demonstrate the linear dependence on pressure. For the first two tests, however, these trends started to falter at temperatures of 30 °C or higher. The propellant was then cooled back down to zero degrees to determine if the initial results could be repeated, however, the new thrust values had decreased to half of their original values. This seemed to indicate a problem with the thruster itself, so a second identical thruster was used for the second test that ended in the same depreciating thrust at a temperature of 30 °C. Rather than show a small decrease in thrust at these higher temperatures, however, the second thruster's performance decreased rapidly. Because both thrusters failed at approximately the same temperature, it was decided that a third test would be conducted without the Lee valve and only the nozzle. Micro Aerospace Solutions was contacted and a new thruster was shipped that was configured with only a nozzle attached to a 1/16" section of tubing. In order to successfully control this test without the Lee valve to control the flow of propellant, a 90 degree ball valve was inserted into the system. When the test was set to begin, one individual opened the valve at the same time another individual activated the computer program and recorded the experiment data. The first two tests are shown in Figure 3.9 and the third test is shown in Figure 3.10.

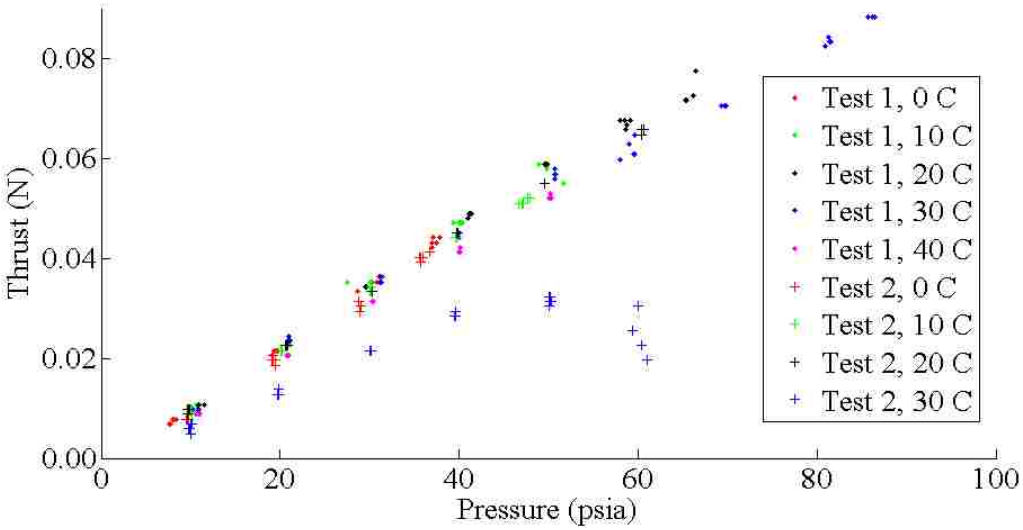

Figure 3.9. Thrust Performance Data from Thruster with Lee Valve

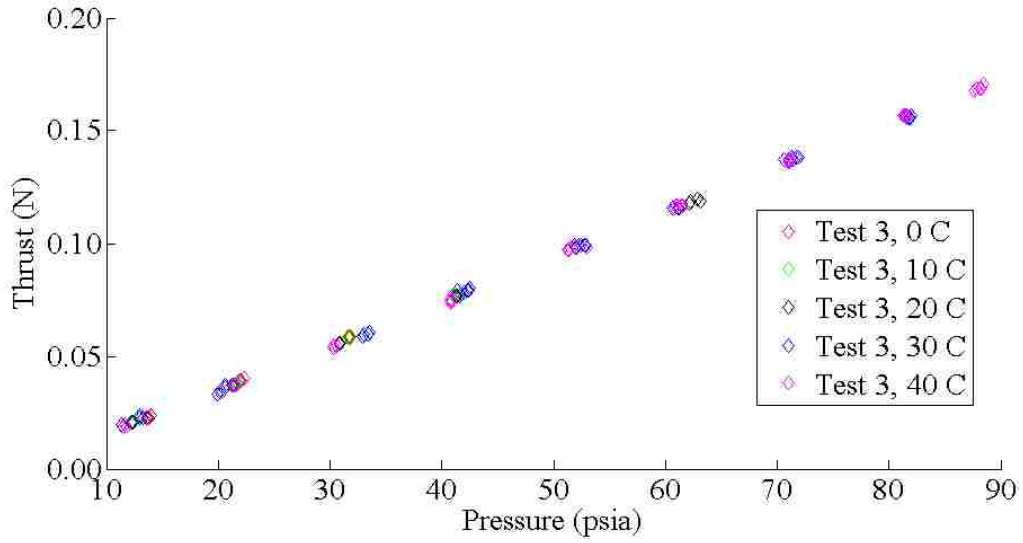

Figure 3.10. Thrust Performance Data from Thruster without Lee Valve

It is clear that removing the Lee Company valve identified the valve as the source of the degrading thrust observed in the first set of tests. However, an unexpected

observance was that the amount of thrust generated with only the nozzle was greatly increased. It is believed that the valve itself caused a significant decrease in the flow pressure in the thruster which significantly reduced the amount of thrust that the system was capable of producing. This increase can be clearly seen in Figure 3.11.

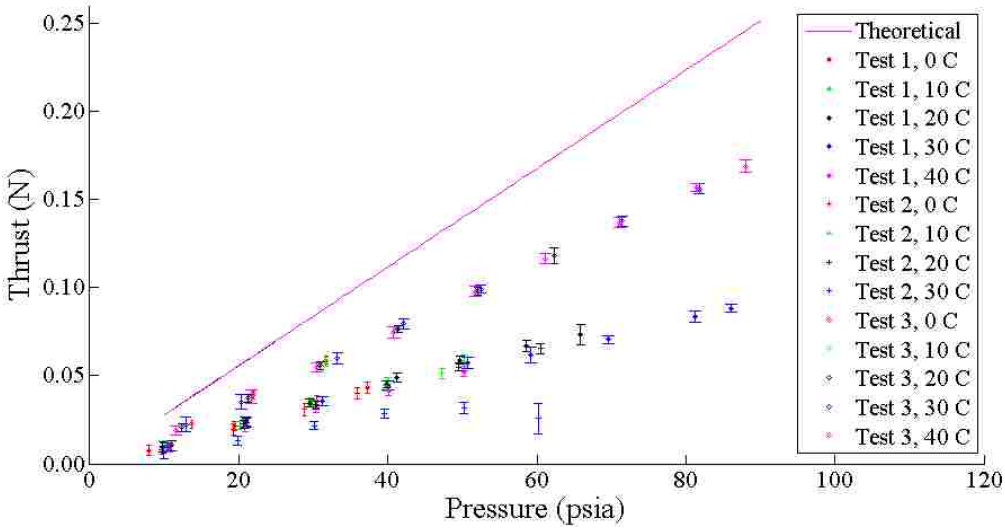

Figure 3.11. Thrust Data Comparison

Figure 3.11 appears to only show the theoretical data corresponding to 40 °C; however, recall that the theory shows that thrust is independent of temperature, and therefore all the lines corresponding to the theoretical thrust lie on top of each other. Additionally, the thrust for the thruster without the Lee valve produced approximately 44.5% more thrust on average than the thruster with the Lee valve. Based on the cutaway view of the thruster in Figure 3.12 [36], it is clear that the flow must maneuver around several sharp turns to pass through the valve which may be resulting in a significant loss in fluid pressure and velocity resulting in decreased thrust.

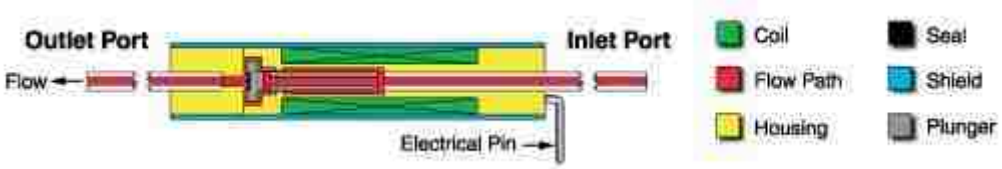

Figure 3.12. Lee Company Valve Cutaway View

Based on the results of the third test, correction factors shown in Table 2.9 were recalculated showing that removal of the Lee Company valve improved performance and are shown in Table 3.1.

Table 3.1. Revised Correction Factors for MR SAT Propulsion System

	Symbol	Predicted Correction Factor	Correction Factor with Valve	Percent Error of Thruster with Valve Relative to Predicted	Correction Factor without Valve	Percent Error of Thruster without Valve Relative to Predicted	Percent Error of Thruster without Valve to Thruster with Valve
Discharge (m)	ζ_d	1.08	1.00	-	1.00	-	0.00
Velocity (Isp)	ζ_v	0.900	0.401	124.49	0.682	31.89	41.25
Propulsive Capability (ΔV)	ζ_p	-	0.401	-	0.682	-	41.25
Force (Thrust)	ζ_F	0.972	0.383	153.85	0.652	49.15	41.25

The performance is substantially better once the Lee Company valve was removed as seen by the approximately 30% increase in performance. It is currently unclear as to why this discrepancy is present; however the team is working with Lee Company and Micro Aerospace Solutions to determine the cause of the inefficiencies and the best way to correct these deficiencies. Additionally, in the event that the Lee Company valve issue cannot be easily solved, the team in investigating other valve

manufacturers such as Vacco to determine whether another vender may exist that can supply valves that maximize the MR SAT propulsion system.

An error analysis shown in Figure 3.11 indicates the value of thrust expected with a confidence level of 95%. A statistical analysis [37] of the data yielded a standard deviation from the average thrust and was combined with the error in the system hardware. Based on observations conducted during testing, at an ambient pressure of 14.7 psia, the transducers fluctuated by +/- 0.1 psia. Using the data from the first two tests, a linear curve fit was found giving thrust as a function of pressure. From this curve fit, the amount of pressure deviation could be transformed into a thrust variation. For the pressure transducers, the manufacturer and calibration error led to a variation of +/- 0.19 mN. Further testing showed that at the maximum pressure, a line loss of approximately nine psia was seen between the two transducers. While the second transducer was located near the thruster to minimize line losses, it is likely that some losses may still occur. To account for this, a variation of +/- 1 psia was assumed, yielding an error of +/- 1.90 mN. Finally, the scale was accurate to +/- 0.1 grams, meaning that a variation of +/- 0.981 mN was possible. The resulting error in the hardware was thus calculated to be +/- 2.18 mN.

3.5. RECOMMENDATIONS

Based on the results of this test, it seems clear that R-134a can be successfully used as a propellant in a vacuum environment to generate moderate levels of thrust for small satellites that require orbital maneuvering capability. The data trends seem to correlate with theory; however, losses in the system significantly reduce the system capability. One of the primary initial concerns was the length of tubing used to deliver the propellant from the tank to the thruster. It was postulated that as the thruster was fired, the propellant would experience significant amounts of frictional losses and fully developed flow resulting in boundary layer choking that would reduce the pressure and thus thrust. However, during testing it was found that the pressure losses between the upstream and downstream transducers only measured two psia for a regulated pressure of 20 psia and approximately nine psia for a regulated pressure of 90 psia. However, during

testing all pressures used in calculations were from the downstream transducer so the line losses were not a factor in these tests.

Another source of error resulted from the testing setup using both 1/4” and 1/8” diameter tubing made of both plastic and metal that could have adverse effects on the performance. The flexible plastic tubing was needed to connect tank and thruster as both rested on scales so that mass flow and thrust readings could be made. The use of rigid tubing would act as a moment arm and introduce large amounts of error. It is possible that the plastic tubing has a higher coefficient of friction which would result in a larger pressure drop relative to the stainless steel tubing. Since the actual system will use all stainless steel tubing it is likely that the system performance may increase. Also, once on orbit, the thrusters will operate in a pulsed fashion, which will reduce the likelihood of the flow fully developing minimizing boundary layer choking.

Additionally, one improvement that can be made is the use of a scale with faster data acquisition so smaller firing times can be achieved. During testing some combinations of temperature and pressure would allow for sustained thruster operation without significant degradation of thrust, however, at the higher pressures the thrust dropped off rapidly, which could have increased the amount of error. Because of the fully developed flow, it was desired to fire the thruster long enough to reach a steady state condition at which point the thrust and downstream pressure could be read and recorded. At the higher pressures, a steady state condition was never reached. Because of the slow acquisition rate of the scale, accurately determining the thrust and pressure presented a larger challenge. This was partially overcome by firing for as short of a duration as possible and averaging the pressure readings from the LabVIEW program. If a faster acquisition scale were procured it would remove some of the error introduced by having to average the pressure over the firing duration. Also, if the LabVIEW program could read the thrust from the scale, more accurate data could be obtained. However, based on the data presented in Figure 3.11, it is clear that even with these sources of error present, the linearity of the data indicate that the results are accurate within an acceptable margin of error.

Finally, the temperature data for the parametric study were recorded by a thermocouple placed in the water bath. As a result, the temperature data presented in this

parametric study corresponds to the initial temperature, and does not change at the same rate as the propellant temperature inside the can. To account for this, a simple calculation was done to determine the amount of time needed to heat the propellant to the same temperature as the water bath. Based on Eq. 3.1 below, it was shown that one minute would be sufficient time to heat a full can of R-134a (340 g) at 20 °C to 40 °C assuming a one millimeter thick steel shell.

$$\dot{Q} = \frac{kA\Delta T}{x} \qquad [3.1]$$

The conductive surface area was found by approximating the can to be a simple cylinder, neglecting the irregular shape of the top of the can. When the can of R-134a was added to the water bath, rather than starting the one minute count down, the system was allowed to sit until the water bath reached equilibrium as the introduction of the relatively cold mass would lower the temperature of the bath by a few degrees. Once the water bath reached equilibrium, the bath was left to sit for two minutes ensuring that the propellant temperature was the same as the water bath. Because the thruster firings lasted only a few seconds, it was assumed that the fluid temperature did not vary much and what little energy was transferred out during the short firing duration was transferred back into the fluid by the water bath before the tank pressure dropped.

4. ENDURANCE TEST

4.1. THEORETICAL PREDICTIONS

4.1.1. Purpose. While total ΔV is a primary concern for the M-SAT propulsion system, one key aspect that makes refrigerant-based systems unique is the need to compensate for the evaporation of liquid propellant to counterbalance the expulsion of gaseous propellant. The goal of this test is to determine the total firing duration of the MR SAT propulsion system before either the propellant is consumed or until the system pressure drops below the regulated pressure resulting in reduced thrust. If the propulsion system can only be fired for 30 seconds before the thrust decreases and the system becomes unresponsive then the maximum ΔV that the system is capable of producing may become the limiting factor in a formation flight mission, regardless of total ΔV potential. If a ΔV requires a longer firing duration to complete than the maximum exhaust duration the system is capable of, then the propulsion system will be unable to complete the mission.

In addition to providing sufficient thrust for a given mission, the other challenge that an R-134a-based system must overcome is generating enough ΔV to achieve mission goals. As mentioned previously, the M-SAT mission requires a separation of MR and MRS SAT via a release mechanism and the propulsion system is then used to overcome the separation velocity and establish the formation. Based on available release mechanisms, there are two candidates that the team is currently pursuing: Planetary Systems Corporation (PSC) Lightband and Non Explosive Actuation (NEA). Currently, the main concern from a propulsion standpoint is the ejection velocity that each release mechanism imparts as this will represent the minimum amount of ΔV that MR SAT's propulsion system will need to overcome in establishing the formation.

4.1.2. Lightband. Lightbands have been successfully used to deploy satellites on several mission [38] and it is the mechanism that the AFRL is purchasing for the winning NS6 team to release their satellite from the launch vehicle [25]. The (second) Lightband under consideration for use in securing MRS SAT to MR SAT during launch ascent uses a motorized system to hold both halves of the Lightband together prior to deployment. Once on orbit, the motor is activated which releases the leaves allowing them to retract.

Finally, the separation springs force the two halves apart and impart a separation velocity. Figure 4.1 shows a Motorizes Lightband (MLB) just after separation [38].

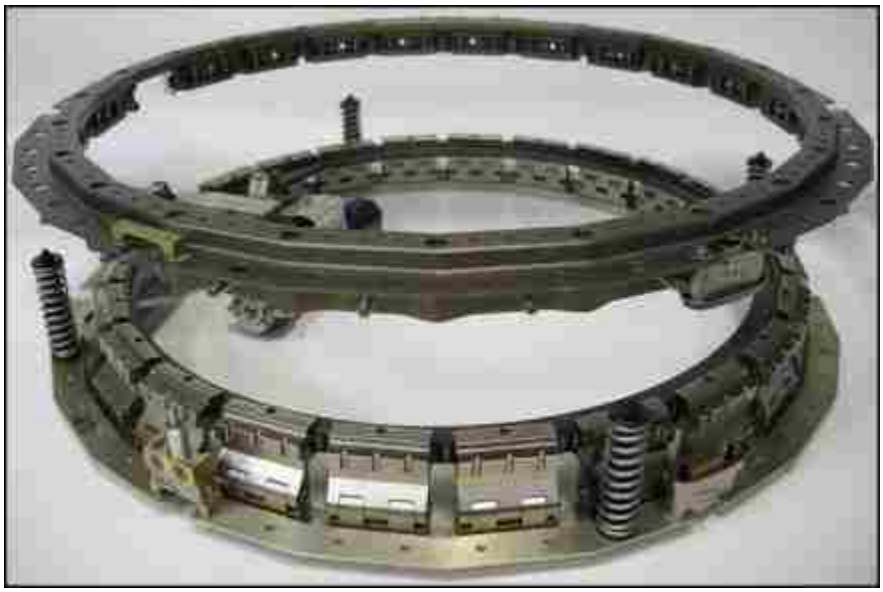

Figure 4.1. Motorized Lightband Release Mechanism

Based on calculations performed by team members using equations provided by PSC, the standard, off-the-shelf Lightband will impart a relative velocity of approximately 1.1 m/s. In an effort to minimize this ejection velocity, the team contacted PSC and was informed that the Lightband must have at least four separation springs, otherwise a successful separation could not be guaranteed. Using this information, the team consulted with PSC to customize the four separation springs to lower the ejection velocity. After resizing the springs, the ejection velocity that the Lightband could deliver was lowered to around 0.9 m/s. Based on the values in Table 2.8, the MR SAT propulsion system lacks the necessary ΔV to establish the formation and complete the formation flight phase of the mission. This presented a significant challenge for the team

that required either dropping the Lightband as a viable option in favor of pursuing alternative methods of separation, or engineering a creative solution. After consulting again with PSC, it was proposed that a nichrome wire retaining mechanism could be used that would arrest the ejection velocity immediately after deployment, and then the nichrome wire would be electrically burnt through to separate the satellites. This would result in a near-zero separation velocity, enabling the propulsion system to more readily establish the formation and complete the mission requirement of one orbit of formation flight and possibly meet the goal of three complete orbits of formation flight.

Two drawbacks of the PSC Lightband system are the significant lead time and cost associated with the system. According to PSC, the typical lead time is around eight months at a cost of roughly $70,000-$80,000. However, the system is easy to integrate and can be reset in-house without having to return the unit to the manufacturer, thus avoiding potentially significant delays and costs. The nichrome wire addition to the stock Motorized Lightband (MLB) will require significant analysis and verification to meet AFRL safety requirements that may result in a design/build time that extends beyond the NS6 competition.

4.1.3. NEA. The NEA component utilizes a bolt-holder mechanism to secure two halves of a system. The bolt is attached to one half of the system while the bolt-holder is attached to the other half. A coil of wire is wound around the bolt threads securing the bolt in place during launch. Once on orbit, the satellite sends an electronic signal to the NEA component that results in a four amp pulse at four volts DC that lasts for less than 35 milliseconds [39]. This electrical pulse burns through the wire securing the bolt, releasing the bolt from the bolt-catcher and allows the satellites to separate. Because of the relative simplicity of the system, the ejection velocity is easily controlled by either pre-tensioning the system or by adding springs to increase separation velocity. Figure 4.2 shows a standard NEA release mechanism for small spacecraft [39].

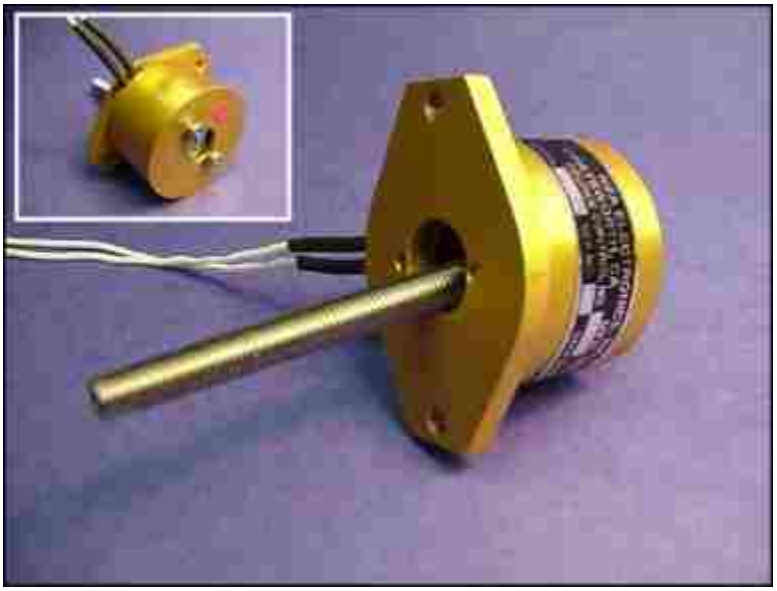

Figure 4.2. NEA Release Mechanism

The NEA release mechanism allows for wide variety of ejection velocities including a near-zero release velocity which would provide sufficient ΔV reserves to satisfy the M-SAT requirement to complete one orbit of formation flight. Additionally, the cost of the NEA component (approximately $6,000-$8,000) is an order of magnitude lower than the Lightband system, presenting a significant advantage to university satellites programs that generally operate on a modest budget. However, the NEA component does present a few unique challenges to the M-SAT team. First, the NEA component must be returned to the manufacturer for reset after each test which results in a delay of a few weeks and at a cost of a few thousand dollars, which means that multiple NEA components must be ordered so that one component is always available. Second, the NEA component requires a more complicated assembly as the satellites will have to be assembled around the NEA release mechanism. Any testing of the NEA component will then result in the need to disassemble the satellites and re-integrate later. This poses a potential problem when presenting the satellite to AFRL which requires testing the satellite on a shaker table to simulate the rigorous conditions that will be encountered

during launch. After the shaker-test, the release mechanism will have to be tested to show that it survived. Even if the test is successful, the satellite will have to be disassembled and the NEA part sent back to the manufacturer. This will potentially invalidate the shaker test as the satellite configuration that was just tested no longer exists. Once the NEA component returns and the satellites are re-integrated, the system will have to re-undergo testing to revalidate the assembly which may require a retest of the release mechanism. It is easy to see that this may result in a catch-22 type of testing and retesting unless there is a suitable process of validating the NEA release mechanism without having to actuate it.

Recently, a shaker test was performed at the Caterpillar testing facility in Peoria, Illinois, which used a simulated NEA component to hold the two satellites together and a cup-cone arrangement on the top panel of MR SAT and bottom panel of MRS SAT to help prevent the rotation of MRS SAT on top of MR SAT. During testing it was found that the single NEA component was insufficient to adequately secure MRS SAT to MR SAT as it provides only a single connection point. To compensate for this, the team is considering adding one or two more NEA mechanisms to provide the satellite either two or three total connection points between the satellite pair to distribute the load. This provides an increased cost associated with the system as $18,000-$24,000 of NEA parts are now needed; in addition a test release would require the reset of several NEA components, not just one, doubling or tripling the reset cost. Furthermore more, one NEA component was proving difficult to integrate. Integrating two or three NEAs concurrently might be beyond the capabilities of the M-SAT team. Finally, one last concern is the release of MRS SAT on orbit. With only one NEA, the release is easy to control. With two or three NEA components, a misfire could add an undesirable tipoff velocity, requiring that a method to fire all NEA components simultaneously needs to be developed (or a release sequence found that minimizes these negative effects).

4.1.4. Previous Calculations. During the Nanosat 4 competition, calculations were made that predicted the total ΔV of the system at various pressures assuming satellite dry mass of 25 kg. The different pressures are simply in multiples of 100 psia for simplicity and ease of component selecting. However, the pressure dictates the mass of R-134a that can be stored in the system. At a maximum temperature of 70 °C with the

100 psia limit, a maximum of 67.36 grams of R-134a can be stored in the propulsion tank. The 200 and 300 psia correspond to 152.06 and 275.03 grams of propellant respectfully [40]. However, during the Nanosat 4 competition, all calculations were based on a more conservative temperature estimate of 100 °C which results in propellant masses of 60.52, 130.80, and 215.87 grams respectfully which will be considered in this analysis for direct comparison [28]. Table 4.1 shows the amount of ΔV each pressure setting can produce and the total firing time (exhaust duration) assuming a constant mass flow rate [28].

Table 4.1. Nanosat 4 Ideal ΔV and Exhaust Duration

Max Tank Pressure at 100 °C [kPa (psia)]	**ΔV (m/s)**	**Total Thrust Exhaust Duration (mins)**
689.48 (100)	0.943	7.10
1378.96 (200)	2.041	15.34
2068.44 (300)	3.374	25.31

Then, applying the correction factors discussed in Section 3, more conservative values can be obtained which are shown in Table 4.2 [28].

Table 4.2. Nanosat 4 Conservative ΔV and Exhaust Duration

Max Tank Pressure at 100 °C [kPa (psia)]	**ΔV (m/s)**	**Total Thrust Exhaust Duration (mins)**
689.48 (100)	0.935	11.34
1378.96 (200)	2.024	24.52
2068.44 (300)	3.345	40.46

Using the conservative values, it appears that the satellite is theoretically capable of achieving a minimum of 0.935 m/s of ΔV; however, based on the laboratory parametric study, it is likely that the actual system performance will be far lower. From the values in Table 3.1, use of the Lee Company valve incurs a corresponding correction factor of $\zeta_p = 0.401$ relative to ideal, making the adjusted ΔV available 0.378 m/s. Based on the testing discussed in Section 3, a value of 0.477 m/s was found using a satellite dry mass of 26 kg which is one kilogram larger than the predicted Nanosat 4 design. This then requires that any separation mechanism used in this mission must have an ejection velocity less than 0.4 m/s to ensure that sufficient propellant remains after establishing the formation to complete one orbit or formation flight.

4.2. TESTING SETUP AND PROCEDURE

The testing setup for this experiment was very similar to that in the parametric study as shown in Figure 4.3.

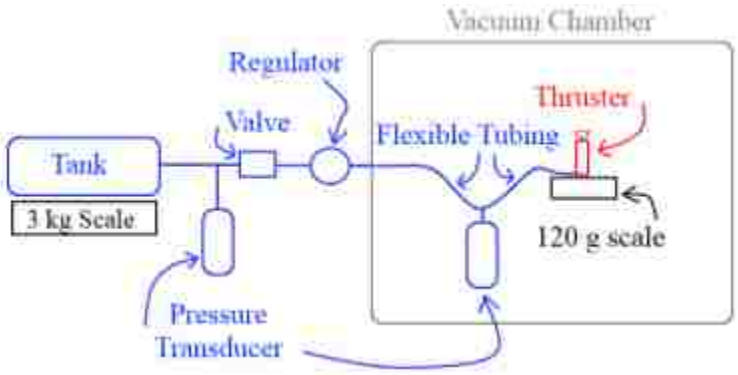

Figure 4.3. Endurance Test Schematic

The same vacuum bell jar chamber was used to simulate space-like conditions and the same electronics package was used to acquire data during testing. One of the primary differences in this setup was the use of the actual propulsion tank rather than a small can of R-134a. This allows for the data to be directly related back to the performance of the M-SAT mission while still providing qualitative data for refrigerant based systems in general. The propulsion tank was connected via flexible tubing to the first pressure transducer so that the tank pressure could be monitored while the propellant was heated. A 90 degree ball valve immediately followed the transducer was to isolate the tank from the rest of the system to ensure that nearly all the R-134a was confined to the tank and didn't disperse to the rest of the system. The Swagelok regulator from the M-SAT mission was located after the ball valve, which regulates the flow to 24.7 psia. While any regulated pressure could have been chosen, it was decided that the M-SAT regulator would be used so that the data was again more directly applicable to the MR SAT propulsion system and still qualitatively valuable to refrigerant-based systems in general. The propellant exited the distributor and was then piped into the vacuum chamber at which point it was fed into the second pressure transducer as in the previous experiment. Finally, after the second transducer, the propellant made its way into the thruster and was then evacuated into the vacuum chamber. Due to performance degradation during prolonged testing, in the interest of consistent data, the thruster without the Lee Company

valve was used. Future tests should be performed with the actual flight valves once the situation with the Lee Company valves has been resolved.

To begin, the vacuum chamber was turned on and allowed to reach an equilibrium pressure of approximately 30 mTorr. Next, the propellant tank was placed on a scale as shown in Figure 4.4 and the 90 degree ball valve opened so that the propulsion tank was evacuated of air to ensure that only R-134a would occupy the tank during the experiment. Once the scale reading stabilized implying that the tank has been completely evacuated, the 90 ball valve was closed and the tank filled with the desired propellant mass. The tank was then left idle until the temperature of the tank equalized to the ambient room temperature. Finally, the data acquisition system was activated and the ball valve opened. Once the scale showed that the tank mass had returned to the initial dry weight, the data acquisition system was deactivated and the data saved.

Figure 4.4. Measuring Propellant Mass in Propulsion Tank Using Scale

For the second part of the experiment, the propellant tank heaters were activated to determine the effect that active heating has on system performance. Since I_{sp} is directly proportional to temperature, any increase in temperature should also increase the efficiency of the system and increase the ΔV capabilities of the satellite. For the M-SAT mission, the heaters have been allocated 3.63 W at 6.9 V. To mimic on-orbit conditions, a power supply was acquired and set to 6.9 V. As before, the tank must be given sufficient time to reach thermal equilibrium after being filled with propellant.

For the endurance test, several different propellant masses were tested to determine how long the system can operate with a given initial mass both with and without heaters. For each heated and unheated case, the goal was to have the same initial mass, however this proved to be a challenge. Table 4.3 shows the actual initial mass of each test and the percent difference between the heated and unheated cases.

Table 4.3. Initial Masses of Endurance Test

Mass (g)					
	No Heater		Heater (6.93 V)		% Error in
Target	Initial	Final	Initial	Final	Initial Mass
60	59.20	-	60.10	0.50	1.50
120	120.35	5.10	117.05	1.65	2.82
180	180.10	7.50	177.85	1.55	1.27
250	249.60	-	251.10	2.25	0.60
350	350.20	8.40	350.55	-0.05	0.10
460	460.40	13.70	458.50	6.80	0.41

Note that the percent error between any one mass did not exceed 2.82% which was been deemed an acceptable margin of error for this test. This was a result of the heater and thermocouple wires. Because these wires were not secured, they hung off the tank influencing the mass read by the scale. When re-orienting the tank during filling and

for the vertical test cases, the amount of wire hanging off the scale changed causing a small change in mass. Also, for some of the final cases, a significant amount of frozen condensation was present which resulted in higher final masses in some cases.

4.3. RESULTS

The results presented in this section are broken up into three parts: superheated vapor, saturated liquid with small amounts of liquid propellant, and saturated liquid with moderate amounts of liquid propellant. Unfortunately, insufficient propellant existed at the time of testing to do higher masses, however, it is predicted that the trends observed in the saturated liquid sections should be mirrored closely in the cases with over one or two kilograms of R-134a. Future testing will focus on higher massed systems due to their obvious desire for providing the maximum mission capabilities.

4.3.1. Superheated Vapor. Tests on the 60 gram case were conducted first and showed a total exhaust duration of only 392 seconds (6.53 minutes) for the unheated case compared to 444 seconds (7.40 minutes) for the heated case, indicating that the heaters-only configuration increase the firing duration by only 13.27 %, as seen in Figure 4.5.

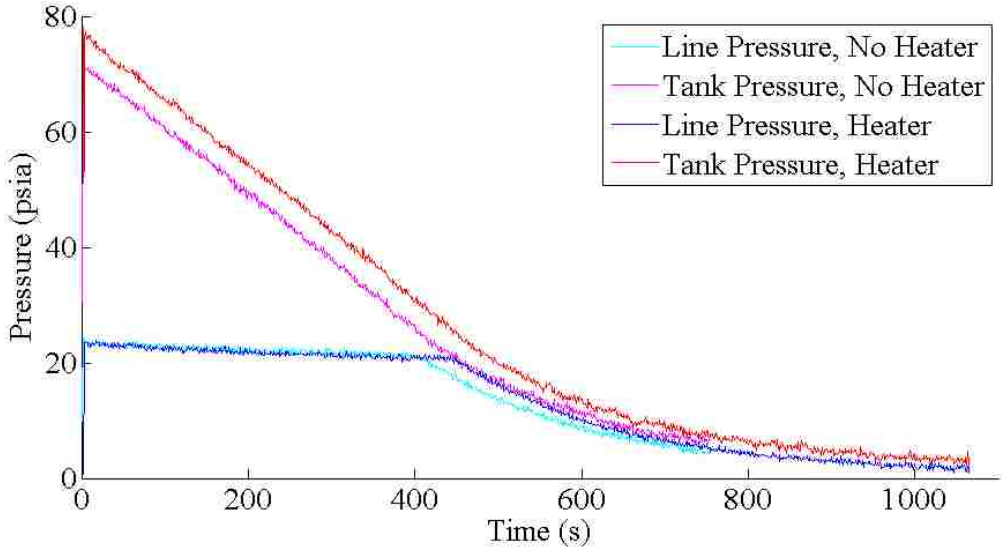

Figure 4.5. Pressure vs. Time for 60 Grams of R-134a

In this case and each of the subsequent pressure plots, the dark red line corresponds to the tank pressure with the heaters on while the purple line represents the tank pressure with the heaters off. Additionally, the dark blue line represents the line pressure with the heaters on while the light blue line shows the line pressure without heaters. The temperature plots of the heated and unheated case are shown in Figure 4.6.

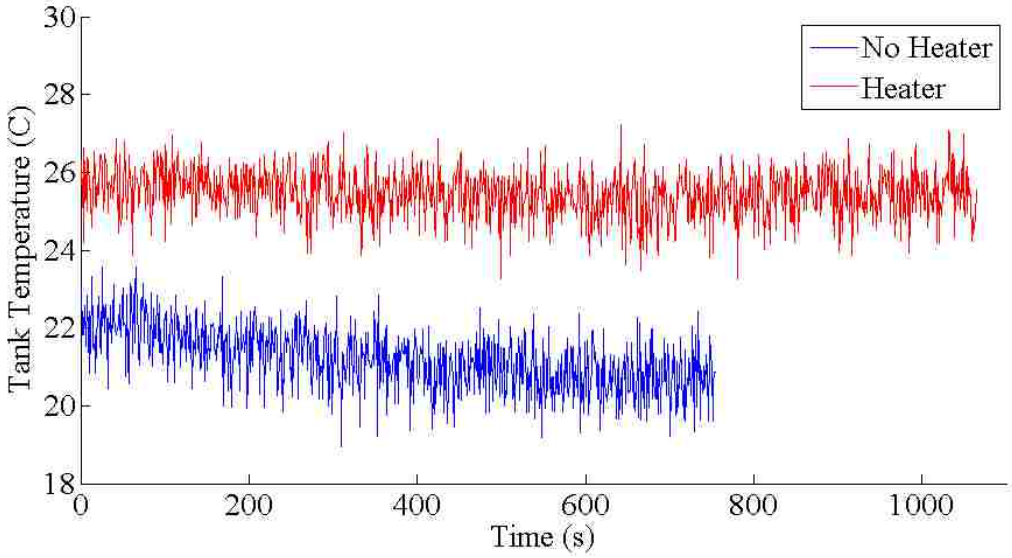

Figure 4.6. Temperature vs. Time for 60 Grams of R-134a

From Figure 4.6 it is clear that the heated case had a much higher initial temperature of approximately 25.75 °C compared to 22.25 °C for the unheated case. This temperature difference is responsible for the difference in initial tank pressures seen in Figure 4.5. At 20 °C, the 60 grams of R-134a is in the superheated vapor state [40], meaning no liquid is present in the system. As a result, with only gaseous propellant, no liquid propellant exists to evaporate and maintain equilibrium. Without the vaporization of R-134a, there is no significant energy draw from the tank and outside environment, which explains why the temperature in both cases did not differ much. While the heated

case did decrease by approximately half a degree Celsius, the cold case only experienced a temperature loss of approximately one degree. Because the heated case only offers approximately a half of a degree difference, it may be prudent to leave the heaters off if power availability is an issue. For the M-SAT mission, power is in high demand during the formation flight portion of the mission. As a result, it is advised that the heaters be run prior to separation and formation flight modes of operation to heat the system to a higher initial temperature when the power requirements of the satellite are lower. This would give a small boost to system performance without taxing the power system of the satellite during the mission. Additionally, this shows that if the ambient conditions of the satellite remain near 20 °C, then the propulsion system will be capable of operating throughout the entire mission without ever using the heaters. However, if power is at a surplus, then the extra performance, while small, will prolong the mission capabilities of the satellite by a few more orbits which may be critical when the entire mission may only last seven to ten orbits.

4.3.2. Saturated Liquid - Small Amounts of Liquid Propellant. For the next analysis, the majority of the discussion focuses on the cases with volumes of liquid less than ten percent of the total volume. Additionally, the 120 gram case is discussed in detail, however the 180 and 250 cases are very similar in both pressure and temperature profiles as functions of time and their graphs and the same explanation for the results seen in the 120 gram case can be applied to the 180 and 250 gram cases. The figures corresponding to the 180 and 250 gram cases can be found in Appendix D. Figure 4.7 shows the pressure trends of the 120 gram case while Figure 4.8 shows the temperature profiles.

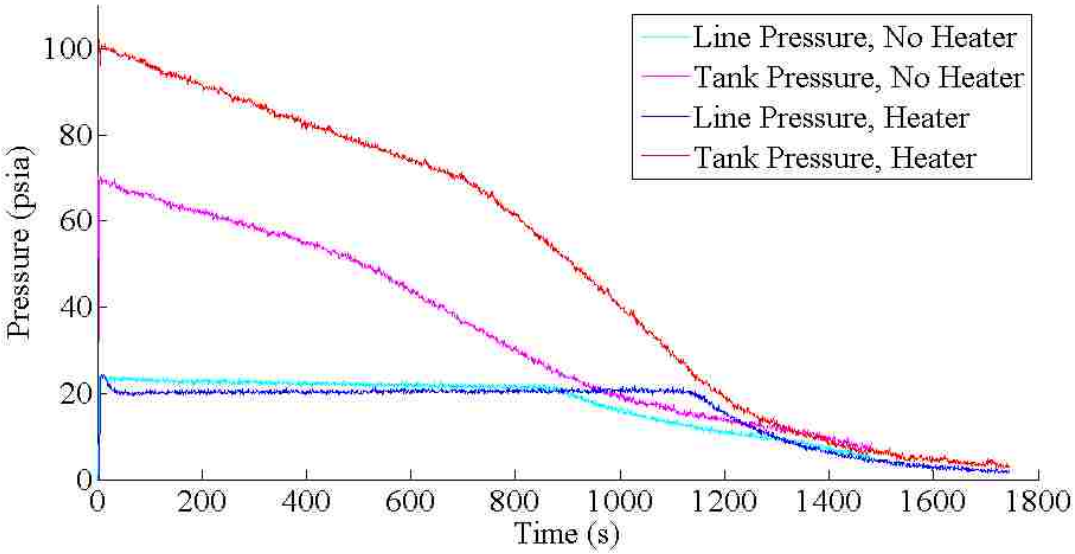

Figure 4.7. Pressure vs. Time for 120 Grams of R-134a

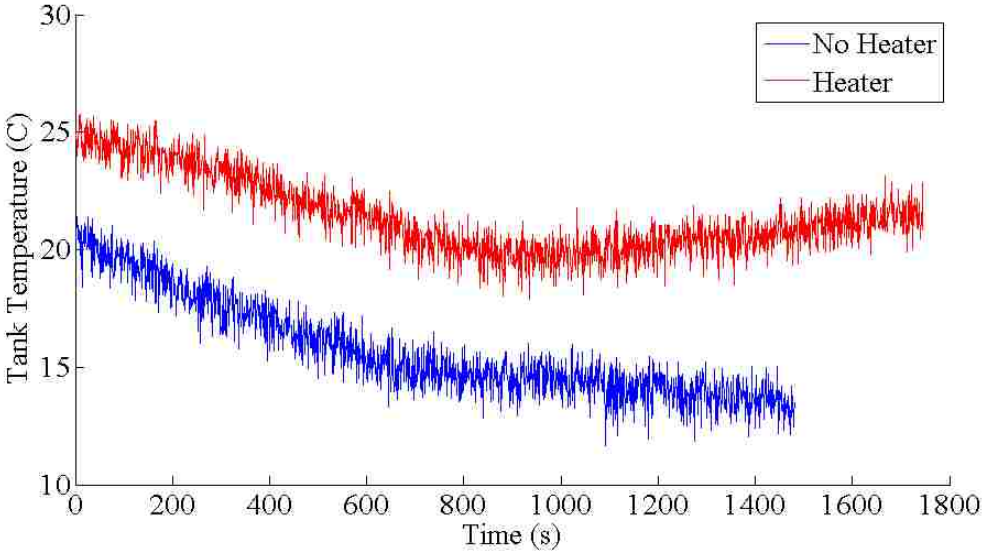

Figure 4.8. Temperature vs. Time for 120 Grams of R-134a

From Figure 4.8 it is clear that the initial temperature for the heated case was approximately 25 °C while the cool case was near 20.5 °C. For the case of 180 grams, the hot case is approximately 26 °C while the cold case is close to 17 °C. Finally the 250 gram case has hot and cold temperatures of 25 °C and 20 °C respectfully. Clearly the 180 gram case has the largest difference in initial temperatures of any mass tested. The reason for the discrepancy was due to a fluctuation in the ambient room temperature. The cold case was conducted after leaving the propellant in the tank overnight and starting the next morning. This experiment was performed in the winter which means the building heating system was active. Because of the automatic environmental controls, the lab is set to warm up by a few degrees when occupied, and to cool off when the room is vacant to conserve power. This results in a lower ambient temperature in the room and when the test was started early in the morning, the tank was at equilibrium with the ambient room temperature, which was a few degrees colder than in the other cases. Based on measurements conducted throughout the day, the lab cooled to a temperature of approximately 18 °C during the night and rose to approximately 23 °C after a few hours of room occupation. While this does present a slight source of error, due to the qualitative nature of this analysis, the variation in temperatures is not very significant. However, it is advised that a future setup be designed that places the propulsion tank inside the vacuum chamber to isolate it from variations in ambient conditions. Regardless, the trends in the data are clear and similar for 120, 180, and 250 grams with the 180 gram case being more exaggerated than the other two cases due to the large temperature difference.

In both the heated and unheated cases for 120 grams, there is a distinct negative slope in the data that becomes steeper at approximately 500 seconds for the cold case and 700 seconds for the hot case. At 20°C, the 120 gram case is a saturated liquid mixture with a quality of 56.80% which means there is 68.15 grams of gaseous R-134a and 51.85 grams liquid. But the percent liquid by volume is only 1.69% which means nearly half of the system's mass occupies only 42.2 mL of the total 2.5 L. The presence of liquid propellant results in the distinct change in the slope of the pressure trends. In an isothermal system, as gaseous propellant is extracted from the system, the liquid propellant evaporates to maintain equilibrium conditions in the tank such that the

pressure remained constant until all liquid R-134a was consumed. Since evaporation is an endothermic process, to maintain isothermal conditions, enough energy must be added to the system by the heaters to match that needed to vaporize the same amount of propellant being ejected by the propulsion system. However, based on the trends seen in Figures 4.6 and 4.7 it is clear that both the pressure and temperature are decreasing as functions of time indicating that the system is not reaching equilibrium and is not isothermal. From the data it is clear that as gaseous propellant is extracted, the liquid propellant continues to evaporate to maintain equilibrium, but the tank heater does not supply sufficient energy to the system to maintain equilibrium. As a result, the internal energy of the fluid must be used to evaporate propellant, lowering the temperature of the system. As the temperature of the system decreases, the vapor pressure decreases as well, enabling the system to continue prolonged operation. If the vapor pressure remained constant while the temperature decreased, eventually a point would be reached at which there would be insufficient energy to vaporize the R-134a effectively crippling the system. Not until enough energy is added to the fluid to vaporize sufficient propellant could the tank pressure be increased above the regulated pressure, restoring nominal operations. But because of the reduced vapor pressure, the fluid can boil at a much lower temperature. Therefore, even though the fluid is cooling leaving less energy to vaporize propellant, it is also becoming easier to evaporate the R-134a. This results in gaseous R-134a being continuously produced up to the point where the temperature drops low enough to decrease the vapor pressure to the regulated pressure or until all the propellant has been consumed. This trend explains why both the heated and unheated cases have the same initial slope. Because the temperature is relatively close, the mass flow rate remains relatively constant between the two cases, meaning that both systems are losing mass at approximately the same rate. However, it is clear via Eqns. 2.3, 2.4, and 2.6 that as temperature increases, the ambient speed of sound increases resulting in an increased characteristic velocity and thus a lower mass flow rate, but in this case the difference is minimal. The 25 °C case has a mass flow rate of 0.136 grams/s where the 21 °C case has a mass flow rate of 0.137 grams/s for a difference of only 0.68 %. But because the heated case had a higher initial temperature, it essentially shifts the entire curve up prolonging exhaust duration by maintaining higher pressures. As mentioned above, as

mass is extracted the temperature decreases driving the pressure down. For the heated case, the initial pressure is much higher due to the higher initial temperature. Since the heated case has this initial offset, it takes longer for the vapor pressure to drop to the regulated pressure, resulting in increased exhaust duration. However, this does not fully explain the change of slope seen clearly in the heated case and slightly in the cold case. While the quality could not be directly determined based on the data collected, it is believed that the points of inflection represent the points where the fluid transitions from saturated liquid to superheated vapor. Clearly there is still mass left in the system after the pressure drops below the regulated pressure, however, the rate at which the propellant is extracted is proportional to the pressure gradient. As the gradient decreases, the thrust and mass flow rate suffer from an exponential decrease in extraction rate until all propellant has been exhausted.

As seen in the 60 gram case, a constant pressure slope was observed because there was no transition point. In the 120, 180, and 250 gram cases, there is a clear and distinct change. To this point, the reason for the change in slope at the transition point has been discussed, but the magnitude of the slopes has not been explicitly explained. For the first slope, there is liquid in the system which is continuously vaporizing in an attempt to restore equilibrium to the system. As the pressure drops due to the removal of gaseous propellant, the pressure is slightly increased by the evaporation of some of the liquid R-134a, negating some of the pressure loss. Because the system is not isothermal as discussed previously, the system cannot keep pace with the endothermic process and ultimately lacks sufficient energy to maintain equilibrium. After the transition point, the magnitude of the slope increases and matches that of the 60 gram case because the fluid is now a superheated vapor. The pressure is still decreasing because of the removal of gaseous propellant, but without liquid propellant to boil off to negate some of this pressure loss, the pressure drops more rapidly than when liquid was present in the system. One interesting quality to point out is the temperature trend after the inflection point. Remembering that the thermocouple is affixed to the exterior of the tank, the temperature reading is of the tank and not directly of the fluid, meaning there will be a small lag before the fluid can cool the tank off to the actual fluid temperature. This is seen in when comparing the transition point of Figure 4.7 to that of Figure 4.8. For example, the

heated case in Figure 4.7 shows the transition point at 11.67 minutes while Figure 4.8 is closer to 15.42 minutes. But what is interesting is that the temperature for the hot case begins to make a rebound once the system crosses over to the superheated vapor region. As mentioned previously, the evaporation of R-134a draws significant amounts of energy from the system, rapidly cooling the fluid and therefore the tank. Once the system is void of liquid propellant, no evaporation occurs, allowing the heater to heat the system more quickly – which appears to contradict Figure 4.5. In Figure 4.5, the 60 grams of propellant were already in the superheated vapor state, but never experienced an increase in temperature relative to the initial condition. This is again explained by environmental factors. Because the system is not in the vacuum chamber, convective currents cool the tank while the heater attempts to actively heat the system. From the 3.63 W provided by the heater, it seemed apparent during testing that the heater could only heat the tank approximately three degrees Celsius above the ambient room temperature. This explains why the 60 gram heated cases temperature did not increase above initial temperature. For the higher mass cases, the system was cooled by the evaporation process which means that the tank temperature dropped below the ambient room temperature, at which point the heater could make a noticeable difference.

For those planning on using R-134a in the saturated liquid state during their mission, heaters provide significant boosts to performance and should be used power as permits. If sufficient power exists to heat the system during the primary portion of the mission, heaters should be used to provide an initial "charge" to the system just prior to the onset of propulsive maneuvers. Additionally, thermal models become increasingly important with saturated systems as they will cool far more rapidly than simple cold gas systems or refrigerant-based systems that are only in the superheated region. If thermal models predict favorable ambient conditions, then the heater may again be turned off during the power intensive portion of the mission; however, if the thermal model predicts colder temperatures, heaters and thermal coatings must be used to provide sufficient energy to keep the saturated pressure above the regulated pressure.

4.3.3. Saturated Liquid - Moderate Amounts of Liquid Propellant. The last portion of the endurance test focused on propellant masses that have between nine and thirteen percent liquid by volume as these will pose possible challenges due to slosh

effects and liquid propellant ingestion. Due to limited resources and time, only the 350 and 460 gram cases are covered in this thesis, however future endurance testing will be conducted with masses as high as 2.67 kg. The 350 and 460 gram cases have percent volumes of liquid of approximately 9.18% and 12.92% respectfully.

As in the previous case, only one of the two masses are analyzed in detail, but the analysis is still applicable to both. For this section, the 460 gram case is covered. Figure 4.9 shows the pressure trends for 460 grams in the MR-SAT propulsion system and Figure 4.10 shows the associated temperature trends.

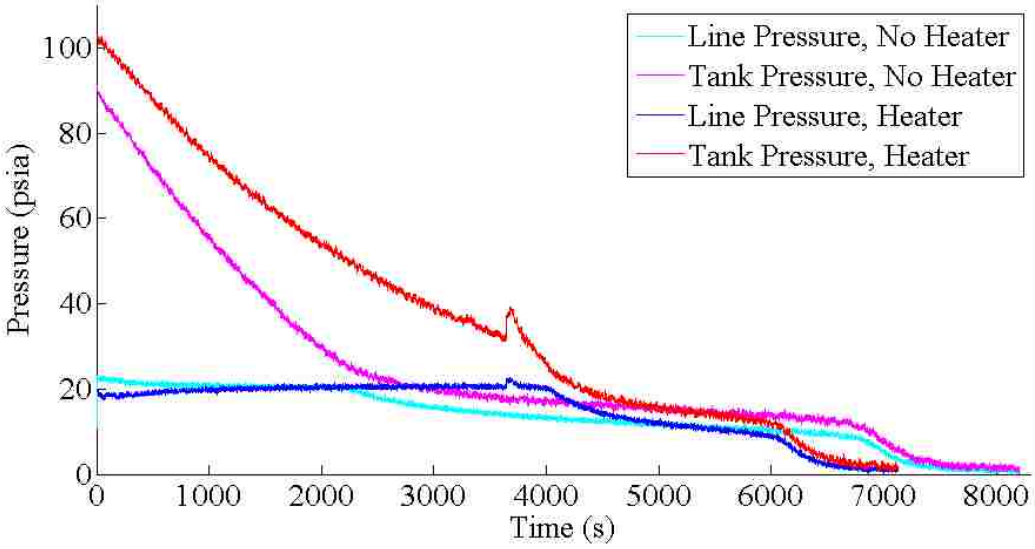

Figure 4.9. Pressure vs. Time for 460 Grams of R-134a

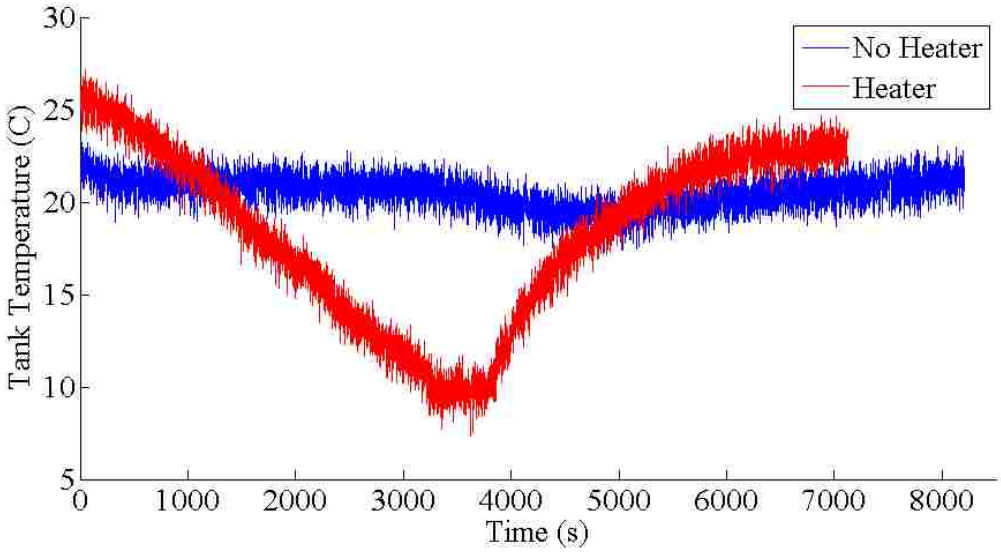

Figure 4.10. Temperature vs. Time for 460 Grams of R-134a

A key difference in the cases with a moderate amount of liquid present in the system is the fact that the system reaches the regulated pressure with a significant amount of propellant still in the tank. This results in a tank and line pressure that hovers near the regulated pressure. In Figure 4.9 it is clear that once the tank pressure reaches the regulated pressure, the line pressure drops by the same Δp that is present in all the figures. As mentioned previously, this Δp corresponds to the line losses and boundary layer losses due to fully developed flow. Because of the regulator used in this test, even though the system has reached the regulated pressure at approximately 4,600 seconds for the heated case, the system was still capable of functioning with lower thrust production. However, this may not be the case in all systems. If the system's regulator cannot operate below the regulated pressure, the system will lockup until enough energy is added to raise the tank pressure above the regulated pressure. In the case of this system, gaseous propellant is still being extracted resulting in decreasing temperature and pressure, however it is a relatively slow change in pressure compared to previous tests. The smaller masses saw a sharp decrease in pressure until the regulated pressure was reached. These moderate fluid massed systems seem to reach the regulated pressure prior

to experiencing the exponential decrease. Again, as temperature decreases, the pressure of the system will decrease as well. It is likely that the reason the pressure drop was not as sharp as previous cases was because of this increase in temperature. The propellant is still in the superheated state, which means that as propellant is extracted, the pressure of the system will decrease, but since there is no phase change, the heater inputs more energy than is removed which results in a net increase in tank temperature. This increase in temperature tends to increase the pressure of the system and will negate a portion of the pressure loss due to loss of mass. Based on Figure 4.9, it appears that the heaters are nearly capable of sustaining indefinite operation of the system at the regulated pressure.

The exception in this case is the spike that is present in both the 350 and 460 gram cases that is not present for the other masses. Comparing Figures 4.8 and 4.9, it seems that the spike corresponds to the lowest point on the temperature plot. Based on trends observed in the previous tests, the change in temperature slope corresponds to the transition from saturated liquid to superheated gas. Unfortunately, a change in the experiment setup may be the cause of the anomalous spike seen in Figure 4.9, however, the exact cause is difficult to determine with certainty. After collecting the first round of data, the experiment was disassembled so that the vacuum chamber could be used by another group for a different series of tests. Upon analysis of the 350 and 460 gram cases, it was determined that the tests need to be re-run, meaning that the experiment had to be reassembled. This may have introduced inconsistencies such as different leak rates. By examining the data, it appears the point where the fluid transitioned to superheated vapor was approximately 3,600 seconds, suggesting a higher mass flow rate than was seen in previous tests that may indicate a possible leak in the system that went undetected. Additionally, the original tests of the 350 and 460 gram tests indicated that liquid may be ingested into the system which dictated that the tests be re-run with the tank in a vertical fashion as shown in Figure 4.11.

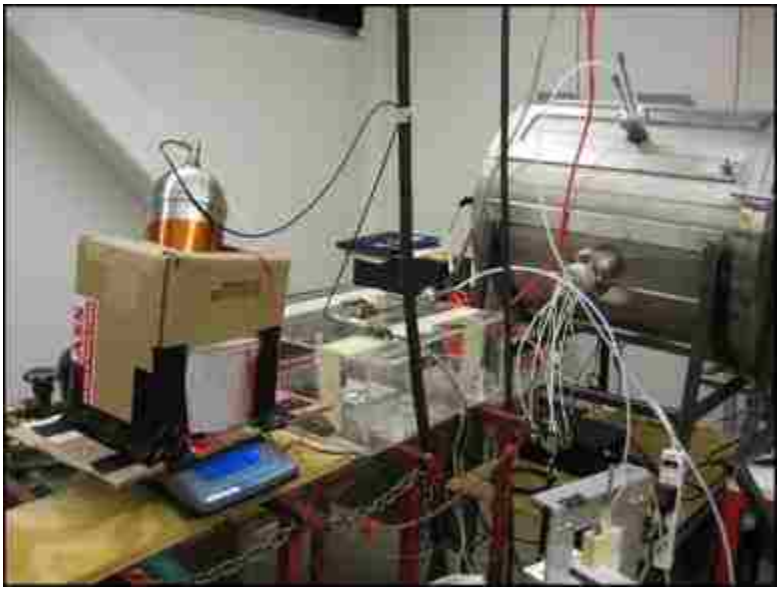

Figure 4.11. Vertical Tank Configuration for Endurance Test

Because the thermocouple measuring the tank temperature is on the downstream side of the tank, when oriented in the vertical configuration the thermocouple is on the opposite side of the tank relative to the liquid propellant. While the coldest temperatures were still recorded for the 460 gram case, it does not accurately reflect the true minimum temperature to which the system fell. For example, after the completion of both 460 gram tests, frozen condensation was found on the lower section of the tank was not present for the horizontal orientations. In microgravity the PMD should be capable of preventing liquid ingestion; however, it appears that with gravity present, testing the tank with significant amounts of liquid present results in various challenges that need to be addressed prior to the next round of tests.

Another interesting trend noticed was that the temperature of the unheated case only decreased by a few degrees Celsius but then leveled off, whereas the heated case changed drastically and then rebounded nearly as fast. It is possible that the vertical tank orientation may have placed the thermocouple too far from the phase change to readily measure the temperature change, however it was capable of measuring the temperature

change for both heated cases that suggests thermocouple location is not the primary issue. It was first believed that a failure of the thermocouple during the unheated case had yielded this result. To test this hypothesis, an ice cube was placed on the thermocouple. The temperature dropped immediately indicating that the thermocouple was functioning normally. Currently, the cause of this anomalous result cannot be explained; however, additional testing will be conducted to determine the cause of this anomaly. Future testing will account for tank orientation and will maintain a consistent orientation for the entire test and with additional thermocouples used.

4.3.4. Summary. The 60, 120, and 460 gram cases represent three different sets of trends and have been discussed in detail in the previous sections. The remaining masses had similar trends to the masses analyzed in this thesis. For figures depicting the firing duration and temperature variation as function of time for the remaining masses, refer to Appendix D. For convenience, the firing durations of all six masses have been tabulated for both the heated and unheated cases and are presented in Table 4.4.

Table 4.4. Maximum Exhaust Duration of MR SAT Propulsion System

	Firing Duration in Minutes (seconds)		Percent
Mass (g)	No Heater	Heater	Increase (%)
60	6.53 (392)	7.40 (444)	13.27
120	14.58 (875)	18.70 (1122)	28.23
180	17.80 (1068)	39.95 (1797)	68.26
250	32.38 (1943)	42.85 (2571)	32.32
350	30.42 (1825)	44.88 (2693)	47.56
460	37.98 (2279)	66.58 (3995)	75.30

Clearly, the heaters add significant firing time to all the systems when examining raw percentages. However, the absolute values still need to be considered. For example, the 60 gram case shows an increase of 13.27% which seems to suggest that heaters would

be a wise addition, but looking at raw numbers the heaters only add 52 seconds of additional firing time, which may or may not be significant depending on the individual system and mission requirements.

4.4. DISCUSSION

4.4.1. Comparing to Theory. Based on the research conducted in this study, it can be concluded that for lower mass systems, assuming a constant mass flow rate can give approximate exhaust durations within ten percent error; however, it appears that this trend does not always hold true. Unfortunately, due to the lack of theoretical values from Nanosat 4, it is hard to confirm this trend. Additionally, due to the fact that the 180 gram case had the increased temperature range (Table 4.5), it is likely that the actual value will increase, reducing the amount of error associated with that value.

Table 4.5. Comparison of Nanosat 4 Predicted Firing Duration to Nanosat 6 Results

	Firing Duration in Minutes (seconds)		Percent
Mass (g)	NS4 Predicted	NS6 Actual	Error (%)
60	7.10 (426)	6.53 (392)	8.73
120	15.34 (920)	14.58 (875)	5.21
180	25.31 (1518)	17.80 (1068)	42.19

4.4.2. Heated Versus Unheated. One of the main goals of this test was to determine the effect of heaters on various initial masses. Based on the data shown in Table 4.4, if the mass of propellant is likely to be in the saturated liquid state while on orbit, then heaters provide a significant amount of performance enhancement. However, for systems operating in the superheated vapor region, this gain is almost negligible at which point the benefit of the heater may be outweighed by the power budget of the satellite. What may be feasible in all situations, saturated or superheated, would be to

"charge" the system prior to start of the propulsive intensive portion of the mission, which would give a significant boost to the system while power requirements are at a minimum. For those systems that have low steady state temperatures within the satellite (< 0 °C), then heaters may be a must; however testing in this study did not include temperature ranges that low. However, assuming a propellant mass of 60.52 grams in the MR SAT propulsion tank at zero degrees Celsius, the internal tank pressure is only 42.64 psia which means that it will only take a couple of minutes to reach the regulated pressure, minimizing the ΔV that can be produced before the tank temperature drops to the regulated pressure. Thermal coatings and multilayer insulation (MLI) should also be considered to maximize the initial "charge" imparted to the propulsion system. However, if a given mission was provided with an abundance of power, then increasing the power of the heaters will not only help negate pressure decreases in the tank but may be used to provide isothermal-like conditions or even supply more energy that is used during propellant vaporization. A word of caution should be mentioned at this point that most small satellites and university-class satellites will not typically provide abundant power due to the small size of the satellite and thus minimal area to place solar panels. As a results, any design for a refrigerant-based cold gas system should revolve around only using the heaters prior to the start of the actual mission and sparingly, if ever again (power permitting).

For the Nanosat 4 mission, the intended modes of operation had the propulsion system heaters on for the entire mission while only having a maximum of 60.52 grams of propellant in the tank. The propulsion system subsequently consumed almost three quarters of the entire power being produced by MR SAT's solar arrays. The obviously presented a significant challenge to the team. However, based on the results of this test and a propellant mass of 60.52 grams, the revised Nanosat 6 modes of operation should include a "heater on" mode during the detumble phase of the mission prior to the release of MRS SAT. While the magnetic torque coils are being used to align MR SAT with Earth's magnetic field, the propulsion system can be heated to its maximum steady state value. Once the satellite formation has achieved the desired attitude, the propulsion tank heater can be turned off and the satellites separated. This would drastically increase the

amount of available power for other subsystems, such as Earth-to-sat and sat-to-sat communications.

Based on the results presented here, if the M-SAT mission chooses a release mechanism that produces a separation velocity of 0.4 m/s or less, then the 100 psia limit of 60.52 grams would be capable of establishing the formation and maintaining it for the required one orbit. However, if the propulsion system gets a waiver to use pressures exceeding 100 psia, then ΔVs up to approximately 20 m/s can be achieved, well in excess of that demanded by the release mechanisms currently under investigation.

4.4.3. Thermal Model. Shortly after beginning testing, it was recognized that a thermal model of the propellant tank would facilitate a better understanding of some of the trends observed in the system. Currently, the thermal model is still a work in progress due to the complexity of modeling the energy transfer from the tank to the propellant. This complexity arises as a result of the changing temperature of the fluid and tank (and the resulting temperature gradient), the amount of mass in the system, the quality of fluid and input from the heaters. Modeling the fluid independent of the tank resulted in temperature and pressure values far colder than what was observed in the experiment and the fluid never reached the superheated state, which was also another indication that a problem existed. Additionally, the temperature of the tank changes as a result of the fluid extracting energy from it. Furthermore, the conductive nature of the tank becomes more difficult to model because the amount of liquid in contact with the tank changes with time, meaning that the fluid will absorb energy from the tank at a changing rate. Finally, modeling the energy transfer from the heater to the tank is contingent on the available power and radiation losses to the environment must also be considered. Currently, the model loosely predicts the results of the test. The rate at which the quality approaches one and the fluid goes superheated appears to be consistent with experimental data within acceptable error margins. The temperature and pressure trends have the same basic shape as the testing results; however the values differ by a significant amount, meaning that the tank modeling aspect of the program still needs to be adjusted. However, this thermal analysis is beyond the scope of this thesis and will be further analyzed and documented in a future publication.

4.4.4. Maximizing MR SAT Propulsion Capabilities. In order to extend the mission capabilities of the M-SAT mission, it was decided that the propulsion system would be filled to the maximum allowable value if a pressure waiver was granted by AFRL. David Gibbon of SSTL was consulted due to his extensive experience with the small satellite saturated liquid cold gas systems. Additionally, Mr. Gibbon worked on the DMC mission that made use of the same Marotta tank used in the MR SAT propulsion system. Mr. Gibbon recommended that the tank be filled to 87% volume by liquid which would allow for maximum propellant while still avoiding slosh effects and accounting for increased pressure if the temperature were to increase to 40 °C. Assuming an 87% fill ratio at 20 °C in a 2.5 L tank with a dry mass of 26 kg yields a maximum propellant mass of 2.671 kg of R-134a. Because the thrust is a function of regulator pressure and I_{sp} is a function of fluid temperature, both of these values will remain unchanged as a result of increasing the propellant mass. The primary advantage of increasing the propellant mass comes in the form of ΔV. Using the new mass and assuming the use of the Lee Company valves, a maximum ΔV of 20.916 m/s was calculated.

By increasing the mass to 2.671 kg, the system is capable of 43.84 times as much ΔV compared to 60.52 grams of R-134a. The next step is to conduct an endurance test for propellant masses that range between 0.460 and 2.671 kg to determine if there are any variations in the trends relative to what was observed in these smaller masses. Since increasing the mass from 60.52 grams to 2.671 kg is a factor of 44.13, it can be roughly assumed, based on testing, that doubling the mass corresponds to a doubling in exhaust duration. Under that assumption, if the 60 gram case lasted approximately 7.10 minutes, then the maximum propellant case would correspond to roughly 313.35 minutes (5.22 hours) of continuous firing. However, before this value is finalized, it will be necessary confirm this through additional testing.

5. MR SAT NANOSAT 6 PROPULSION SYSTEM INTEGRATION

5.1. CORE HARDWARE LAYOUT

Due to the highly restricted volume associated with small and micro-class satellites, the layout of one subsystem is typically dependent on space and location needs of the other subsystems. For example, the various components of MR SAT reside in aluminum boxes that are secured to the side panels that limit where thrusters can be placed, propellant lines run, or propulsion hardware attached. This section focuses on the author's analysis of propulsion tubing length and thruster layout which will be implemented on the Nanosat 6 propulsion system.[1]

5.1.1. Nanosat 4 Design. Due to the relatively large size of the propulsion tank, the combination of possible orientations was limited. The only panels large enough to secure the tank to were the top and bottom panels, and only if the tank was placed along a diagonal as seen in Figure 5.1. Because of center of gravity concerns, the tank was attached to the panel closest to the launch vehicle, which in this case was the bottom panel.

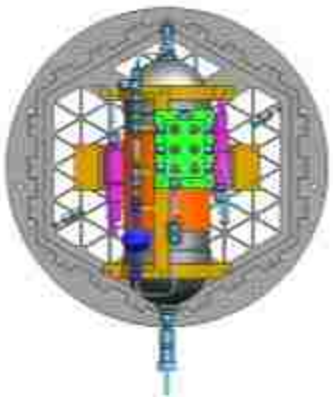

Figure 5.1. Propulsion Tank Layout

[1] Assistance was provided by Missouri S&T undergraduate student Eric Murray

In order to prevent losses due to excessive lengths of propellant tubing, it was desired that the core hardware components be located closely together and as close to the tank as possible. However, due to the masses of the regulator and pressure transducers, these components had to be secured to the satellite to prevent damage resulting from vibrational loading. Because the side panels were already being used to hold component boxes, it was decided that a "bridge" would be made for the tank that would be attached to the mounting brackets used to hold the tank to the bottom panel. The bridge was manufactured to contain attachment points for the regulator and isolation valve while the mounting brackets for the tank were designed with attachment points for the transducers. Finally, the last core component was the propellant line heater, which needed a minimum of four inches of straight tubing to which to adhere. Because of the limited space, a U-bend was made that provided a space for the line heater but added extra tube length and bends which increased system losses. This core hardware layout is shown in Figure 5.2.

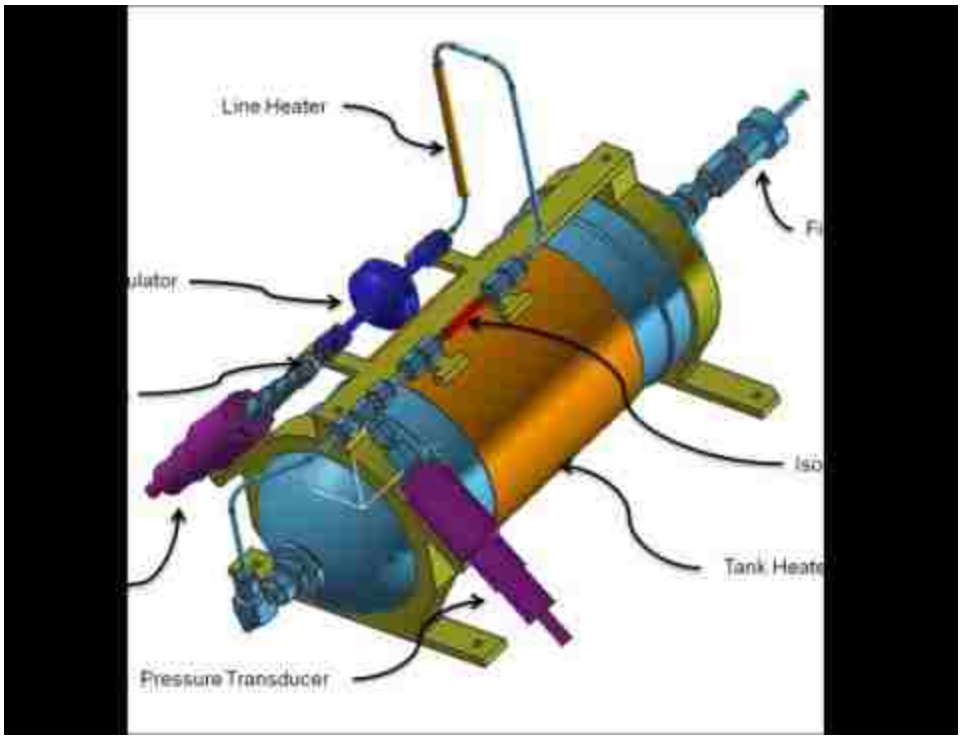

Figure 5.2. Core Hardware Layout for Nanosat 4

5.1.2. Nanosat 6 Design. In order to improve the propulsion system for the Nanosat 6 competition, some modifications were incorporated into the system to reduce unnecessary tube lengths and connections. The main cause for re-designing the core hardware layout was the addition of a "distributor" to the system. The distributor is larger than most of the components and therefore takes up a greater amount of space. Using the same component "bridge concept" from the previous Nanosat 4 design, a new bridge was designed that would allow for the integration of the distributor in addition to containing attachment points for the regulator and isolation valve while the transducers are again attached to the tank mounts (Figure 5.3).

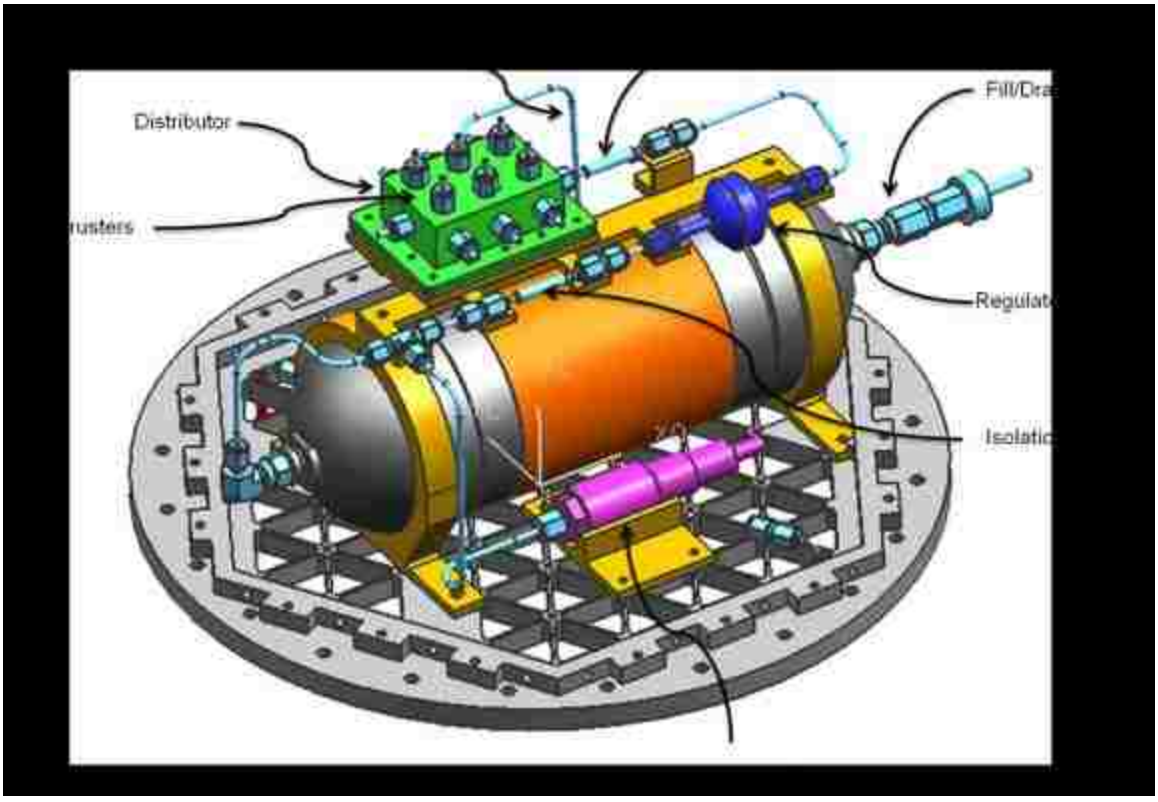

Figure 5.3. Core Hardware Layout for Nanosat 6

With the addition of the distributor, it was decided that having an internal heater within the distributor would allow for greater heat transfer to the propellant than an exterior line heater, negating the need for the large U-bend. Removing the U-bend removes over 20 cm. of tubing and two 90 degree turns, reducing losses and increasing system performance with more efficient heat transfer. Furthermore, the second transducer is located on the other side of the tank in a similar fashion the transducer seen in Figure 5.3, but rotated 180 degrees.

5.2. THRUSTER LAYOUT

5.2.1. Nanosat 4 Thruster Layout. In past designs, the propellant lines were run along the top panel of MR SAT and then branched out to the various side panels using several tee and four-way fittings as shown in Figure 5.4 in order to avoid interfering with the various component boxes. Additionally, only eight thrusters were used in this first-generation design (Figure 5.4 [28]) in order to save on cost while sacrificing one translational DOF.

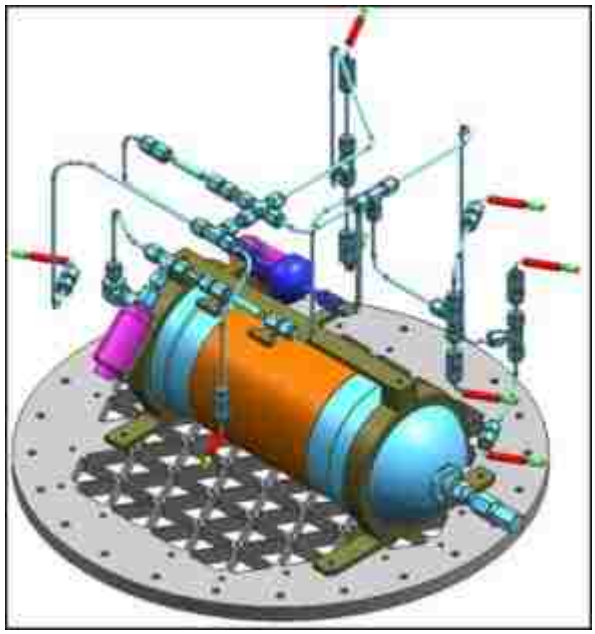

Figure 5.4. Nanosat 4 Thruster Layout

While this design did reduce cost, the loss in the degree of freedom was undesirable. The Nanosat 4 design did not provide thrusters along the Z-axis, which presented a complication when MR and MRS SAT detached and MR SAT was required to maneuver to establish the nominal formation. To arrest the drift of MRS SAT, MR SAT was required to first negate the initial ΔV associated with separation and then continue thrusting until the distance between MR and MRS SAT was within the limits of the mission parameters. Without thrusters placed along the direction of separation, MR SAT needed to perform a 90 degree turn to gain translational capability along the Z-axis. Once the turn was completed, then MR SAT could begin closing the distance with MRS SAT. Unfortunately, for this system two significant problems arise for this mission. First, the communication range between the satellites is limited to approximately 200 m. Depending on the separation velocity, it is possible that MRS SAT could reach the limit of the communications range or even beyond before MR SAT even completes the 90 degree turn. Once MRS SAT drifts out of range of MR SAT, the possibility of successfully establishing the required formation with MRS SAT are remote and the mission would likely end in failure. Second, assuming that MR SAT could complete the turn and establish formation with MRS SAT before it drifts out of range, the propulsion system would likely suffer from reduced thrust as a result of lower vapor pressure. As the system expels gaseous propellant, the tank heater adds energy into the liquid propellant to promote continued phase change of liquid R-134a into gaseous form, maintaining equilibrium. Because of the limited electrical power typically available on small satellites, the heaters are only capable of restoring a modest amount of energy to the satellite. If the energy draw is greater than what the heaters are capable of replacing, then the fluid temperature will begin to decrease, lowering the vapor pressure of the system resulting in reduced thrust, I_{sp}, and ΔV. The amount of energy required to be restored to the propellant to complete the 90 degree turn and establish formation is likely greater than what the heater can provide, which could result in thrust levels diminishing to point where it would be impossible to establish formation with MRS SAT before it drifts out of range.

Another concern to the M-SAT team arises based on UNP regulations (but would not typically be a concern in general to satellite developers not bound by UNP constraints

for this type of propulsion system). A sealed container pressure limit of 689.48 kPa (100 psia) at the maximum possible temperature is imposed for safety purposes, which, based on the volume of the tank and a maximum temperature of 70 °C (a rather high (conservative) value defined by UNP), results in a maximum allowed propellant mass of 67.36 grams (60.52 grams from the 100 °C temperature assumed in Nanosat 4). Based on preliminary models and assuming a separation velocity of 0.5 m/s, the vast majority of this propellant will be used to complete the 90 degree turn and establish formation, with insufficient propellant remaining to complete even a single orbit of formation flight. However, if the sealed container limit is waived, then sufficient propellant can be added to the system to complete both the 90 degree turn and establish formation assuming MRS SAT stays within range and the thrust levels do not diminish excessively as a result of insufficient energy input from the propellant tank heater.

Finally, the eight-thruster configuration relied on several thrusters being balanced by only one thruster opposite to them for moment generation (Figure 5.4). For example, one panel contained four thrusters located at the top and bottom centers of the panel and on the left and right sides of the panel. These four thrusters were coupled with a single thruster located at the center of the opposite panel that provided very small moment arms and no redundancy if that single thruster was to stop functioning (Figures 5.5 and 5.6).

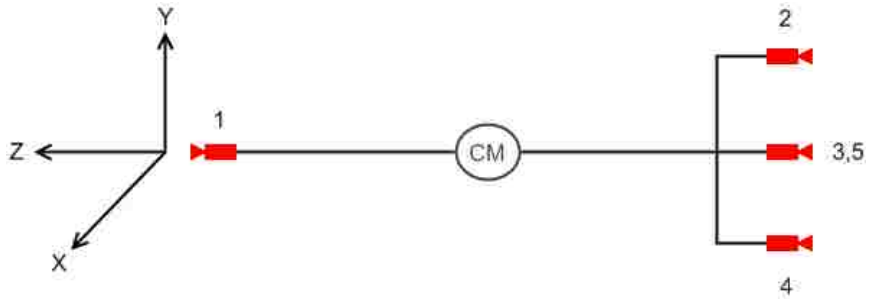

Figure 5.5. Thruster Over-Coupling Side View

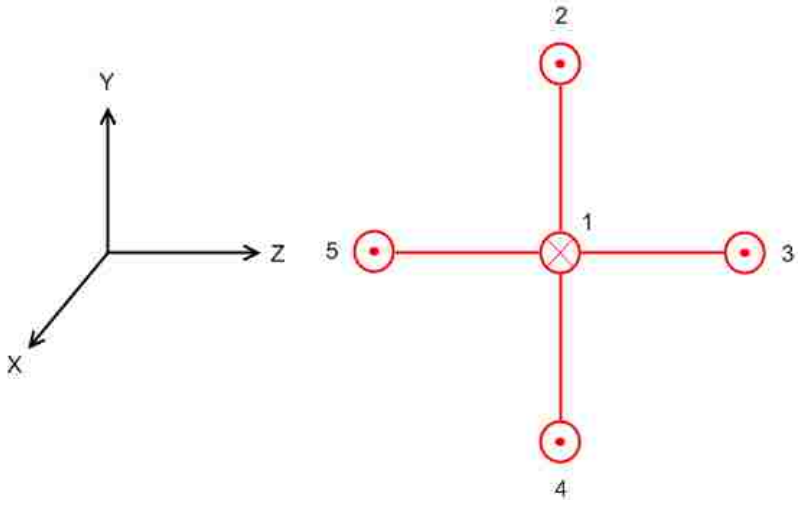

Figure 5.6. Thruster Over-Coupling Front View

By pairing Thruster 1 with another thruster, moments could be generated along the ±Y-axis and ±Z-axis and thruster one provides translational motion along the –X-axis. Using Thrusters 1 and 4 as examples, when both are fired the translation effects are canceled by the opposing forces, but since Thruster 4 is offset from the center of mass (CM), a rotation is induced along the +Z-axis. However, rather than contributing to the rotational motion, Thruster 1 only counters translation effects, meaning that propellant is being consumed without any actual benefit to the system. In addition to the problem of reduced system efficiency, another significant problem exists. Since both Thrusters 1 and 4 allow translation along the X-axis, if Thruster 4 fails Thrusters 2, 3, and 5 can provide redundancy in the +X-axis. The problem arises if Thruster 1 ceases to function. If Thruster 1 fails, then translational control along the –X-axis along with rotation about the Y and Z axis is no longer possible since Thrusters 2-5 rely on Thruster 1 to negate translational motion when rotating the satellite. This means that three out of the original five DOFs are lost with the failure of only one thruster, which is undesirable from a fault tolerance point of view. In most mission critical systems, double or even triple redundancy is standard, meaning that the original thruster configuration presents a high-risk situation that can reduce the flyability of the satellite.

5.2.2. Nanosat 6 Thruster Layout. Because of the limited capabilities of the original Nanosat 4 design, it was decided that the team would pursue a more conventional thruster layout, namely the H-pattern configuration shown in Figure 5.7.

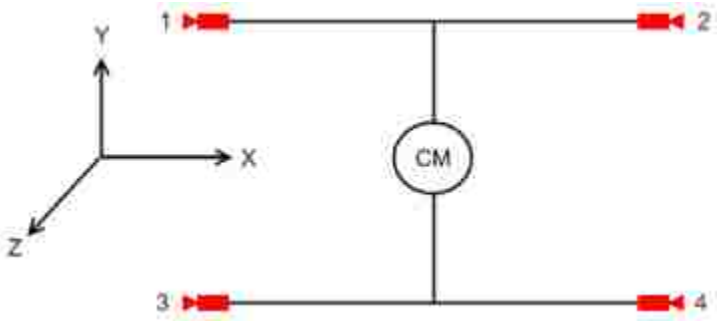

Figure 5.7. H-Pattern Configuration

While the original layout used a centered thruster to cancel translational motion, the H-pattern configuration uses diagonally positioned thrusters to achieve the same result. For example, a clockwise rotation can be initiated by firing Thrusters 1 and 4. Rather than simply negating translational motion generated by Thruster 1, Thruster 4 also contributes to the moment being induced, increasing the efficiency compared to the previous design. Additionally, if Thruster 4 were to fail, translational control can still be achieved in the –X-axis with Thruster 2 but an undesired clockwise rotation would result, which would need to be negated by firing other thrusters in similar H-pattern configurations on the satellite. This may seem wasteful at first glance, but this thruster arrangement allows the satellite to recover from a single thruster failure and still continue its mission, although slightly compromised. The final thruster layout is shown in Figure 5.8 with a total of three H-patterns being used to provide all six DOFs.

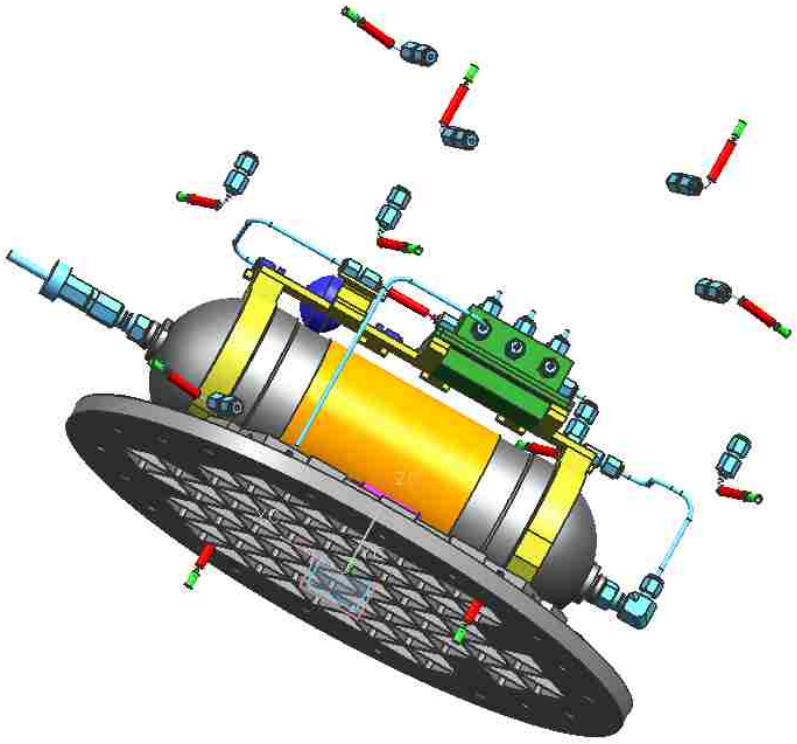

Figure 5.8. Nanosat 6 Thruster Layout

However, because of the complex nature of the thruster layout, it is necessary to further break-down Figure 5.8 into smaller views to understand the relative positioning of each thruster. Figure 5.9 shows one of the side panels for MR SAT which has four thrusters located on it. Both Panels 1 and 4 utilize this layout, accounting for two of the H-patterns and eight of the twelve thrusters.

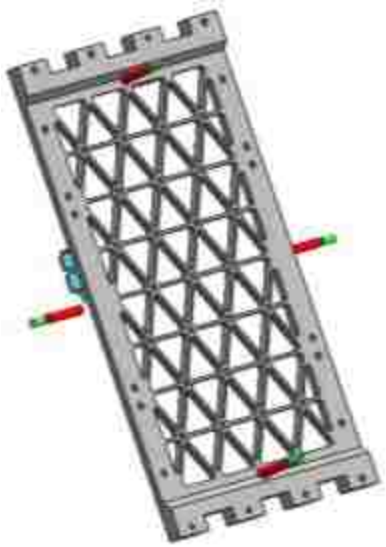

Figure 5.9. Thruster Layout on Panels 1 and 4

The remaining H-patter is split between the top and bottom panels as shown in Figures 5.10 and 5.11. This H-pattern represents the primary divergence from the Nanosat 4 mission as now MR SAT has the ability to thrust along the Z-axis rather than having to perform the 90 degree turn before having the capability to chase MRS SAT.

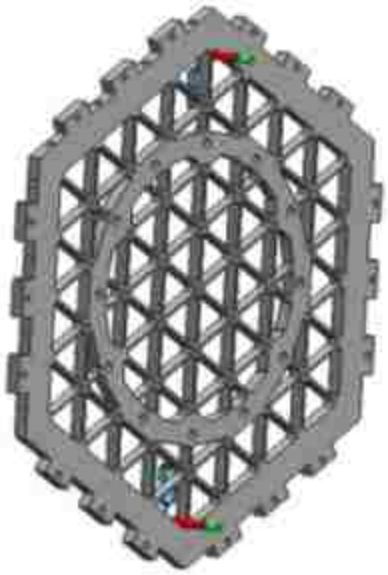

Figure 5.10. Thruster Layout on Top Panel

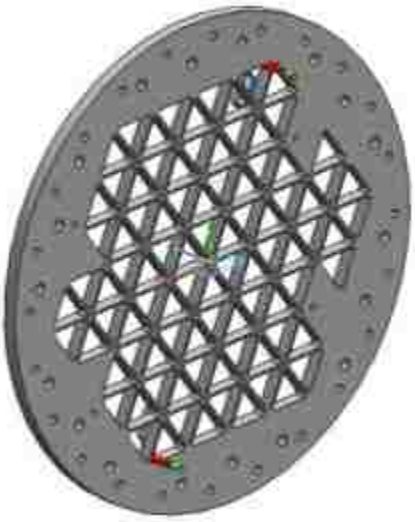

Figure 5.11. Thruster Layout on Bottom Panel

To better illustrate the thruster coupling used in the MR SAT mission, wire-frame drawings of the satellite were made and thrust vectors inserted for simplification. These wire-frame drawings are shown in Figure 5.12 and better illustrate the three H-patterns used in MR SAT propulsion system.

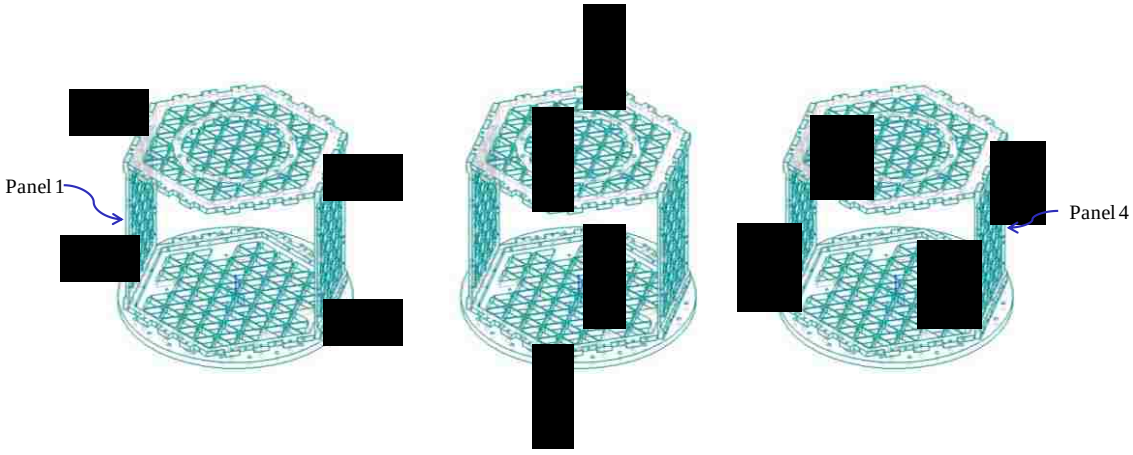

Figure 5.12. Wire-Frame Schematic of MR SAT H-Patterns

While the new design includes the addition of four thrusters, increasing the cost of the system, based on the added performance and redundancy it was deemed an acceptable expenditure.

5.3. DISTRIBUTOR DESIGN

Because of the much needed thruster layout re-design, the team took a step back to determine how the propulsion system would be integrated in the future. In the original Nanosat 4 design, the propulsion system is configured with a primary propellant line emanating from the propellant tank that divides into various branching lines with additional subsequent divisions as needed (see Figure 5.4). In order to integrate the system, tubing is run along the top panel of MR SAT and then down the various panels

that are fitted with thrusters. Using the top and side panels for support is beneficial from a structural point of view, but creates integration difficulties. The integration of the original propulsion system required multiple team members and partial assembly of the subassemblies of the propulsion system. For example, a side panel would need to be affixed with the thrusters and tubing separate from the main structure and then added as a subassembly, and then could be incorporated into the rest of the system. However, because the tubing must align exactly, the sub-assemblies connections could only be hand-tight so that the parts could still be adjusted if needed when integrated with the rest of the system. These hand-tight connections did not fully secure the tubing which meant that they were difficult to work with. On more than one occasion the subassembly came apart during the integration procedure requiring a complete disassembling of the entire system. Two concerns arise: integration time greatly increased, and extra wear on parts that need to be disassembled. In order to address these concerns in addition to the performance issues mentioned previously, it was decided that a centralized distributor could be used to address both deficiencies. Because of the limited volume inside MR SAT, all tubing must run out of the top of the distributor rather than the sides or bottom, which resulted in a longer than desired distributor increasing the mass of MR SAT. However, the reduction of required tube lengths helps to offset this increase in satellite mass. Because all thruster tubing originates at the distributor, the distributor can be integrated to the tank and then all twelve thruster propellant lines can be connected directly to the distributor. With the relatively low mass of both thruster and tubing, these components can be hand-tightened and remain in place while the rest of the satellite is integrated around it. Finally, when the side panels are integrated to the bottom panel of MR SAT, the thruster can be properly aligned and secured to the structure and the Swagelok connectors fully tightened. This drastically reduces the current integration time and complexity as well as reduces the number of disassemblies required saving on wear of components.

One of the concerns associated with the distributor was the way in which the tubing attaches to the distributor and the allowable length of a section of unsupported tubing before vibrational concerns arise. First, the team worked on methods of connecting the propellant lines to the distributor. One idea was to weld the tubes into

place, however, due to the thin walls and close proximity to each other, the likelihood that a leak would result was too high. Additionally, any mistakes in measuring tube and cutting tube lengths or producing a perfect bend with tube benders would mandate that all tubing be made prior to welding which meant that the placement would have to be exact otherwise the entire distributor and propellant lines would need to be re-manufactured. The second idea was to use the same Swagelok compression fittings that were used on the rest of the propellant line connections. To minimize connections, all fourteen stems on the distributor (twelve thrusters, one tank inlet, and one pressure transducer) will be manufactured with threads so that all tubing can be directly connected to the distributor with no special adaptors required (Figure 2.11).

Additionally, because it is desired to manufacture the distributor using as few pieces as possible, a single piece of stainless steel is machined into a hollow rectangular prism with the fourteen stems on the exterior with a separate hollow rectangular prism for the bottom. This design lends itself to significant possible leaks where the bottom plate and distributor are mated. Two methods of connections were considered: first was to use a gasket/O-ring and bolt the two pieces together, second was sending the distributor off campus to be welded by a third party. After consulting the Nanosat User's Guide [25], it was determined that welding the distributor would be in violation of NS6 guidelines and the team chose to bolt the distributor together. There are two primary concerns with this approach: material compatibility and leaks. Materials exist that are R-134a compatible, but from the extensive research conducted with respect to the Lee Company valves, it was found that some compatible materials may be difficult to mold to a desired shape. This may lead to some complications; however, copper gaskets are used in high vacuum applications and will be a backup consideration for an R-134a material. Second, due to the internal pressure of the fluid on the distributor top and bottom surfaces, it is possible that stress will stretch the distributor bolts sufficiently to create a gap in the distributor halves resulting in a leak. To that end, calculations were performed to determine how far the bolts will stretch as a result of the internal pressure. Because the regulator is on the downstream side of the regulator, it will experience a pressure of only 24.7 psia regardless of tank pressure. A factor of safety of approximately two was employed and 50 psia was used in the calculations. Based on the dimensions of the distributor shown in

Figure 5.9, the area on which the pressure is acting that would result in bolt stretching is shown in Eq. 5.1, and the force that must be carried by the distributor bolts is shown in Eq. 5.2.

$$A_D = 2l_d w_d = 2(69.85\ mm * 44.45\ mm) = 6.210 * 10^{-3}\ m^2 \quad [5.1]$$

$$F = PA_D = 3.4474 * 10^5\ Pa * 6.210 * 10^{-3}\ m^2 = 2140.82\ N \quad [5.2]$$

After the total force is found, it is then necessary to determine force that each individual bolt must carry. This is accomplished using Eq. 5.3.

$$F_n = \frac{F}{N} = \frac{2140.82\ N}{14} = 152.92\ N \quad [5.3]$$

The elongation of each bolt is then calculated by first finding the cross-sectional area of the bolt using Eq. 5.4 and then substituting all values into Eq. 5.5. For these calculations, and elastic modulus for the bolts was taken to be 193 GPa [41] and the length of the bolt was taken to be the effective length that must carry the load which is the region between the bolt head and the nut. This length was found to be the sum of the thickness of the two distributor flanges. Each flange is 1/8" thick so the resulting bolt length is thus ¼" (6.35 x 10^{-3} m).

$$A_b = \frac{\pi}{4}d^2 = \frac{\pi}{4}(3.175 * 10^{-3}\ m)^2 = 7.917 * 10^{-6}\ m^2 \quad [5.4]$$

$$e = \frac{F_n L}{A_b E} = \frac{(152.92\ N)(6.35 * 10^{-3}\ m)}{(7.917 * 10^{-6}\ m^2)(193\ GPa)} = 6.355 * 10^{-7}\ m \quad [5.5]$$

Based on these calculations, it is clear that so long as the distributor O-ring/gasket is compressed by a millimeter, no leakage will occur due to pressure expansion at the interface of the distributor halves. For more information, please refer to M-SAT document, "04-016 Minimum Distributor Gasket Compression" [42].

While the two-part distributor posses an increased leak risk, it also allows for the distributor to be dual purposed without much additional work. As mentioned previously, the amount of energy delivered to the propellant directly correlates to how efficient the system is and how long the thrusters can fire before losses in thrust performance occur. Because of this, adding the heat directly to the propellant is highly desired. While the tank heater covers a majority of the surface area of the tank, it relies on convection through the stainless steel to transfer its energy, which results in increased inefficiencies. To help overcome this challenge, it was decided that a heater could be directly placed into the distributor before it was assembled that would allow for heat transfer directly to the propellant increasing the temperature of the propellant and increasing system performance as shown in Section 3. The next challenge is then how to power the heater inside the distributor without allowing any leaks. Clearly, all electrical leads need to be conductively isolated from one another to prevent shorts, requiring any material used to be non-conductive. Emulating an idea from a high-voltage pass-thru in a vacuum chamber, each individual lead will be inserted into a small cylindrical piece of alumina and then soldered at one end to completely seal any gaps to prevent leaks. Then, a hole a few thousands of an inch larger than the alumina cylinder will be drilled into the side of the distributor and the alumina covered electrode fed through this hole and finally soldered in place around the alumina to finish the integration. This method is commonly used on vacuum chamber components and can be easily accomplished in-house or by a third-party.

The final consideration for the proposed setup was how the new tubing layout will be attached to the satellite. As previously mentioned, one end of the tubing will be attached to the distributor and the other end attached via Swagelok to a thruster. The thrusters are then mounted to the satellite using either mounting brackets or zip-ties to secure them in place and then potted with Arathane 5753 for vibration dampening. A concern, however, is the unsupported lengths of tubing that will run across the inside of

the satellite. Because both ends can be considered clamped, a simple calculation can be done to determine the maximum length of tubing can be used and still ensure that the natural frequency is greater than 100 Hz which stems from UNP guidelines for NS6 (so defined to avoid catastrophic resonance with the launch vehicle during ascent). Treating the tubing as a simple beam, basic beam equations [43] can be used to determine the maximum allowed tube length. The governing equation for this analysis is

$$\omega = (kl)^2 \sqrt{\frac{EI}{\mu l^4}} \qquad [5.6]$$

where:

ω is the natural frequency, $\left[\frac{rad}{s}\right]$

μ is the mass of the beam per unit length

l is the length of the beam

E is the Elastic Modulus of the propellant line

I is the moment of inertia of the beam (propellant line) along its central axis

kl is the derived parameter of the supports, end conditions, and the harmonic being found

As a result of the clamped-clamped boundary conditions, a kl value of 4.73 is used [43] to find the first natural frequency of the tubing. Using a materials database [41], the Elastic Modulus for stainless steel is 207 GPa and the density is 7.86 x $10^3 \frac{kg}{m^3}$. Because the mass per length is needed (rather than density), μ can be found by multiplying the density by the cross-sectional area of the tubing to give

$$\mu = A\rho = \frac{\pi}{4}(d_0^2 - d_i^2)\rho \qquad [5.7]$$

where d_o is the outer diameter of tubing = 3.18 mm (0.125 in), and d_i is the inner diameter of tubing = 1.59 mm (0.0625 in).

Substituting known values to Eq. 5.7 gives

$$\mu = \frac{\pi}{4}[(0.00318)^2 - (0.00159)^2](7.86 \times 10^3) = 5.9567 \times 10^{-6} \quad [5.8]$$

From theory, the moment of inertia of a tube is given as

$$I = \frac{\pi}{64}(d_0^2 - d_i^2)\rho \quad [5.9]$$

Again, substituting in the values from the geometry of the tubing gives

$$\mathrm{I} = \frac{\pi}{4}[(0.00318)^4 + (0.00159)^4] = 4.706 \times 10^{-12}\ \mathrm{m} \quad [5.10]$$

Next, the natural frequency of 100 Hz needs to be converted to $\frac{rad}{s}$ as

$$\omega = 100\ Hz = 100 * 2\pi\ \frac{rad}{s} = 628.1385\ \frac{rad}{s} \quad [5.11]$$

Finally, by substituting all values into Eq. 5.6, a maximum length can be calculated as

$$628.3125 = (4.73)^2\sqrt{\frac{(207\times10^{9})(4.706\times10^{-12})}{(0.0468)l}} \quad \Rightarrow \quad l = 0.396\,m \qquad [5.12]$$

Based on these calculations, a maximum tube length of 0.4 meters, which is approximately the same as MR SAT's entire height, can be used. Since the distributor is located near the geometric center of MR SAT, no tube length could approach this design limitation.

With these proposed design changes, the MR SAT propulsion system can be constructed with greater ease and speed with minimal wear on the various components. Additionally, the propulsion system will function with higher efficiencies and for a longer duration enabling greater mission capabilities while on orbit.

6. CONCLUSION

6.1. SMALL AND UNIVERSITY-CLASS SATELLITE APPLICATION

During the design, construction, testing and integration of the Nanosat 6 version of the MR SAT propulsion system many challenges were encountered and most of them have been either been overcome or plans are in place to address them in the short term.

6.1.1. Lee Company Valves. One example of a key challenge is the type of valve being used in the propulsion system. The Lee Company valves were recommended by Micro Aerospace Solutions (MAS) as a cheap and effective method of controlling the flow of propellant within the propulsion system. Of the other systems considered, it was found that many of the COTS valves have MEOPs in the 20-30 psia range whereas the Lee Company valve offers pressures over 300 psia. Also, the Lee Company valves with Swagelok integration only cost $800 per isolation valve and $1,000 per thruster compared to custom thrusters used by SSTL that incur costs of approximately $5,000 as quoted by Mr. Gibbon. Currently, MAS is endeavoring to space qualify these valves for use in a hydrazine-based system. However, commonly observed leaks are a source of concern with the system and their cause has yet to be determined. Currently three potential causes are currently under investigation: silver solder, electronics control circuitry, and R-134a incompatibility.

6.1.1.1 Silver solder concerns. Because the valves were not originally designed to be used in this fashion, they do not come with a standard connector that easily integrates into a propulsion system. Because Swagelok connectors are the primary form of connections used in the MR SAT propulsion system, it was desired that the valves and thrusters be easily integrated with the other Swagelok components. For simplify integration and to minimize weight and connections, MAS opted to attempt a new method of attaching the Swagelok connectors which involved using a high temperature silver solder to attack Swagelok fittings as seen in Figure 2.9. At first this appeared to be a suitable solution. Testing, however, showed otherwise. While great care was always taken when working with or near flight hardware, integration resulted in the formation of cracks in the silver solder joints near the tubing that caused a leak that would have ended the M-SAT mission prematurely. The valves were sent back for repairs, but even the

refurbished valves suffered from the same defect. While there may be some mass savings by soldering the connections, unless extreme care is taken to ensure that the tubing is not stressed (even in the slightest amount) during integration, leaks are likely to result. One possible solution to prevent the joints from moving is with the use of brackets designed to fit around the Swagelok connector so that the torque applied during integration is taken by the bracket and not the valve. Also, the valves were found to have internal leaks in addition to the leaks caused by the joints. It is possible that the high heat required to solder the Swagelok connectors caused damage to the internal components such as melting a portion of the EPDM o-ring. However, this has yet to be proven as the cause because of yet another factor not related to the silver solder joints. To eliminate this leak, the team decided to go back to simple Swagelok compression fittings. The valve tubing has an outer diameter of 1/16" which is a standard size of Swagelok components and can then be attached to the 1/8" tubing via 1/16"-1/8" adapter. This valve was connected to a can of R-134a and showed no sign of leaks; however, the thruster has yet to be fired to ensure that the electronics package is not at fault.

6.1.1.2 Electronics control circuit. The other source which may be responsible for causing internal leaks may be the Miners In Space electronics cart which has been used to test the thruster both in zero gravity and on the ground. This cart was specifically designed for the Lee Company thrusters to provide a 24 V pulse for no more than nine milliseconds to open the valve and then switch to a five volt signal to hold the valve open. The first version of the cart electronics was not tested extensively prior to connecting some of the hardware which resulting in anomalous operations of the thrusters. Just before the first flight of the experiment, the team was creating a program that would interface with the data acquisition (DAQ) system to fire the thruster and record the resulting thrust, pressure, and temperature data. The team had little experience with LabVIEW and was informed by a technician that the hardware needed to be powered-up in order to program the system. The team abided by this suggestion and began creating a program until the odor of burnt electronics was detected. After some initial inspecting, it was found that the isolation valve used in the experiment had heated to the point that the resin holding the solenoid in place melted and the solenoid unwound itself, rendering the valve unusable. (As a side note however, the valve did fail closed,

confirming that safety feature of the valve.) However, the integrity of the thruster was now in question as the control system for the thruster is identical to that for the valve. While the thruster downstream showed no outward sign of damage, it was assumed that it was not damaged and the team chose not to reconnect it into the system until further testing could be done using an oscilloscope that the team did not have access to while in Houston.

After returning to campus, the team met with the electrician and it was determined that the design was faulty in that it was possible that the circuit that switches from the 24 V to 5 V could get "stuck" and send a continuous 24 V pulse to the valve, resulting in the overheating issue. The issue was corrected and the system fully tested with an oscilloscope to verify the voltage step down occurred within the given time. Based on readings it appeared that the electronics circuit waited the full nine milliseconds before stepping down. Further testing with valves sent by MAS were connected to the MIS cart and test fired for functionality, but all thrusters were found to have internal leaks in addition to the previous leaks caused by the silver solder. After again consulting with MAS, the team was told that the valves are tested prior to shipping and that it must be something that the team was doing that caused the valves to malfunction. The first consideration was particulate contamination; however, the valves come with a built-in filter which should prevent clogging. Nonetheless, the team purchased a 0.5 micron filter and integrated it into the testing setup to ensure the propellant is free of possible sources of contamination. Unfortunately, the problem persisted. The next consideration for the leak source was that the in-house electronics controller circuit may be sending the 24 V signal slightly too long, resulting in damage that is accumulating over time as seen in the parametric study. A small electronics circuit was sent by MAS to allow the team to test the valves independent of the MIS cart. The current plan is to use the MAS electronics circuit to test a new isolation valve sent by MAS (that has no leaks to date). The team is setting up a machine that will allow for the successful testing of the new thruster with the new valve; however at the time of this writing, the testing has not yet been completed. Future documentation will be released this year to record the resolution of this issue. If the valve can be successfully tested with the MAS electronics package and still has no leaks, but is then tested with the MIS cart and starts leaking, then it will be clear that the

in-house electronics controller circuit is at fault. If the valve passes both electronics package testing, then it is likely that either the silver solder was at fault or an incompatibility of the internal components with R-134a may exist.

6.1.1.3 R-134a incompatibility. During the initial valve selection process, care was taken to select a valve material that is compatible with R-134a and meets outgassing requirements. After consulting with Lee Company, it was decided that the standard off-the-shelf valve contained an R-134a incompatible material. The search then began for a material that would meet both requirements. A sample of EPDM was obtained for in-house testing. To test for R-134a compatibility, the team first took the mass of the EPDM and placed a sample in a small container of R-134a. The sample was removed the next day and reweighed to determine if any mass loss occurred. Based on this simple test, it was determined that the mass did not change, suggesting that EPDM is R-134a compatible. The next step was to verify outgassing properties. Lee Company was again contacted and asked to see if they had relevant data available. However, as previously mentioned EPDM is not the standard application for these valves and outgassing data apparently does not exist or is not readily available for this material. Additionally, due to proprietary concerns, Lee Company could not disclose the exact composition of the EPDM, and the team could not investigate further without sending the material off campus for outgassing testing. Currently, such testing is beyond price range of the M-SAT budget. It is possible that exposing the thruster to prolonged vacuum and R-134a has resulted in the degradation of the o-ring material that resulted in internal leaks. However, if this is the case it will be difficult to determine which of the two issues is at fault. One option may be to measure the mass of the valve and then bake it to force it to outgas, and then re-weigh the valve and calculate how much mass was lost due to outgassing. However, the team is hesitant to expose their hardware to conditions that may be damaging.

6.1.2. Regulator Pressure Concerns. Due to limitations shown in the endurance test, one of the limiting factors of a saturated refrigerant-based cold gas system is the need to maintain a saturated pressure greater than or equal to the regulated pressure. If sufficient energy is not added to the flow to maintain isothermal conditions, the tank will slowly cool due to the need to vaporize liquid propellant (an endothermic process). As

the temperature decreases, the saturated pressure of the system also decreases to maintain equilibrium. If a regulator is not used, then the thrust being produced by the satellite will fluctuate greatly, causing complications with the orbit and attitude control if the thrust models (as functions of temperature, pressure and time) are not pre-programmed. Otherwise the controller will likely demand a thrust value that can no longer be produced, which may cause it to try to over compensate resulting in wasted propellant. It is highly recommended that a regulator be used to ensure production of a constant thrust value. However, if the system is fired sufficiently long, it is possible that the saturated pressure may drop below the regulated pressure rendering the satellite inoperable if the regulator is incapable of operating at pressures below the regulated pressure. Otherwise, even if the regulator can operate below the preset pressure, the same depreciating thrust will exist and may cause the satellite to expend an unnecessarily large amount of propellant. One final consideration to keep in mind: if the regulated pressure is set higher, the thrust will increase, but the ΔV and exhaust duration will both decrease significantly. Only short bursts can be used before the system needs to "recharge." And conversely, if the regulated pressure is too low, then the opposite will occur. The ΔV and exhaust velocity are both adequate, but the thrust may be too low to complete the mission.

6.1.3. Team Communication. One of the other concerns that any student or engineer must consider when designing a system is the relative location of the specified component and what other components are present in the vicinity. In the process of designing the Nanosat 6 version of the propulsion system, many changes were incorporated to increase the performance of the system. Unfortunately, many of the other subsystems made improvements as well. For example, the Structures subsystem employed an interlocking dovetail pattern as seen in Figures 2.2 and 2.3, with the goal to increase the stiffness of the entire structure and simplify integration. A communication breakdown between the Propulsion and Structures subsystems resulted in a satellite configuration that was too small to accommodate the propulsion tank. The two subsystems worked together to resize the satellite to a "final" structures design. Propulsion began to place hardware and run tubing until it was discovered that new hardware had been added that now intersected propulsion components that had already been placed. For example, the battery box was split in half and then placed on two

different panels. One of these new boxes intersected with parts of the distributor, transducer and tubing requiring Propulsion to redesign again. Had all the subsystem leads meet prior to original construction and addition of components, it is likely that the propulsion redesigns would have not been necessary or at least more minor in nature. Open communication will result in significant savings in time and resources that may make the difference in making a deadline for a customer or in completing a quality spacecraft for the Nanosat program.

6.2. CONCLUDING REMARKS

6.2.1. Road Map to Success. The purpose of this thesis is to provide a road map for the design of refrigerant-based saturated liquid cold gas propulsion systems. At the team level, the mission objectives should be defined for the satellite as a whole and for individual subsystems. For example, one of the MR SAT requirements is to complete a minimum of one orbit of formation flight with a goal of three. This requirement involves more than just the propulsion system. Communications is needed to ensure the satellites are still talking to coordinate the formation, Attitude Determination And Control (ADAC) is needed to develop the code to ensure that the satellite orientation is conducive for constant communication between satellites, Orbit is needed to calculate orbital position and the thruster inputs to ensure the satellites maintain the formation. Propulsion's task is to provide three translational and three rotational degrees of freedom for full maneuverability on orbit and to ensure that the propulsion system can deliver sufficient thrust and ΔV to complete the mission. Then, once the propulsion system has their requirements for performance quantities, the information in this thesis will allow student or engineer take the minimum thrust value needed to complete the mission design and apply the correction factors mentioned in this document to determine the appropriate inlet conditions. Depending on whether the reader has chosen the Lee Company valves used in the M-SAT mission or a different vendor, the correction coefficients can be used to estimate the actual thrust that will be produced for a given setup. For example, if the Lee Company valve is used, then the thrust can be directly read off Figure 3.9. If a different valve is used, the reader can use the "valveless" setup to get an estimate of the maximum thrust a given inlet condition can produce. However, if the valve type is unknown, the

student or engineer should apply a conservative factor of safety on the predicted loss coefficient; however, it is likely that most other systems will lie between the valveless test and the Lee Company valve test. Next, the ΔV from the mission requirements and the rocket equation (Eq. 2.1) can be used to find the minimum propellant mass needed to complete the mission. Then, depending on the valve choice, a realistic ΔV can be found using the correction factors shown in Table 3.1. Again, the Lee Company valve can likely be used as a conservative value if the intended system will be using actual space-rated valves, such as those available through Vacco. In addition to a performance road map, the majority of the hardware used in this system are COTS components that are readily available with minimal lead time. The primary exception to this is the Marotta tank. The list price for the propulsion tank was $50,000 at the time of purchase. However, due to a manufacturing defect that would not allow its integration into the DMC satellites, the M-SAT team was able to purchase the tank for only $10,000. Other tanks may be available or constructed, however due the nature of the Nanosat program and the AFRL, the flight heritage of this particular model help justify the additional cost. If less regulation was to be placed on the propulsion tank, a simple vessel could be fabricated and welded by a third party for minimal cost; however no flight heritage would be available and proof, fracture and fatigue tests would likely be required prior to having the system launched.

6.2.2. Looking Ahead. Refrigerant-based saturated liquid cold gas propulsion systems are the future of safe and affordable propulsion systems for small satellites, particularly at the university level. The testing presented in this thesis outlines how to construct, test and integrate a functional propulsion system at the system level. However, more work can always be done to further enhance the capabilities of refrigerant-based systems. To that end, future testing should make use of the entire propulsion system, eventually in the flight configuration in a thermal-vacuum chamber to simulate on-orbit conditions. Due to the limited size and electrical pass-throughs available on the bell jar vacuum chamber, several workarounds were used such as the construction of a custom electrical pass-through with DB-9 connectors. The thermal-vacuum chamber should be large enough to house the entire MR SAT assembly to determine how the propulsion system will behave with the other subsystems. For example, the thrusters create a

magnetic field to retract the poppet to allow the propellant to flow. This magnetic field should be fairly localized as it is not very strong; however, the magnetic torque coils are sensitive enough to pick up Earth's magnetic field, meaning that they may be sensitive to interference. Ideally a full systems test will enable both subsystems to determine the functionality of their respective hardware when both systems are operating.

Based on the information provided in this thesis, it is clear that a refrigerant-based saturated liquid cold gas propulsion system is relatively cheap and simple to assemble and due to the nature of the propellant, easy to test within a university laboratory setting. And not only can this system provide sufficient thrust for station keeping, but can even be used to complete the complicated and propulsively-intensive mission involving formation flight. If not for the restriction placed on the propulsion system by AFRL, the system can easily achieve a ΔV over 20 m/s and sustained thrust output for several hours. However, even with the strict limitation imposed by AFRL, the satellite is still capable of meeting the mission requirement of one orbit of formation flight. The Satellite will simply require a release mechanism that produces a separation velocity less than 0.4 m/s. With these capabilities, university satellites can attempt missions that would have previously required complicated and expensive electric propulsion systems or other systems that present unneeded dangers due to high pressures, or corrosive/toxic/explosive propellants.

APPENDIX A
CURRENT PROPULSION TECHNOLOGIES

This appendix expands on the current technologies available for chemical and electrical propulsion systems.

A.1. CHEMICAL PROPULSION SYSTEMS

A.1.1. Solid-Chemical Propulsion Systems. Solid rockets generally consist of ammonium perchlorate, powdered aluminum, and some type of organic polymer. This method of propulsion is very simple, extremely reliable, and relatively low cost, but it has significant disadvantages. One drawback is the inability to throttle a solid-rocket motor. Once ignited, the chemical reaction continues until the fuel is exhausted, limiting the rocket's potential application. Additionally, safety is another issue due to the volatile nature of the solid-rocket propellant [10].

A.1.2. Liquid-Chemical Propulsion Systems. Liquid propellants have characteristics similar to those of solid propellants except that they require additional hardware to operate. In general, most liquid-chemical propulsion systems require the use of pumps to feed the propellant into a combustion chamber where it combines with an oxidizer and is then ignited. The advantage of these types of propulsion systems is that they are easily throttled, providing increased mission flexibility [10].

A.1.2.1. Liquid-Chemical Monopropellant Systems. The most common propulsion systems for attitude and velocity control on spacecraft are liquid-chemical monopropellants. Injectors are used to spray an iridium-impregnated bed of alumina pellets with a catalyst, typically hydrazine or hydrogen peroxide, which causes the pellets to decompose rapidly; the vapor is then expelled to generate thrust. This method of spacecraft propulsion is simple, reliable, and inexpensive. It yields excellent handling characteristics and remains relatively stable under normal storage conditions. However, monopropellants tend to have lower performance and higher mass than liquid-chemical bipropellants [10].

A.1.2.2. Liquid-Chemical Bipropellant Systems. To gain greater efficiencies than is typically possible with liquid monopropellants, a system using liquid fuel and oxidizer is used. These bipropellant systems use two or more tanks so that the oxidizer and propellant can be stored separately, and they have internal plumbing that prevents these chemicals from mixing until they reach the combustion chamber. Like the

monopropellant thruster, this type of propulsion system is easily throttled, permitting precise maneuvers with better overall performance. The downside, however, is such systems are more complex because they require extra tanks and pumps that add significant mass. Additionally, the nature of storing the fuel and oxidizer raises safety concerns. In some cases, helium is stored at a pressure of 4,000 psia, which could result in a catastrophic incident if the tank were to rupture; in other instances, the chemicals used can be hazardous [10].

A.1.2.3. Liquid-Chemical Hybrid Propellant Systems. One form of liquid propulsion seeks to combine the best of both monopropellant and bipropellant systems. Hybrid systems use a solid form of fuel with a liquid or gaseous oxidizer (e.g., liquid oxygen and rubber). This approach permits a throttleable reaction that can be set to idle (10% thrust) or even completely stopped and restarted later. Although hybrids have poorer performance than bipropellants, the nonexplosive, nontoxic, and environmentally clean nature of their byproducts makes development of these systems safer and cheaper (because they can be made to produce no hydrochloric acid or ammonium oxide exhaust). The downside of hybrids is that they tend to be more massive than basic solid rockets because of the need to store and pump of the oxidizer [10].

A.2. ELECTRIC PROPULSION SYSTEMS

A.2.1. Electrothermal Propulsion Systems. To increase the performance of spacecraft propulsion systems, electrothermal systems use electric power to heat a gaseous propellant. However, such systems are limited by the amount of heat that can be added to them directly. Once the propellant reaches a sufficiently high temperature, the energy being added to it is gets absorbed to facilitate the dissociation and eventual ionization of the fuel, thus creating an upper bound on performance capabilities [11].

A.2.1.1. Resistojet Propulsion Systems. By adding simple resistive heating elements to the propulsion system, however, large amounts of energy can be added to a system directly at the thruster rather than at the propellant tank. Thermal losses incurred between the tank and the thruster can reduce overall performance. Resistojets perform well with simple feed systems, but the complicated interface makes integration difficult. Additionally, these systems require little power compared to other forms of electric

propulsion. Some typical propellants used in resistojet systems are nitrogen, ammonia, hydrazine, and hydrogen. As mentioned before, hydrazine, like ammonia, is hazardous and requires additional ground support equipment and staff, increasing development time and costs. Hydrogen is nontoxic but highly flammable, a property that presents a different but no less dangerous hazard to personnel and launch vehicles [10].

A.2.1.2. Arcjet Propulsion Systems. Arcjet systems use an electric arc generated at the nozzle rather than resistive means to add energy to the flow, and they generate local temperatures greater than 20,000 K. These systems are capable of higher specific impulses and greater thrust than resistojets, but at the cost of increased power consumption. As with a resistojet, the propellant feed system is simple, but the interface is complicated, adding time and costs to a project. Furthermore, the propellants typically used in arcjets are ammonia, hydrazine, and hydrogen, the dangers to personnel and hardware have already been noted [10].

A.2.2. Electrostatic Propulsion Systems. In general, electrostatic systems generate strong electrical fields that propel charged ions out of the satellite, generating thrust. To generate these fields, a neutral gas is first injected and stripped of electrons, resulting in a mixture of ionized and neutral gases called *plasma*. Electrostatic systems use ions as the means of propulsion due their large mass relative to electrons. By generating electric field potentials of several thousand volts, the charged ions "fall" through the engine, gaining speed. They are discharged focused out the back of the nozzle at extremely high velocity, generating thrust. This method of propulsion accommodates a higher specific impulse than other means of spacecraft propulsion, but at the cost of thrust. The amount of thrust generated by such a system is so small that the engine must often be run for several consecutive hours to gain any significant velocity. Electrostatic systems have several additional disadvantages: The electrodes in such systems degrade over time, limiting the mission lifetime. They require an enormous amount of power. And, because positive ions are being constantly expelled, the satellite tends to take on a net negative charge, which can pose a hazard to sensitive electrical hardware. To counter the later problem, electrostatic systems use an electron injector that collects the electrons resulting from the ionization of the propellant and injects them into the ion flow, keeping the spacecraft at a net neutral charge [11].

A.2.2.1. Ion Propulsion Systems. The most common electrostatic thruster is the ion propulsion system in which positively charged ions are injected into an acceleration region that consists of a set of grids that control the potential distribution and ion motion [12]. Ion propulsion systems are well known for having a larger specific impulse than any other form of spacecraft propulsion and nearly the lowest level of thrust production. Typical propellants for ion thrusters are mercury, argon, xenon, and cesium. Both mercury and cesium are hazardous and require additional safety measures during handling. Argon and xenon are the standard propellants of choice because they have a higher molecular weight than other compounds. With a heavier molecule, more thrust can be generated by the ions ejected from the spacecraft. The downside to ion systems is that they require large amounts of energy and are extremely complicated to design and operate. Further, the power supplies that are needed to supply such a large voltage potential are quite heavy [13]. Because the ions are expelled from the engine, a net charge remains on the satellite, and this charge must be negated to ensure that charge buildup does not damage any systems. An equal current of electrons injected near the thruster exit by a thermionic emitter neutralizes the flow of high-speed ions [12], thus preventing charge buildup.

A.2.2.2. Colloidal Propulsion Systems. Another type of electrostatic propulsion system, colloid systems produce thrust by accelerating very fine droplets of an electrically charged, conductive fluid that are formed through a needle with a diameter on the order of hundreds of microns and biased with a potential of 5-10 kilovolts (with respect to ground). As the fluid exits the needle, it is accelerated by an electrode placed near the needle which has been biased several thousand volts negative. Because of the electrostatic forces on it, the charged droplet breaks off with a net positive charge and is accelerated out of the nozzle [14]. Using glycerine ($C_3H_5(OH)_3$) as a propellant, colloid thrusters produce the lowest thrust and specific impulse of all electrostatic propulsion systems. Additionally, the high power consumption and complexity of such systems are often a deterrence to their use [10].

A.2.2.3. Hall-Effect Thruster (HET) Systems. Hall-effect thrusters represent a bridge between the ion thruster and the electromagnetic thruster [13]. The Hall effect occurs when applied magnetic fields force the current to flow in spiral paths, increasing

the total voltage potential of the system. Typically, it occurs at low particle densities [12]. Hall-effect thrusters provide excellent performance with a relatively high power-to-thrust density, and thus typically use only xenon as a propellant due to its large molecular weight. Like most systems, however, Hall-effect thrusters suffer from the same power consumption challenge as other electric propulsion systems. They have a high power draw and have a high incidence of beam divergence and electrode erosion [13].

A.2.3. Electromagnetic Propulsion Systems. Similar to electrostatic systems, electromagnetic propulsion systems expel ions rather than neutral particles to increase exhaust velocity potentials. The difference between these two systems lies in the method used to accelerate the ions out of the engine. Electromagnetic systems use magnetic fields to accelerate the ions to speeds on the order of 50 km/s, resulting in very high specific impulse values. Again, the tradeoff for this high specific impulse is the large amount of power needed to ionize the propellant (and power the magnetic field if an electromagnet is used). In addition, extra wires and electrical components often increase the system's mass [13].

A.2.3.1. Magneto-Plasma-Dynamic (MPD) Systems. Based on the Lorentz force, MPDs generate electrical and magnetic fields that interact with the charged particles, accelerating them out of the nozzle at high speed given by

$$\bar{F} = q(\bar{E} + \bar{V} \times \bar{B}). \qquad [A.1]$$

The construction of MPDs is similar to that of thermal arcjets, with electrodes at the nozzle exit that produce a high temperature arc. They use a much stronger magnetic field, however, to increase the acceleration of the propellant [13]. Thus, MPDs generate more thrust than any other electric propulsion system using argon as the propellant. Although MPDs perform much better than other systems, their high power draw and great expense make them less desirable [10].

A.2.3.2. Pulsed Plasma Thruster (PPT) Systems. PPTs use high voltage to arc current from one electrode to the other over a Teflon® core that oblates and ionizes a

small amount of the fuel. The resulting plume contains both neutral and ionized particles that are expelled through a nozzle by two different methods. The ionized particles experience a force as a result of interaction between the magnetic and electrical fields, resulting from the initial arcing as shown above in Eq. 2. The remaining neutral particles are either expanded thermally through the nozzle as a result of the heat added to the particles or are ionized by a subsequent arcing [15]. The efficiency of PPTs is modest compared to other forms of electric propulsion, but it is the lowest among other electromagnetic thrusters. Additionally, the high power consumption and the risk components may be contaminated by Teflon makes PPTs a less desirable form of propulsion [10].

A.2.3.3. Pulsed Inductive Systems. In pulsed inductive thrusters, both coil and plasma currents are aligned along the azimuthal ($\overline{\boldsymbol{E}} \times \overline{\boldsymbol{B}}$) direction so that the plasma is accelerated parallel to the axis of symmetry due to the radial intervening magnetic field [12]. The two most common forms of propellant are argon and hydrazine. As mentioned above, the hazards associated with the use of hydrazine propellant can increase both the cost and development time of a project. Pulsed inductive systems have very high performance and moderate thrust; the trade-off is that their development is risky, they are typically very complicated, and they use large amounts of power [10].

APPENDIX B
MISSOURI SATELLITE TEAM

This Appendix outlines the mission objectives of the M-SAT mission, the satellites, and the propulsion system used in MR SAT.

B.1. MISSOURI SATELLITE TEAM (M-SAT)

The Missouri Satellite Team operates out of the Space Systems Engineering Lab (SSE) at the Missouri University of Science and Technology. It is one of the universities participating in the Nanosat 6 competition. The 40 team members represent many disciplines, primarily aerospace engineering, in addition to mechanical and electrical engineering, computer science, and computer engineering.

B.1.1. Mission Objectives. Most satellites today have one thing in common: All of the hardware needed to carry out the mission is enclosed in a single structure. Although this may seem like a logical approach, a single failure in a critical hardware component can jeopardize the success of an entire mission. Currently, S&T is investigating distributed systems using fractionated spacecraft [26]. If the critical hardware is spread among several small spacecraft, the chance that a single piece of hardware will cause a catastrophic failure is drastically reduced. If one small satellite fails, it can more easily be replaced, whereas replacing a large, complicated satellite can cost millions of dollars.

Additionally, the M-SAT mission seeks to prove the viability of new technologies. One of the key factors limiting formation flight of small satellites is the lack of an effective propulsion system. The M-SAT mission will use a refrigerant-based saturated-liquid cold-gas propulsion system capable of establishing and maintaining formation. Furthermore, the team is also designing a flight controller that uses the θ-D algorithm (designed at S&T) for real-time magnetometer-only attitude determination and control [27]. Finally, the team is using Bluetooth technology for inter-satellite communications. Bluetooth is an off-the-shelf, low-power technology that has never been used in space.

By demonstrating these technologies on the M-SAT mission, the team hopes to better facilitate future formation flight missions, challenging the traditional approach to spacecraft design and mission execution.

B.1.2. M-SAT Satellites. The team has designed two satellites, known as the Missouri Rolla Satellite (MR SAT) and the Missouri Rolla Secondary Satellite (MRS SAT), to be flown in close formation to validate the Bluetooth technologies and cold-gas propulsion system. Both satellites will be launched in a stack configuration with MRS SAT attached to the top of MR SAT, as shown in Figure B.1.

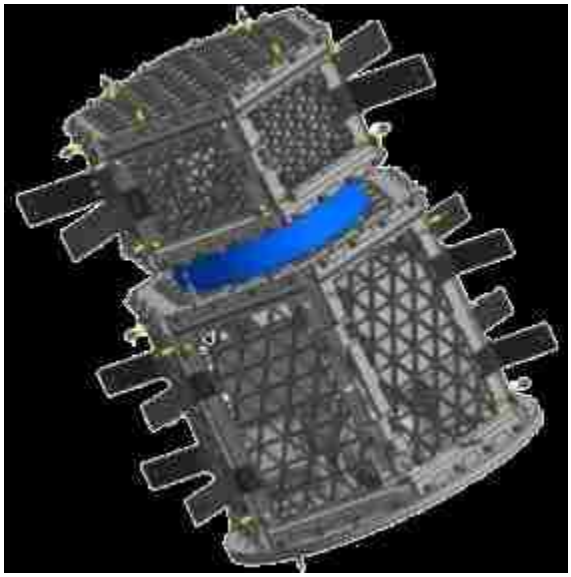

Figure B.1. MR and MRS SAT Launch Configuration

Once it orbit, a Lightband system will be used to eject the pair from the launch vehicle, and magnetic coils aboard both satellites will be used to detumble and align the satellites to ensure intrasatellite communication via Bluetooth. Once the orbit is achieved, the satellites will decouple, and MR SAT will enter chase mode to establish a formation with MRS SAT using a cold-gas propulsion system.

B.1.2.1. Missouri Rolla Satellite (MR SAT). The primary satellite is the only one of the two equipped with an onboard propulsion system permitting orbital maneuvers and space-to-ground antennas for relaying data back to the ground station. Because the

flight control system (FCS) is designed to have minimal input from the ground, MR SAT is also the only one of the pair that communicates with the ground station. MRS SAT is designed to communicate only with MR SAT, which then activates the necessary thrusters to maintain the formation without input from human controllers. If, however, a problem arises, the ground control station can override the onboard system and command the satellites directly.

Recently, both MR SAT and MRS SAT have undergone a redesign to be outfitted with a dovetail interlocking pattern on the side panels. While enhancing structural integrity, this outfit increased satellite mass relative to the previously analyzed Nanosat 4 design. The updated mass for MR SAT is now approximately 25 kg. All the analysis presented here, therefore, uses a total mass of 26 kg to provide a margin of safety that accounts for any increase in mass that may occur later in the design phase. Additionally, the current dimensions of MR SAT are 48.7 x 48.7 x 33.0 cm. Although a proposed redesign, however, will alter these dimensions slightly, this analysis considers only the current dimensions as this will affect hardware layout. Figure B.2 shows a CAD image of MR SAT.

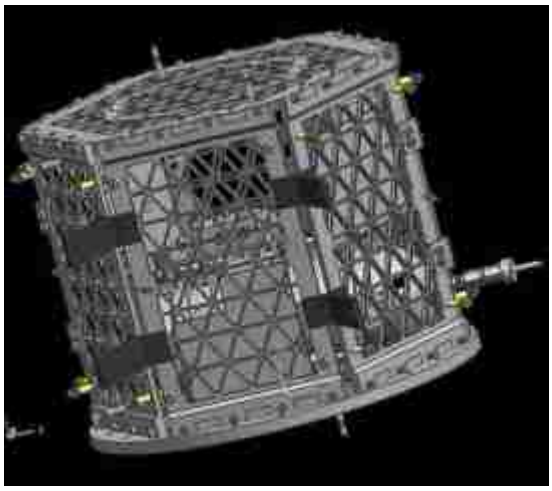

Figure B.2. MR SAT

B.1.2.2. Missouri Rolla Secondary Satellite (MRS SAT). The second satellite of the M-SAT pair serves as a target for the primary spacecraft. MRS SAT uses magnetic coils to align itself with the Earth's magnetic field for attitude control, but no means exist to change MRS SAT's orbit. Thus, it relies on the cold-gas system of MR SAT to maintain the formation. Figure B.3 shows the current design of MRS SAT.

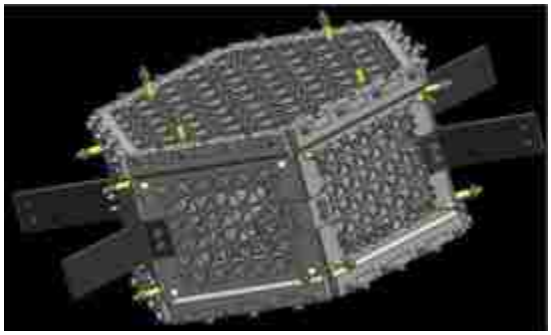

Figure B.3. MRS SAT

The current mass and dimensions of MRS SAT are 11.07 kg and 48.7 x 48.7 x 19.4 cm; however, due to the redesign mentioned above, these figures are likely to change slightly as various components are redesigned to integrate with the new structure.

B.2. MR SAT PROPULSION SYSTEM

Among the propulsion systems available on the market today, only cold-gas systems appear to be capable of providing the levels of thrust needed by typical micro- and nanosatellites given their volumetric and power constraints. MR SAT uses twelve thrusters in an H-pattern configuration, permitting full six degrees of freedom (DOF) control, while maximizing the applied moments to the spacecraft. Figure B.4 illustrates the thruster arrangement for MR SAT.

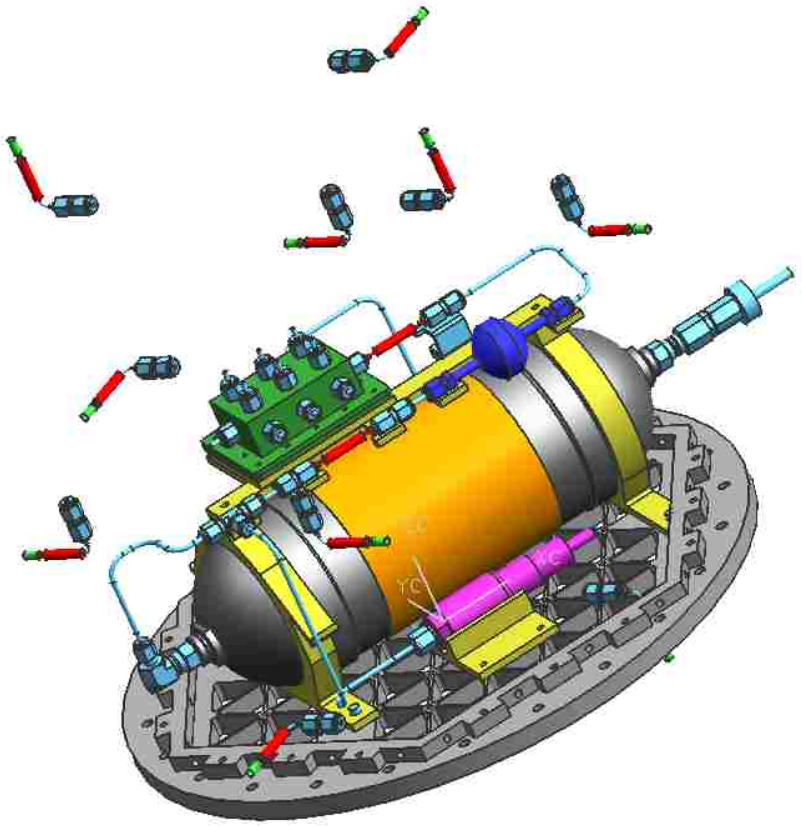

Figure B.4. MR SAT Propulsion System

B.2.1. Two-Phase Refrigerant-Based Propellant. The refrigerant R-134a has recently replaced the freon once commonly used in vehicle and household air conditioners and refrigerators because it is a more ozone-friendly chemical. Because of its low vapor pressure (84 psia at 21 °C), R-134a can be stored as a saturated liquid at relatively low pressures while maintaining a mass sufficient to provide enough ΔV to complete a spacecraft's mission. More simply, once the R-134a reaches its vapor pressure inside the propellant tank, any propellant added later is condensed into the liquid phase. Thus, the internal pressure of the system remains constant as more propellant (R-134a) is added to the system. As mentioned above, the quality of the fluid determines the amount of gaseous propellant available for expulsion to generate thrust for the satellite.

After a certain point, however, the propellant becomes fully saturated and only liquid propellant remains. Full saturation presents a potential problem because vapor pressure could be increased only by heating the propellant and thus converting some of the liquid fuel into a gaseous state. This conversion costs energy, resulting in higher temperatures and pressures and thus creating a potentially more dangerous system. Care should be taken initially to determine the amount of ΔV needed to complete the mission so that a propulsion system can be properly sized to ensure sufficient gaseous propellant at the desired temperature and pressure. Given the exhaust velocity, the necessary ΔV can be calculated using the Tsiolkovsky (ideal) rocket equation:

$$\Delta V = V_e ln\left(\frac{m_0}{m_1}\right) \quad \text{[B.1]}$$

where m_0 is the total initial mass of the spacecraft including propellant and m_1 is the final mass. The exhaust velocity can be calculated as

$$V_e = I_{sp} g_0 \quad \text{[B.2]}$$

where g_0 is the gravitational acceleration due to gravity. Using this method, the propellant mass can be determined by taking the difference of the total initial and final masses. Using equations 1.3-1.5, the quality of propellant needed to complete the mission in its early phases can then be determined.

B.2.2. System Hardware. In addition to the propellant, many hardware components must function together to produce a propulsion system capable of meeting mission objectives. When selecting hardware for any system the primary concern is safety. Not only does the system have to pose no risk to persons in the immediate area, but also to the launch vehicle. Most launch providers will not fly a satellite that could damage the million dollar launch vehicle or the primary payload. All components of the MR SAT propulsion system meet or exceed NASA's recommended specifications for

hazard mitigation. After safety, cost and availability drive the hardware selection. Because designing custom parts for a single satellite can be very costly, where possible, inexpensive, commercial-off-the-shelf (COTS) components were incorporated into the M-SAT design. However, COTS hardware has a low technology readiness level ranking because much of it lacks flight heritage, which provides additional hurdles, such as complex analyses, to overcome when pursuing a possible launch opportunity. The components used in the MR SAT propulsion system are briefly described here; however, Seubert [28, Section 5] provides a detailed component trade study. Figure B.5 shows a schematic of the propulsion system; the function of each component is described in the following sections.

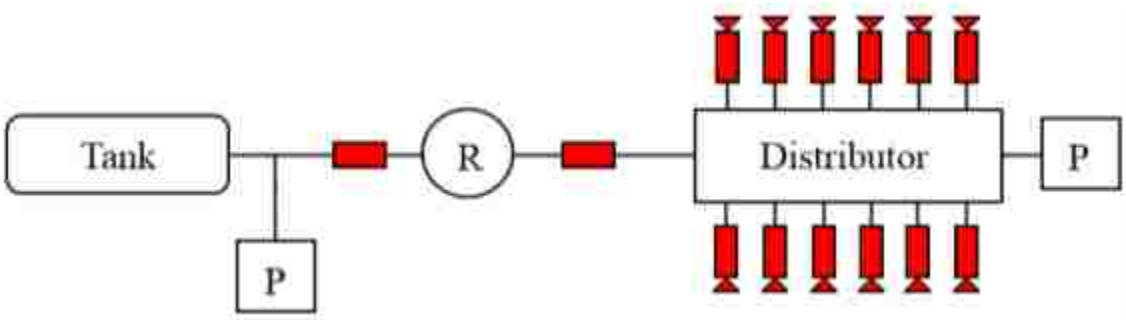

Figure B.5. Propulsion System Schematic

In Figure B.5, the system's pressure transducers are represented by the squares with a "P" and the circle with an "R" is the regulator. The red rectangles signify a valve and the red triangles represent thruster nozzles. The combination of both red squares and triangles designate the system thrusters.

B.2.2.1. Propellant Tank. In most cold-gas propulsion systems, the tank must withstand only the pressure applied to it by the propellant. As a result, typical cold-gas tanks are relatively simple and easy to construct. Two-phase systems, however, are

complicated by the presence of both the liquid and gaseous propellant. To maintain high system efficiency, the propellant must be ejected from the thruster only in the gaseous state, a requirement that simple cold-gas tanks cannot consistently meet. Additionally, the use of a two-phase propellant is complicated by the potential for propellant sloshing. Liquids tend to form large globules in space due to surface tension in the weightless environment. These globules can shift inside the propellant tank, causing a sudden shift in the satellite's center of mass that can affect the stability of the spacecraft's attitude control. To address both issues, the M-SAT project uses a tank with a propellant management device (PMD). The PMD uses a series of screens and baffles (similar to a sponge) to separate and collect the propellant, preventing sloshing and keeping liquid from being ingested by the propellant lines.

A BSS01 tank was purchased from Marotta UK Ltd. It is constructed from stainless steel, has an internal wetted volume of 2.5 liters, and a dry mass of 1.4769 kg. This tank model is currently in use on four SSTL disaster monitoring constellation (DMC) satellites in low Earth orbit, giving the tank flight heritage. The first satellite, Alsat-1, was launched in November 2002, and the remaining three, UK-DMC, NigeriaSat-1, and BilSat-1, were launched almost a year later in September 2003 [28]. The DMC uses saturated butane stored at a maximum absolute pressure of 400 kPa (58 psia) at 40 °C, combined with a 50 mN resistojet [29]. Since the M-SAT mission will use R-134a instead of butane, the team consulted with engineers from Marotta. The Marotta engineers advised that the tank should operate safely with R-134a, but they were unsure whether the PMD would be effective. The tank has been proof tested to 1.62 MPa (235 psi), and it has a burst pressure of 9.8 MPa (1,421 psi), well above the operational limits expected for the M-SAT mission. The term *burst pressure* is somewhat misleading in this case, however. For increased safety, the tank was designed to leak before burst, meaning that it will develop a leak rather than fail catastrophically. This characteristic is important for university-built satellites because launch providers generally consider these satellites to be a higher risk. If a satellite's propulsion tank could decompress explosively, potentially damaging a multi-million dollar vehicle, it is not likely to be launched. If the worst-case scenario were only a leak, however, the odds of securing a launch opportunity increase. Figure B.6 displays the propulsion tank (with the attached

heater) integrated into MR SAT, and Table B.1 [28], [30] shows the associated data sheet.

Figure B.6. MR SAT Propulsion Tank (with Heater)

Table B.1. MR SAT Tank Properties and Configuration – Marotta BSS01-01

Mass of Empty Tank - Measured	1.4769 kg (3.256 lb)
Volume - Measured	2.459 L
Temperature Range	-40 °C to 75 °C
Proof Pressure - Measured	1.62 MPa (235 psi)
Burst Pressure (Minimum Recorded - Leak no Burst)	9.8 MPa (1,421 psi)
Factor of Safety (Burst Pressure : Proof)	6.05
Leak Rate (He - 0.81 MPa) - Measured	2×10^{-10} std. cm^3/sec
Mesh Baffles (PMD)	Aluminum Alloy
Insert Disks (PMD)	Aluminum
20 Micron Filter	Stainless Steel
Purchase Price	$9,800 USD

B.2.2.2. Regulator. To guarantee consistent thrust values despite potential changes in tank pressure, a regulator was added to the MR SAT propulsion system. A Swagelok HFS3B regulator was selected for its compact size and leak-before-burst design. Additionally, the HFS3B has no reference pressure port or vent hole that could create incompatibility issues in a vacuum environment. The HFS3B regulator is capable of handling inlet pressures ranging up to 6.89 MPa (1,000 psig), well beyond the maximum design pressure of the MR SAT propulsion system, and it is capable of functioning even when the tank drops below the regulated pressure. During production, an inert gas is used to charge the regulator to determine the preset outlet pressure. Based on theoretical calculations [28], a regulated pressure of 20 psia was determined to provide sufficient thrust to establish the formation while still maintaining relatively high efficiencies and thus enough ΔV to complete the mission. However, the Swagelok HFS3B does not offer 20 psia as a stock selection, therefore, a 24.7 (10 psig) setting was deemed acceptable. Figure B.7 shows the regulator integrated into the MR SAT propulsion system, and Table B.2 provides a data summary.

Figure B.7. Swagelok HFS3B-WU5-P10 Regulator

Table B.2. Swagelok HFS3B-WU5-P10 Data Sheet

Preset Outlet Pressure	24.7 psia (10 psig)
Mass - Measured	176 grams
Temperature Range	-40 °C to 70 °C
Inlet Pressure Range	Vacuum to 6.89 MPa (1,000 psig)
Operating Temperature Range	-23 °C to 65 °C
Orifice Size	3 mm (0.12 in)
Flow Capacity	100 std. L/min
Leak Rate (He)	1×10^{-9} std. cm^3/sec

B.2.2.3. Pressure Transducers. To ensure safety and high performance, the pressure of the entire propulsion system must be monitored at all times. To permit constant monitoring of both the tank and the rest of the system, it was decided to integrate two pressure transducers were integrated into the MR SAT propulsion system. The first transducer is located immediately downstream of the tank and is used to monitor the pressure inside the tank and up to the regulator. Past the regulator the pressure drops and a second transducer is used to measure the pressure in the distributor and propellant lines.

The pressure transducer used in the MR SAT propulsion system is the Honeywell/Sensotec COTS model AS17A, selected because it has been customized for aerospace application [28]. The AS17A is extremely durable and accurate, but it has a low total mass. It was designed for a maximum pressure of 68.9 MPa (10,000 psia), thus providing a factor of safety that exceeds launch vehicle and government requirements for the M-SAT system. The transducers are preset to read an absolute pressure between zero and 1378.96 kPa (0 to 200 psia), a range suitable for the pressures expected in all scenarios envisioned for the Nanosat 6 mission. However, a waiver is currently being sought from AFRL to allow pressures greater than 100 psia. The waiver will permit the addition of more propellant to the tank, increasing the maximum pressure to 307 psia; therefore, the tank pressure transducer must be capable of measuring this value. The

AS17A model meets this requirement. Figure B.8 provides a photograph of the transducer, and Table B.3 lists product specifications [28].

Figure B.8. Sensotec AS17A Pressure Transducer

Table B.3. Sensotec AS17A Pressure Transducer Specifications

Pressure Range	0 to 1,378.96 kPa (0 to 200 psia)
Mass - Measured	140 grams
Operating Temperature Range	-54 °C to 121 °C
Material	Stainless Steel
Pressure Port	7/16-20 UNF
Electrical Connection	PTIH-10-6P

B.2.2.4. Isolation Valves and Thrusters. To control the flow of the propellant in the system so that propulsive maneuvers occur only when needed, the team investigated several COTS valves. Several microdispense solenoid valves from Micro Aerospace Solutions have been integrated into the propellant feed lines. The valve selected is the INKX0507800A model manufactured by the Lee Company [28], and as shown in Figure B.9; Table B.4 lists the specifications.

Figure B.9. INKX0507800A Lee Company Valve

Table B.4. Lee Company Valve Specifications

Mass	7 grams
Proof Pressure (Lee Co. Rating)	5.17 MPa (750 psi)
Burst Pressure (Lee Co. Rating)	7.76 MPa (1,125 psi)
Rated Thermal Environment	-18 °C to 70 °C
Open Response Time - 689.48 kPa (100 psig)	0.25 ms
Close Response Time - 689.48 kPa (100 psig)	< 3.0 ms
Actuation Voltage	24 V spike
Actuation Power (Maximum Average)	0.75 W

To open these valves, a 24 V signal must be initiated, followed by a continuous 5 V signal to hold them open. As a safety precaution, these valves are designed to close when electric power is no longer applied, preventing the system from performing thrusting maneuvers until instructed to do so by the control system. The valve uses a high-density rubber, ethylene propylene diamine monomer (EPDM), seal, and it constructed from Stainless Steel 316. For added simplicity, the thrusters were manufactured using the same valve. A nozzle design was analyzed, manufactured, and integrated by Micro Aerospace Solutions to create a thruster assembly [28]. Figure B.10 shows the nozzle and valve.

Figure B.10. Lee Company Valve with Integrated Nozzle on MR SAT Side Panel

Compliance with NASA NSTS 1700.7B requires a minimum of three separate inhibits (i.e., valves) along any path from the tank to any system exit. Two isolation valves were integrated into the system, as shown in Figure B.5. One is located immediately downstream of the first transducers so that the pressure in the tank can be monitored even when the valves are closed; the other was installed just before the

distributor, isolating the thruster network from the rest of the core hardware. The final inhibits are the thrusters themselves, giving every path from tank to exit three independent inhibits.

B.2.2.5. Distributor. To minimize the number of possible leak sources, the team designed a propellant distribution device. One of the primary concerns was the number of Swagelok connectors used in previous versions of the MR SAT propulsion system. Originally, the team designed an eight-thruster configuration to provide five DOF. This approach reduced the cost by sacrificing one dimension of translational motion [28], [31]. This design used several Swagelok tees and crosses to minimize propellant lines, but this approach made the system more complex. Additionally, the tubing was run along the panels, requiring that the propulsion system be partially assembled on a panel before that panel could be integrated into the system. Because the Swagelok connectors could not be tightened until the entire assembly was in place, the team struggled to manage the loose tubing which often fell apart during assembly of the rest of the system. To reduce complication and minimize the number of connections in the current system, a distributor was designed with a separate line branch for each thruster in a twelve-thruster configuration. This new design reduced the number of connections from 26 to 24 and shortened tubes, thus reducing frictional losses. Although these design changes appear to decrease the number of connection points by only two while adding a significant amount of mass with the addition of the distributor, the 26 connections in the original design accommodated only eight thrusters. The new design, runs tubing routes to twelve thrusters with only 24 connectors. The eight-thruster configuration, extrapolated to a twelve thrusters and relying on the original method of splitting the propellant lines, would require as many as 39 different connection points. The new design, therefore, represents a more significant improvement than is immediately apparent.

Based on an analysis of the propellant tubing, and assuming a clamped-clamped boundary condition, a maximum length of 0.396 m can be used while maintaining a natural frequency of 100 Hz. The length of the tubing, therefore can be roughly equal to height of the MR SAT's height without concern [32]. The longest tube length in this configuration is approximately 24.75 cm; the shortest and longest connections on the original eight-thruster configuration were approximately 28.84 and 55.15 cm respectfully.

This change represents a 55.11% reduction from the worst-case tube length for the Nanosat 4 design. Even more surprising, the longest tubing in the new design is 14.17% shorter than the shortest tube length in the Nanosat 4 design, resulting in a significant reduction in frictional tube losses. Figure B.11 shows the current distributor design. (See Section 5 for additional information.)

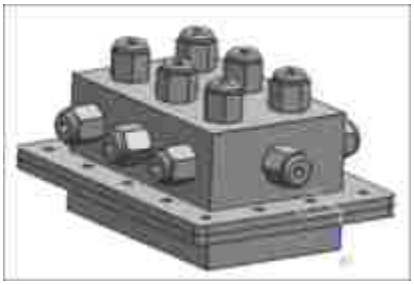

Figure B.11. MR SAT Propellant Distributor

B.2.2.6. Heaters and MLI. To maintain thermodynamic equilibrium and propulsive efficiencies, heaters were added to the system to replace the heat lost when the thrusters are fired. Because the R-134a is stored as a saturated liquid propellant, and because vapor propellant is expelled to generate thrust, some of the liquid propellant must evaporate to replace the vapor and maintain equilibrium. To sustain this equilibrium, heat must be added to the system; otherwise, the tank pressure drops to compensate for the loss of liquid propellant. When tank pressure drops below the regulated pressure, thrust is reduced.

The MR SAT propulsion system is currently designed to use two heaters, one on the propulsion tank and the other inside the distributor. The heater selected for the propulsion tank is manufactured by Minco and consists of a heating element wrapped with a polymide film (Kapton) insulator with an aluminum backing for mounting; it meets all outgassing limitations defined by ARFL's Nanosat 6 User's Guide [25], [28].

The tank heater is rated to a maximum power of 3.63 Watts, and while in orbit, it will be powered by a 24 V bus. Figure B.6 shows the tank heater installed on the propellant tank.

A heater installed in the distributor will heat the propellant for maximum efficiency. This heater serves two primary functions in the MR SAT propulsion system: First, it ensures that if any liquid propellant enters the distributor, it will be supplied with enough energy to change phases to vapor form. Second, although the tank heater helps to maintain thermodynamic equilibrium, the energy transfer relies on conduction through the tank walls into the PMD before absorption by the propellant. Because the heater is located inside the distributor, the gaseous propellant should flow directly over the heater so that heat is transferred efficiently to the fluid. As indicated in Section 3, higher propellant temperatures lead to significant increases in thrust. To maximize the heat transferred to the propellant, the system will use a heat sink structure like those used in computers. Computer heat sinks use vertical fins to create a large surface area so that more energy can be transferred to air as it moves through the structure, cooling the computer. This setup will work in a similar fashion. In the MR SAT propulsion system, a heater will be located on the bottom of the distributor and the heat placed on top. Once the heater is turned on, the heat sink will begin to conduct the heat. As R-134a flows into the distributor, it will remove heat from the heat sink, increasing the fluid's temperature. The heater and heat sink specifications have not yet been determined; however, Figure B.12 a preliminary schematic is shown in Figure B.12.

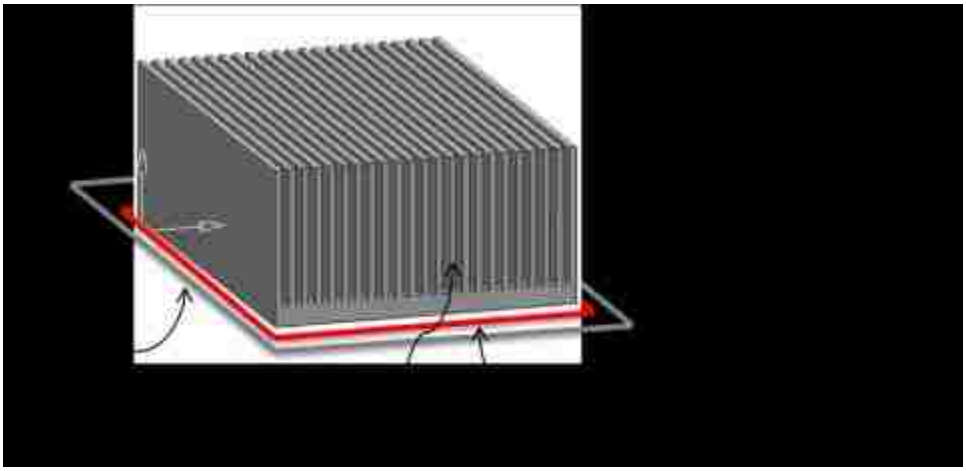

Figure B.12. Distributor Heater Assembly

To ensure optimum efficiency of the propulsion system, multilayer insulation (MLI) will be used to wrap the tank and distributor to minimize heat losses due to radiation. MLI consists of multiple sheets of insulation layered together to provide a thermal blanket that inhibits radiation loss and provides passive temperature control for the propulsion system [28].

APPENDIX C

MATLAB PROGRAMS USED TO ANALYSE EXPERIMENTAL DATA AND PREDICT SYSTEM PERFORMANCE

The MATLAB programs presented in this section were used to analyze the various data files gathered from the parametric study and endurance test and present them in convenient plots.

C1. Parametric Study

```
% MASTER RESEARCH - Parametric Study
%
% This program calculates the performance parameters (Delta V, Isp, and
% thrust) for a range of temperatures and pressures using a thruster
% from the MR SAT propulsion system.
%
% Ryan Pahl
% Oct. 10, 2009


%% Initialize Program

clc;
clear all;
close all;

%% Constants

%%% Satellite properties
mass_MR_dry = 26;   % MR SAT dry mass (kg)
vol_tank = 0.0025;  % Propultion tank volume (m^3)
g_0 = 9.81;         % Earth's gravitational constant (m/s^2)


% Nozzle geometry
D_exit = 5e-3;      % Nozzle exit diameter (m)
AR = 100;           % Nozzle aspect ratio (-)

% R-134a properties
gamma = 1.127;       % Specific heat ratio of R-134a at test conditions
MW = 102.0308928;    % Molecular weight of R-134a [CH2FCF3] (kg/kmol)
R_univ = 8314.51;    % Universal gas constant (J/(kmol-K))
mass_prop = 0.06736; % Propellant mass (kg)
num_props = length( mass_prop );

font = 'Times';      % Sets font for plots
fig_font = 20;       % Sets font size for plots
mark_size = 3;       % Set marker size on figures
exp_err = 0.00218;   % Error due to experiment components (mN)

%% Initialize Arrays

percent_dV = zeros( num_props );
```

```
%% Theoretical Data

% Get data from MATLAB binary file "Theoretical Data".  Origianl
% data can be found in excel file "Theoretical Data.xlsx"

load Theoretical_Data;
T_c_Array = Temperature.Tbl;
P_c_Array = Pressure.Tbl;
Thrust = Thrust.Tbl;
m_dot = m_dot.Tbl;
dV = dV.Tbl;

% Generate theoretical arrays as a function of temperature
% Temperature = 0 C
T_0_theory( : , 1 ) = T_c_Array( 1 , : )';
T_0_theory( : , 2 ) = P_c_Array( 1 , : )';
T_0_theory( : , 3 ) = Thrust( 1 , : )';
T_0_theory( : , 4 ) = m_dot( 1 , : )';
T_0_theory( : , 5 ) = dV( 1 , : )';

% Temperature = 10 C
T_10_theory( : , 1 ) = T_c_Array( 11 , : )';
T_10_theory( : , 2 ) = P_c_Array( 11 , : )';
T_10_theory( : , 3 ) = Thrust( 11 , : )';
T_10_theory( : , 4 ) = m_dot( 11 , : )';
T_10_theory( : , 5 ) = dV( 11 , : )';

% Temperature = 20 C
T_20_theory( : , 1 ) = T_c_Array( 21 , : )';
T_20_theory( : , 2 ) = P_c_Array( 21 , : )';
T_20_theory( : , 3 ) = Thrust( 21 , : )';
T_20_theory( : , 4 ) = m_dot( 21 , : )';
T_20_theory( : , 5 ) = dV( 21 , : )';

% Temperature = 30 C
T_30_theory( : , 1 ) = T_c_Array( 31 , : )';
T_30_theory( : , 2 ) = P_c_Array( 31 , : )';
T_30_theory( : , 3 ) = Thrust( 31 , : )';
T_30_theory( : , 4 ) = m_dot( 31 , : )';
T_30_theory( : , 5 ) = dV( 31 , : )';

% Temperature = 40 C
T_40_theory( : , 1 ) = T_c_Array( 41 , : )';
T_40_theory( : , 2 ) = P_c_Array( 41 , : )';
T_40_theory( : , 3 ) = Thrust( 41 , : )';
T_40_theory( : , 4 ) = m_dot( 41 , : )';
T_40_theory( : , 5 ) = dV( 41 , : )';


%% Actual Data

% Reads in test data from MATLAB binary file Parametric_Study_data
% in the following format:
% [ Temp (C), Pres (psia) , Actual Pres (psia) , Thrust (g) ,
```

```
% Thrust (mN) ]

load Parametric_Study_Data;

% Test 1
T_0_1 = T_0_1.Tbl;
T_10_1 = T_10_1.Tbl;
T_20_1 = T_20_1.Tbl;
T_30_1 = T_30_1.Tbl;
T_40_1 = T_40_1.Tbl;

% Test 2
T_0_2 = T_0_2.Tbl;
T_10_2 = T_10_2.Tbl;
T_20_2 = T_20_2.Tbl;
T_30_2 = T_30_2.Tbl;

% Test 3
T_0_3 = T_0_3.Tbl;
T_10_3 = T_10_3.Tbl;
T_20_3 = T_20_3.Tbl;
T_30_3 = T_30_3.Tbl;
T_40_3 = T_40_3.Tbl;


%% Calculations

% R-134a properties
R = R_univ / MW;    % Gas constant of R-134a (J/(kg-K))

% Nozzle geometry
A_exit = ( pi / 4 ) * ( D_exit ^ 2 );         % Exit area (m^2)
D_throat = sqrt( 4 * A_exit / ( pi * AR ) );  % Throat diameter (m)
A_throat = A_exit / AR;                       % Throat area (m^2)

%%% Find Pressure Ratio, PR (Pe/Pc), using secant method as a funtion
% of area ratio and gamma.
PR_guess_1 = 0.001; % First guess, used in secant method to find root
PR_guess_2 = 0.01;  % Second guess, used in secant method to find root
tolerance = 1e-16;  % Accuracy of root to previous iteration

% Function of Aspect Ratio in terms of Pressure Ratio and gamma
f_PR = @( PR_i ) sqrt( ( ( ( gamma - 1 ) / 2 ) * ( 2 / ...
    ( gamma + 1 ) ) ^ ( ( gamma + 1 ) / ( gamma - 1 ) ) ) / ...
    ( PR_i ^ ( 2 / gamma ) * ( 1 - PR_i ^ ( ( gamma - 1 ) / ...
    gamma ) ) ) ) - AR;

% Solve using secant method solver
PR = Secant_Method( PR_guess_1 , PR_guess_2 , f_PR , tolerance );

% Put all data from a test into a single array
test_1_data = [ T_0_1 ; T_10_1 ; T_20_1 ; T_30_1 ; T_40_1 ];
test_2_data = [ T_0_2 ; T_10_2 ; T_20_2 ; T_30_2 ];
test_3_data = [ T_0_3 ; T_10_3 ; T_20_3 ; T_30_3 ; T_40_3 ];
```

```
% Combine all test arrays into a single array
data_array = [ test_1_data ; test_2_data ; test_3_data ];

%% Determine actual performance values

[ data_rows , data_cols ] = size( data_array );

% create column for actual I_sp
data_array( : , ( data_cols + 1 ) ) = 0;

% create column for actual dV
data_array( : , ( data_cols + 2 ) ) = 0;

for iii = 1 : data_rows

    % Sonic velocity (m/s)
    a_0 = sqrt( gamma * R * ( data_array( iii , 1 ) + 273.15 ) ) ;

    % Characteristic velocity (m/s)
    c_star = a_0 / ( gamma * ( 2 / ( gamma + 1 ) ) ^ ...
        ( ( gamma + 1 ) / ( 2 * gamma - 2 ) ) );

    % Mass flow rate (kg/s)
    m_dot = A_throat * ( ( data_array( iii , 3 ) / 14.6959487560 ) ...
        * 101325 ) / c_star;

    % Specific Impulse (s)
    I_sp = data_array( iii , 5 ) / ( m_dot * g_0 );

    % Delta V (m/s)
    dV = g_0 * I_sp * log( ( mass_MR_dry + mass_prop ) / mass_MR_dry );

    % Insert dV into data_array
    data_array( iii , ( data_cols + 2 ) ) = dV;

    % Insert I_sp into data_array
    data_array( iii , ( data_cols + 1 ) ) = I_sp;
end

%% Determine theoretical values based on actual temperature
% and pressure

% Pre-allocate columns in data_array for speed

% create column for theoretical thrust
data_array( : , ( data_cols + 3 ) ) = 0;

% create column for theoretical Isp
data_array( : , ( data_cols + 4 ) ) = 0;

% create column for theoretical dV
data_array( : , ( data_cols + 5 ) ) = 0;
```

```
% create column for percent of theoretical thrust
data_array( : , ( data_cols + 6 ) ) = 0;

% create column for percent of theoretical Isp
data_array( : , ( data_cols + 7 ) ) = 0;

% create column for percent of theoretical dV
data_array( : , ( data_cols + 8 ) ) = 0;

for iii = 1 : data_rows

    % Nozzle exit pressure (Pa)
    P_exit = ( ( data_array( iii , 3 ) / 14.6959487560497 ) * ...
        101325 ) * PR;

    % Sonic velocity (m/s)
    a_0 = sqrt( gamma * R * ( data_array( iii , 1 ) + 273.15 ) ) ;

    % Characteristic velocity (m/s)
    c_star = a_0 / ( gamma * ( 2 / ( gamma + 1 ) ) ^ ...
        ( ( gamma + 1 ) / ( 2 * gamma - 2 ) ) );

    % Ideal Specific Impulse (seconds)
    I_sp = ( c_star * gamma / g_0 ) * sqrt( ( 2 / ( gamma - 1 ) ) * ...
        ( 2 / ( gamma + 1 ) ) ^ ( ( gamma + 1 ) / ( gamma - 1 ) ) * ...
        ( 1 - PR ^ ( ( gamma - 1 ) / gamma ) ) );

    % Calculate percent of theoretical Specific Impulse
    percent_Isp = data_array( iii , ( data_cols + 1 ) ) / I_sp;

    % Calculate delta V
    dV = g_0 * I_sp * log( ( mass_MR_dry + mass_prop ) / mass_MR_dry );

    % Calculate percent of theoretical dV
    percent_dV = data_array( iii , ( data_cols + 2 ) ) / dV;

    % Force (N)
    Thrust = A_throat * ( ( data_array( iii , 3 ) / 14.6959487560 ) ...
        * 101325 ) * gamma * sqrt( ( 2 / ( gamma - 1 ) ) * ( 2 / ...
        ( gamma + 1 ) ) ^ ( ( gamma + 1 ) / ( gamma - 1 ) ) * ...
        ( 1 - PR ^ ( ( gamma - 1 ) / gamma ) ) ) + P_exit * A_exit;

    % Calculate percent of theoretical thrust
    percent_Thrust = data_array( iii , 5 ) / Thrust;

    % Insert theoretical thrust into data_array
    data_array( iii , ( data_cols + 3 ) ) = Thrust;

    % Insert theoretical I_sp into data_array
    data_array( iii , ( data_cols + 4 ) ) = I_sp;

    % Insert theoretical dV into data_array
    data_array( iii , ( data_cols + 5 ) ) = dV;
```

```
    % Insert percent of theoretical thrust into data_array
    data_array( iii , ( data_cols + 6 ) ) = percent_Thrust;

    % Insert percent of theoretical Isp into data_array
    data_array( iii , ( data_cols + 7 ) ) = percent_Isp;

    % Insert percent of theoretical dV into data_array
    data_array( iii , ( data_cols + 8 ) ) = percent_dV;
end


%% Plot

%%% Plot individual points
figure (1)
hold on

% Plot theoretical data
plot( T_0_theory( : , 2 ) , T_0_theory( : , 3 ) , '-r' , 'MarkerSize' ,
mark_size );
plot( T_10_theory( : , 2 ) , T_10_theory( : , 3 ) , '-g' , 'MarkerSize'
, mark_size );
plot( T_20_theory( : , 2 ) , T_20_theory( : , 3 ) , '-k' , 'MarkerSize'
, mark_size );
plot( T_30_theory( : , 2 ) , T_30_theory( : , 3 ) , '-b' , 'MarkerSize'
, mark_size );
plot( T_40_theory( : , 2 ) , T_40_theory( : , 3 ) , '-m' , 'MarkerSize'
, mark_size );

% Plot test 1 data
plot( T_0_1( : , 3 ) , T_0_1( : , 5 ) , '.r' , 'MarkerSize' , mark_size
);
plot( T_10_1( : , 3 ) , T_10_1( : , 5 ) , '.g' , 'MarkerSize' ,
mark_size );
plot( T_20_1( : , 3 ) , T_20_1( : , 5 ) , '.k' , 'MarkerSize' ,
mark_size );
plot( T_30_1( : , 3 ) , T_30_1( : , 5 ) , '.b' , 'MarkerSize' ,
mark_size );
plot( T_40_1( : , 3 ) , T_40_1( : , 5 ) , '.m' , 'MarkerSize' ,
mark_size );

% Plot test 2 data
plot( T_0_2( : , 3 ) , T_0_2( : , 5 ) , '+r' , 'MarkerSize' , mark_size
);
plot( T_10_2( : , 3 ) , T_10_2( : , 5 ) , '+g' , 'MarkerSize' ,
mark_size );
plot( T_20_2( : , 3 ) , T_20_2( : , 5 ) , '+k' , 'MarkerSize' ,
mark_size );
plot( T_30_2( : , 3 ) , T_30_2( : , 5 ) , '+b' , 'MarkerSize' ,
mark_size );

% Plot test 3 data
plot( T_0_3( : , 3 ) , T_0_3( : , 5 ) , 'dr' , 'MarkerSize' , mark_size
);
```

```
plot( T_10_3( : , 3 ) , T_10_3( : , 5 ) , 'dg' , 'MarkerSize' ,
mark_size );
plot( T_20_3( : , 3 ) , T_20_3( : , 5 ) , 'dk' , 'MarkerSize' ,
mark_size );
plot( T_30_3( : , 3 ) , T_30_3( : , 5 ) , 'db' , 'MarkerSize' ,
mark_size );
plot( T_40_3( : , 3 ) , T_40_3( : , 5 ) , 'dm' , 'MarkerSize' ,
mark_size );

title('Thrust vs. Pressure','FontSize',fig_font,'FontName',font);
xlabel('Pressure (psia)','FontSize',fig_font,'FontName',font);
ylabel('Thrust (N)','FontSize',fig_font,'FontName',font);
set(gca,'FontSize',fig_font,'FontName',font); % changes the size and
font of the axis numbers

hold off

%%% Plot individual points
figure (2)
hold on

% Plot theoretical data
p1=plot( T_0_theory( : , 2 ) , T_0_theory( : , 3 ) , '-r' ,
'MarkerSize' , mark_size );
p2=plot( T_10_theory( : , 2 ) , T_10_theory( : , 3 ) , '-g' ,
'MarkerSize' , mark_size );
p3=plot( T_20_theory( : , 2 ) , T_20_theory( : , 3 ) , '-k' ,
'MarkerSize' , mark_size );
p4=plot( T_30_theory( : , 2 ) , T_30_theory( : , 3 ) , '-b' ,
'MarkerSize' , mark_size );
p5=plot( T_40_theory( : , 2 ) , T_40_theory( : , 3 ) , '-m' ,
'MarkerSize' , mark_size );

% Plot test 1 data
p6=errorbar( T_0_1( : , 7 ) , T_0_1( : , 8 ) , T_0_1( : , 9 ) + exp_err
, '.r' , 'MarkerSize' , mark_size + 2 );
p7=errorbar( T_10_1( : , 7 ) , T_10_1( : , 8 ) , T_10_1( : , 9 ) +
exp_err , '.g' , 'MarkerSize' , mark_size + 2 );
p8=errorbar( T_20_1( : , 7 ) , T_20_1( : , 8 ) , T_20_1( : , 9 ) +
exp_err , '.k' , 'MarkerSize' , mark_size + 2 );
p9=errorbar( T_30_1( : , 7 ) , T_30_1( : , 8 ) , T_30_1( : , 9 ) +
exp_err , '.b' , 'MarkerSize' , mark_size + 2 );
p10=errorbar( T_40_1( : , 7 ) , T_40_1( : , 8 ) , T_40_1( : , 9 ) +
exp_err , '.m' , 'MarkerSize' , mark_size + 2 );

% Plot test 2 data
p11=errorbar( T_0_2( : , 7 ) , T_0_2( : , 8 ) , T_0_2( : , 9 ) +
exp_err , '+r' , 'MarkerSize' , mark_size );
p12=errorbar( T_10_2( : , 7 ) , T_10_2( : , 8 ) , T_10_2( : , 9 ) +
exp_err , '+g' , 'MarkerSize' , mark_size );
p13=errorbar( T_20_2( : , 7 ) , T_20_2( : , 8 ) , T_20_2( : , 9 ) +
exp_err , '+k' , 'MarkerSize' , mark_size );
p14=errorbar( T_30_2( : , 7 ) , T_30_2( : , 8 ) , T_30_2( : , 9 ) +
exp_err , '+b' , 'MarkerSize' , mark_size );
```

```
% Plot test 3 data
p15=errorbar( T_0_3( : , 7 ) , T_0_3( : , 8 ) , T_0_3( : , 9 ) +
exp_err , 'dr' , 'MarkerSize' , mark_size );
p16=errorbar( T_10_3( : , 7 ) , T_10_3( : , 8 ) , T_10_3( : , 9 ) +
exp_err , 'dg' , 'MarkerSize' , mark_size );
p17=errorbar( T_20_3( : , 7 ) , T_20_3( : , 8 ) , T_20_3( : , 9 ) +
exp_err , 'dk' , 'MarkerSize' , mark_size );
p18=errorbar( T_30_3( : , 7 ) , T_30_3( : , 8 ) , T_30_3( : , 9 ) +
exp_err , 'db' , 'MarkerSize' , mark_size );
p19=errorbar( T_40_3( : , 7 ) , T_40_3( : , 8 ) , T_40_3( : , 9 ) +
exp_err , 'dm' , 'MarkerSize' , mark_size );

title('Thrust vs. Pressure','FontSize',fig_font,'FontName',font);
xlabel('Pressure (psia)','FontSize',fig_font,'FontName',font);
ylabel('Thrust (N)','FontSize',fig_font,'FontName',font);
set(gca,'FontSize',fig_font-5,'FontName',font); % changes the size and
font of the axis numbers
l1 =
legend([p5,p6,p7,p8,p9,p10,p11,p12,p13,p14,p15,p16,p17,p18,p19],...
    'Theoretical','Test 1, 0 C','Test 1, 10 C','Test 1, 20 C','Test 1,
30 C','Test 1, 40 C','Test 2, 0 C','Test 2, 10 C','Test 2, 20 C','Test
2, 30 C','Test 3, 0 C','Test 3, 10 C','Test 3, 20 C','Test 3, 30
C','Test 3, 40 C'); % Create legend for figure

hold off


%% Write Data Array (Results) into Matlab Binary or Excel File

% Save data as binary matlab file
data.Lbl = (' Temperature (C) , Pressure (psia) , Actual Pressure
(psia) , Thrust (g) , Thrust (mN) , Avg Temp (C) , Avg Press (psia) ,
Avg Thrust (mN) , Std Dev , Isp (s) , dV (m/s) , Theoretical Thrust
(mN) , Theoretical Isp (s) , Theoretical dV (m/s) , Percent of
Theoretical Thrust , Percent of Theoretical Isp , Percent of
Theoretical dV ');
data.Tbl = data_array;
save Parametric_Study_Results data

% Save data in excel 2007 format
xlswrite( 'Theoretical Data.xlsx', data_array , 'data array' , 'A4' )
```

C2. Calculate Error Bars

```
% MASTER RESEARCH - Calculate Error Bars
%
% This program calculates the average temperature, pressure, and thrust
of
% a set of data points and finds the standard deviation based on a
% statistical approach.
%
% Ryan Pahl
% April 4, 2010
```

```
%% Initialize Program
% Take in a data array, find the averages and append them to the end of
the
% array and return to user.
function [data_array] = Calc_Err_Bars(data_array)


%% Constants

% Number of data points per temperature-pressure combination tested
num_points = 5;

% Counter for array indexing
counter = 0;
n=1;

% Wanted a 95% confidence with only 5 data points, resulting in 4
degrees
% of freedom (v=n-1 -> v=5-1=4) [37]
t_distribution = 2.776;

%% Calculatinos

% Find size of array
[data_rows,data_cols]=size(data_array);

while n <= data_rows
    counter = counter + 1;

    % If more than num_points points remaining
    if (data_rows-n) >= num_points

        % Calculate average temperature
        avg_temp = mean(data_array(n:n+4,1));

        % Calculate average pressure
        avg_press = mean(data_array(n:n+4,3));

        % Calculate average thrust
        avg_thrust = mean(data_array(n:n+4,5));

        % Calculate standard deviation
        std_dev = std(data_array(n:n+4,5));

        % Error in measurements
        err = t_distribution * std_dev / sqrt( num_points );

        for iii = 0:num_points-1
            % Append new values to end of data array
            data_array(n+iii,data_cols+1:data_cols+4) = [avg_temp,...
                avg_press,avg_thrust,err];
        end
    else
```

```
        % Calculate average temperature
        avg_temp = mean(data_array(n:data_rows,1));

        % Calculate average pressure
        avg_press = mean(data_array(n:data_rows,3));

        % Calculate average thrust
        avg_thrust = mean(data_array(n:data_rows,5));

        % Calculate standard deviation
        std_dev = std(data_array(n:data_rows,5));

        % Error in measurements
        err = t_distribution * std_dev / sqrt( data_rows-n );

        for iii = 0:data_rows-n
            % Append new values to end of data array
            data_array(n+iii,data_cols+1:data_cols+4) = [avg_temp,...
                avg_press,avg_thrust,err];
        end
    end

    % Data points were tested in groups of 5.  May need to change for
    % larger sample sizes.
    n=n+5;
end
```

C3. R-134a Heating Time

```
% MASTER RESEARCH - R-134a Heating Time
%
% Determine time needed for can of R-134a to heat to desired
% temperature in a hot water bath given the initial temperature
% of both the R-134a and water bath.
%
% Ryan Pahl
% Dec. 8, 2009


%% Initialize Program

clc;
clear all;
close all;

%% Constants

% Diameter of R-134a can used in test [m]
can_diameter = 0.0762;

% Thickness of R-134a can usid in test [m]
x = 0.004;
```

```
% Height of R-134a can used in test [m]
can_height = 0.1016;

% Heat capacity of R-134a liquid at 25 C [kcal/(kg-K)]
Cp_f = 0.339;

% Heat capacity of R-134a gas at 25 C and 1 atm [kcal/(kg-K)]
Cp_g = 0.204;

% Thermal conductivity of R-134a at 25 C [W/(m-K)]
k = 0.0824;

% Ambient temperature of room (assume this is starting temperature
% for can of R-134a) [C]
T_0 = 20;

% Temperature of hot water bath [C]
T = [ 30 , 40 , 50 ];

% Incremental time step [s]
dt = 0.001;

% Mass of R-134a in can [kg]
m = 0.340;

%% Initialize Arrays

time = zeros( 1 , length( T ) );

%% Calculations

% Cross-sectional area of can of R-134a, A [m^2]
A = ( pi / 4 ) * can_diameter ^ 2;

% Volume of can of R-134a, V [m^3]
V = ( pi / 4 ) * can_diameter ^ 2 * can_height;

% Quality of 340 grams of R-134a in a 4.6333e-004 volume at 1 psi
% and 30, 40 and 50 C respectfully (R-134a Daemon [40])
X = [ 2.010 , 2.558 , 3.200 ];

% Since X ~= 0, assume all R-134a is fluid, therefore
% Cp = Cp_f = 0.339 [W/(m-K)]
Cp = Cp_f;

% If X is not ~= 0, calculate Cp using Cp_g and Cp_f
%{
for iii = 1 : length( X )
    % Caclculate Cp of two-phase fluid using quality
    Cp( iii ) = Cp_f + X( iii ) * ( Cp_g - Cp_f);
end
%}
```

```
for iii = 1 : length( T )

    counter = 0;

    % Set initial temp of R-134a to ambient temperature of room [C]
    T_R134a = T_0;

    while ( T( iii ) - T_R134a ) / T_R134a > 0.0001 %&& counter < 1000

        counter = counter + 1;

        % Determine how much energy, Q [J], is added to the can of
        % propellant in a small 'dt' time.  dQ/dt = k*A*(T-T_0)/x
        dQ = k * A * ( T( iii ) - T_R134a ) * dt / x;

        % Determine the final temperature based on how much energy was
        % transfered to R-134a fluid [K]
        T_R134a = dQ / ( m * Cp ) + T_R134a;

    end
    time( iii ) = counter * dt;
end
```

C4. Endurance Test

```
%% Endurance Test
%
% Program takes the raw data from the MIS cart during the endurance
% test and coverts it to usable values of temperature and pressure
% and then plots the resulting data.  The goal is to analyze the
% duration of firing as funtion of initial propellant mass with
% heaters on versus the case with the heaters off to see what
% difference is made in regard to increasing the firing duration.
% Finally, the data will show precisely how much heat is lost from
% the system when firing continuously by monitoring the temperature
% drop in the system.
%
% Ryan Pahl
% Feb. 17, 2010


%% Initialize Program

clc;
close all;
clear all;

%% Constants

font = 'Times';      % Sets font for plots
fig_font = 20;       % Sets font size for plots
```

```
%% Calculations

% Read raw data from matlab binary files.  Original files are in txts
% format.

load Endurance_Data;

row_array(1) = length(no_heater(60).Tbl);
row_array(2) = length(no_heater(120).Tbl);
row_array(3) = length(no_heater(180).Tbl);
row_array(4) = length(no_heater(250).Tbl);
row_array(5) = length(no_heater(350).Tbl);
row_array(6) = length(no_heater(460).Tbl);
row_array(7) = length(heater(60).Tbl);
row_array(8) = length(heater(120).Tbl);
row_array(9) = length(heater(180).Tbl);
row_array(10) = length(heater(250).Tbl);
row_array(11) = length(heater(350).Tbl);
row_array(12) = length(heater(460).Tbl);

raw(1:length(no_heater(60).Tbl),:,1) = no_heater(60).Tbl;
raw(1:length(no_heater(120).Tbl),:,2) = no_heater(120).Tbl;
raw(1:length(no_heater(180).Tbl),:,3) = no_heater(180).Tbl;
raw(1:length(no_heater(250).Tbl),:,4) = no_heater(250).Tbl;
raw(1:length(no_heater(350).Tbl),:,5) = no_heater(350).Tbl;
raw(1:length(no_heater(460).Tbl),:,6) = no_heater(460).Tbl;
raw(1:length(heater(60).Tbl),:,7) = heater(60).Tbl;
raw(1:length(heater(120).Tbl),:,8) = heater(120).Tbl;
raw(1:length(heater(180).Tbl),:,9) = heater(180).Tbl;
raw(1:length(heater(250).Tbl),:,10) = heater(250).Tbl;
raw(1:length(heater(350).Tbl),:,11) = heater(350).Tbl;
raw(1:length(heater(460).Tbl),:,12) = heater(460).Tbl;

[ rows , cols , sets ] = size( raw );

calibrated(:,:,1:sets) = zeros(size(raw(:,:,1:sets)));

% Copy data from raw to calibrated and apply calibration
for jjj = 1 : sets

    % Uses the calibration curves to convert from voltage to
    % usable values
    calibrated(:,1,jjj)=raw(:,1,jjj);  % time
    calibrated(:,2,jjj)=113.64*raw(:,2,jjj)-79.545; % Tank temp (C)
    calibrated(:,3,jjj)=114.29*raw(:,3,jjj)-80.571; % Line temp (C)
    calibrated(:,4,jjj)=9.6086*raw(:,4,jjj)-0.3421; % Load cell (g)
    calibrated(:,5,jjj)=40.3828*raw(:,5,jjj)-0.6016;% Line press (psia)
    calibrated(:,6,jjj)=40.315*raw(:,6,jjj)+1.3959; % Tank press (psia)
    calibrated(:,7,jjj)=113.64*raw(:,7,jjj)-78.977; % Thruster temp (C)
end

%% Plot

% Plot all pressures vs. time
```

```
figure(1)
hold on
for jjj = 1 : sets
    p1=plot(calibrated(1:row_array(jjj),1,jjj),...
        calibrated(1:row_array(jjj),5,jjj),'-b');
    p2=plot(calibrated(1:row_array(jjj),1,jjj),...
        calibrated(1:row_array(jjj),6,jjj),'-r');
end

title('System Pressure vs. Time','FontSize',fig_font,'FontName',font);
xlabel('Time (s)','FontSize',fig_font,'FontName',font);
ylabel('Pressure (psia)','FontSize',fig_font,'FontName',font);
set(gca,'FontSize',fig_font,'FontName',font); % changes the size and
font of the axis numbers
l1 = legend([p1,p2],'No Heater','Heater'); % Create legend for figure
hold off;

% Plot all temperatures vs. time

figure(2)
hold on
for jjj = 1 : sets
    p3=plot(calibrated(1:row_array(jjj),1,jjj),...
        calibrated(1:row_array(jjj),2,jjj),'-b');
end

title('Tank Temperatur vs. Time','FontSize',fig_font,'FontName',font);
xlabel('Time (s)','FontSize',fig_font,'FontName',font);
ylabel('Temperature (C)','FontSize',fig_font,'FontName',font);
set(gca,'FontSize',fig_font,'FontName',font); % changes the size and
font of the axis numbers
l2 = legend(p3,'No Heater'); % Create legend for figure
hold off;

%%% Plot pressure vs. time for individual masses

% Plot 60 grams pressure vs. time with and without heaters
figure(3)
hold on
% 60 grams without heaters first
p4=plot(calibrated(1:row_array(1),1,1),...
    calibrated(1:row_array(1),5,1),'-c');
p5=plot(calibrated(1:row_array(1),1,1),...
    calibrated(1:row_array(1),6,1),'-m');

% 60 grams with heaters second
p6=plot(calibrated(1:row_array(7),1,7),...
    calibrated(1:row_array(7),5,7),'-b');
p7=plot(calibrated(1:row_array(7),1,7),...
    calibrated(1:row_array(7),6,7),'-r');

title('System Pressure vs. Time for 60
grams','FontSize',fig_font,'FontName',font);
xlabel('Time (s)','FontSize',fig_font,'FontName',font);
```

```
ylabel('Pressure (psia)','FontSize',fig_font,'FontName',font);
set(gca,'FontSize',fig_font,'FontName',font); % changes the size and
font of the axis numbers
l3 = legend([p4,p5,p6,p7],'Line Pressure, No Heater','Tank Pressure, No
Heater','Line Pressure, Heater','Tank Pressure, Heater'); % Create
legend for figure
hold off;

% Plot 120 grams pressure vs. time with and without heaters
figure(4)
hold on
% 120 grams without heaters first
p8=plot(calibrated(1:row_array(2),1,2),...
    calibrated(1:row_array(2),5,2),'-c');
p9=plot(calibrated(1:row_array(2),1,2),...
    calibrated(1:row_array(2),6,2),'-m');

% 120 grams with heaters second
p10=plot(calibrated(1:row_array(8),1,8),...
    calibrated(1:row_array(8),5,8),'-b');
p11=plot(calibrated(1:row_array(8),1,8),...
    calibrated(1:row_array(8),6,8),'-r');

title('System Pressure vs. Time for 120
grams','FontSize',fig_font,'FontName',font);
xlabel('Time (s)','FontSize',fig_font,'FontName',font);
ylabel('Pressure (psia)','FontSize',fig_font,'FontName',font);
set(gca,'FontSize',fig_font,'FontName',font); % changes the size and
font of the axis numbers
l4 = legend([p8,p9,p10,p11],'Line Pressure, No Heater','Tank Pressure,
No Heater','Line Pressure, Heater','Tank Pressure, Heater'); % Create
legend for figure
hold off;

% Plot 180 grams pressure vs. time with and without heaters
figure(5)
hold on
% 180 grams without heaters first
p12=plot(calibrated(1:row_array(3),1,3),...
    calibrated(1:row_array(3),5,3),'-c');
p13=plot(calibrated(1:row_array(3),1,3),...
    calibrated(1:row_array(3),6,3),'-m');

% 180 grams with heaters second
p14=plot(calibrated(1:row_array(9),1,9),...
    calibrated(1:row_array(9),5,9),'-b');
p15=plot(calibrated(1:row_array(9),1,9),...
    calibrated(1:row_array(9),6,9),'-r');


title('System Pressure vs. Time for 180
grams','FontSize',fig_font,'FontName',font);
xlabel('Time (s)','FontSize',fig_font,'FontName',font);
ylabel('Pressure (psia)','FontSize',fig_font,'FontName',font);
```

```
set(gca,'FontSize',fig_font,'FontName',font); % changes the size and
font of the axis numbers
l5 = legend([p12,p13,p14,p15],'Line Pressure, No Heater','Tank
Pressure, No Heater','Line Pressure, Heater','Tank Pressure, Heater');
% Create legend for figure
hold off;

% Plot 250 grams pressure vs. time with and without heaters
figure(6)
hold on
% 250 grams without heaters first
p16=plot(calibrated(1:row_array(4),1,4),...
    calibrated(1:row_array(4),5,4),'-c');
p17=plot(calibrated(1:row_array(4),1,4),...
    calibrated(1:row_array(4),6,4),'-m');

% 250 grams with heaters second
p18=plot(calibrated(1:row_array(10),1,10),...
    calibrated(1:row_array(10),5,10),'-b');
p19=plot(calibrated(1:row_array(10),1,10),...
    calibrated(1:row_array(10),6,10),'-r');

title('System Pressure vs. Time for 250
grams','FontSize',fig_font,'FontName',font);
xlabel('Time (s)','FontSize',fig_font,'FontName',font);
ylabel('Pressure (psia)','FontSize',fig_font,'FontName',font);
set(gca,'FontSize',fig_font,'FontName',font); % changes the size and
font of the axis numbers
l6 = legend([p16,p17,p18,p19],'Line Pressure, No Heater','Tank
Pressure, No Heater','Line Pressure, Heater','Tank Pressure, Heater');
% Create legend for figure
hold off;

% Plot 350 grams pressure vs. time with and without heaters
figure(7)
hold on
% 350 grams without heaters first
p20=plot(calibrated(1:row_array(5),1,5),...
    calibrated(1:row_array(5),5,5),'-c');
p21=plot(calibrated(1:row_array(5),1,5),...
    calibrated(1:row_array(5),6,5),'-m');

% 350 grams with heaters second
p22=plot(calibrated(1:row_array(11),1,11),...
    calibrated(1:row_array(11),5,11),'-b');
p23=plot(calibrated(1:row_array(11),1,11),...
    calibrated(1:row_array(11),6,11),'-r');

title('System Pressure vs. Time for 350
grams','FontSize',fig_font,'FontName',font);
xlabel('Time (s)','FontSize',fig_font,'FontName',font);
ylabel('Pressure (psia)','FontSize',fig_font,'FontName',font);
set(gca,'FontSize',fig_font,'FontName',font); % changes the size and
font of the axis numbers
```

```
l7 = legend([p20,p21,p22,p23],'Line Pressure, No Heater','Tank
Pressure, No Heater','Line Pressure, Heater','Tank Pressure, Heater');
% Create legend for figure
hold off;

% Plot 460 grams pressure vs. time with and without heaters
figure(8)
hold on
% 460 grams without heaters first
p24=plot(calibrated(1:row_array(6),1,6),...
    calibrated(1:row_array(6),5,6),'-c');
p25=plot(calibrated(1:row_array(6),1,6),...
    calibrated(1:row_array(6),6,6),'-m');

% 460 grams with heaters second
p26=plot(calibrated(1:row_array(12),1,12),...
    calibrated(1:row_array(12),5,12),'-b');
p27=plot(calibrated(1:row_array(12),1,12),...
    calibrated(1:row_array(12),6,12),'-r');

title('System Pressure vs. Time for 460
grams','FontSize',fig_font,'FontName',font);
xlabel('Time (s)','FontSize',fig_font,'FontName',font);
ylabel('Pressure (psia)','FontSize',fig_font,'FontName',font);
set(gca,'FontSize',fig_font,'FontName',font); % changes the size and
font of the axis numbers
l8 = legend([p24,p25,p26,p27],'Line Pressure, No Heater','Tank
Pressure, No Heater','Line Pressure, Heater','Tank Pressure, Heater');
% Create legend for figure
hold off;

%%% Plot temperature vs. time for individual masses

% Plot 60 grams tank temperature vs. time with and without heaters
figure(9)
hold on
% 60 grams without heaters first
p28=plot(calibrated(1:row_array(1),1,1),...
    calibrated(1:row_array(1),2,1),'-b');

% 60 grams with heaters second
p29=plot(calibrated(1:row_array(7),1,7),...
    calibrated(1:row_array(7),2,7),'-r');

title('Tank Temperature vs. Time for 60
grams','FontSize',fig_font,'FontName',font);
xlabel('Time (s)','FontSize',fig_font,'FontName',font);
ylabel('Tank Temperature (C)','FontSize',fig_font,'FontName',font);
set(gca,'FontSize',fig_font,'FontName',font); % changes the size and
font of the axis numbers
l9 = legend([p28,p29],'No Heater','Heater'); % Create legend for figure
hold off;

% Plot 120 grams tank temperature vs. time with and without heaters
figure(10)
```

```
hold on
% 120 grams without heaters first
p30=plot(calibrated(1:row_array(2),1,2),...
    calibrated(1:row_array(2),2,2),'-b');

% 120 grams with heaters second
p31=plot(calibrated(1:row_array(8),1,8),...
    calibrated(1:row_array(8),2,8),'-r');

title('Tank Temperature vs. Time for 120
grams','FontSize',fig_font,'FontName',font);
xlabel('Time (s)','FontSize',fig_font,'FontName',font);
ylabel('Tank Temperature (C)','FontSize',fig_font,'FontName',font);
set(gca,'FontSize',fig_font,'FontName',font); % changes the size and
font of the axis numbers
l10 = legend([p30,p31],'No Heater','Heater'); % Create legend for
figure
hold off;

% Plot 180 grams tank temperature vs. time with and without heaters
figure(11)
hold on
% 180 grams without heaters first
p32=plot(calibrated(1:row_array(3),1,3),...
    calibrated(1:row_array(3),2,3),'-b');

% 180 grams with heaters second
p33=plot(calibrated(1:row_array(9),1,9),...
    calibrated(1:row_array(9),2,9),'-r');

title('Tank Temperature vs. Time for 180
grams','FontSize',fig_font,'FontName',font);
xlabel('Time (s)','FontSize',fig_font,'FontName',font);
ylabel('Tank Temperature (C)','FontSize',fig_font,'FontName',font);
set(gca,'FontSize',fig_font,'FontName',font); % changes the size and
font of the axis numbers
l11 = legend([p32,p33],'No Heater','Heater'); % Create legend for
figure
hold off;

% Plot 250 grams tank temperature vs. time with and without heaters
figure(12)
hold on
% 250 grams without heaters first
p34=plot(calibrated(1:row_array(4),1,4),...
    calibrated(1:row_array(4),2,4),'-b');

% 250 grams with heaters second
p35=plot(calibrated(1:row_array(10),1,10),...
    calibrated(1:row_array(10),2,10),'-r');

title('Tank Temperature vs. Time for 250
grams','FontSize',fig_font,'FontName',font);
xlabel('Time (s)','FontSize',fig_font,'FontName',font);
ylabel('Tank Temperature (C)','FontSize',fig_font,'FontName',font);
```

```
set(gca,'FontSize',fig_font,'FontName',font); % changes the size and
font of the axis numbers
l12 = legend([p34,p35],'No Heater','Heater'); % Create legend for
figure
hold off;

% Plot 350 grams tank temperature vs. time with and without heaters
figure(13)
hold on
% 350 grams without heaters first
p36=plot(calibrated(1:row_array(5),1,5),...
    calibrated(1:row_array(5),2,5),'-b');

% 350 grams with heaters second
p37=plot(calibrated(1:row_array(11),1,11),...
    calibrated(1:row_array(11),2,11),'-r');

title('Tank Temperature vs. Time for 350
grams','FontSize',fig_font,'FontName',font);
xlabel('Time (s)','FontSize',fig_font,'FontName',font);
ylabel('Tank Temperature (C)','FontSize',fig_font,'FontName',font);
set(gca,'FontSize',fig_font,'FontName',font); % changes the size and
font of the axis numbers
l13 = legend([p36,p37],'No Heater','Heater'); % Create legend for
figure
hold off;

% Plot 460 grams tank temperature vs. time with and without heaters
figure(14)
hold on
% 460 grams without heaters first
p38=plot(calibrated(1:row_array(6),1,6),...
    calibrated(1:row_array(6),2,6),'-b');

% 460 grams with heaters second
p39=plot(calibrated(1:row_array(12),1,12),...
    calibrated(1:row_array(12),2,12),'-r');

title('Tank Temperature vs. Time for 460
grams','FontSize',fig_font,'FontName',font);
xlabel('Time (s)','FontSize',fig_font,'FontName',font);
ylabel('Tank Temperature (C)','FontSize',fig_font,'FontName',font);
set(gca,'FontSize',fig_font,'FontName',font); % changes the size and
font of the axis numbers
l14 = legend([p38,p39],'No Heater','Heater'); % Create legend for
figure
hold off;
```

APPENDIX D
ENDURANCE TEST FIGURES

This appendix contains the remaining pressure and temperature plots not shown in the endurance test section. Figures B.1 and B.2 correspond to an initial mass of 180 grams or R-134a. Figures B.3 and B.4 correspond to 250 grams and B.5 and B.6 correspond to 350 grams of R-134a.

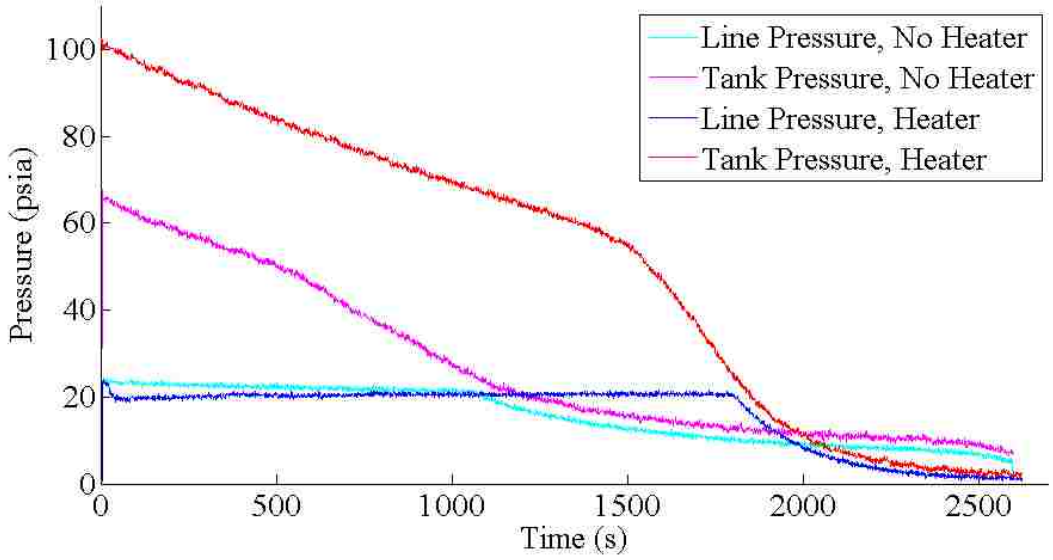

Figure B.1. Pressure vs. Time for 180 Grams of R-134a

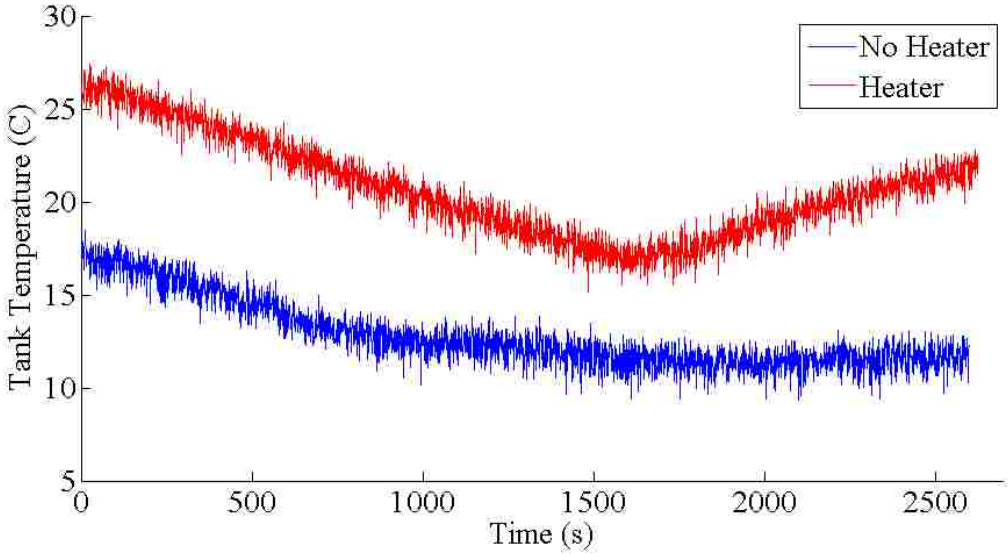

Figure B.2. Tank Temperature vs. Time for 180 Grams of R-134a

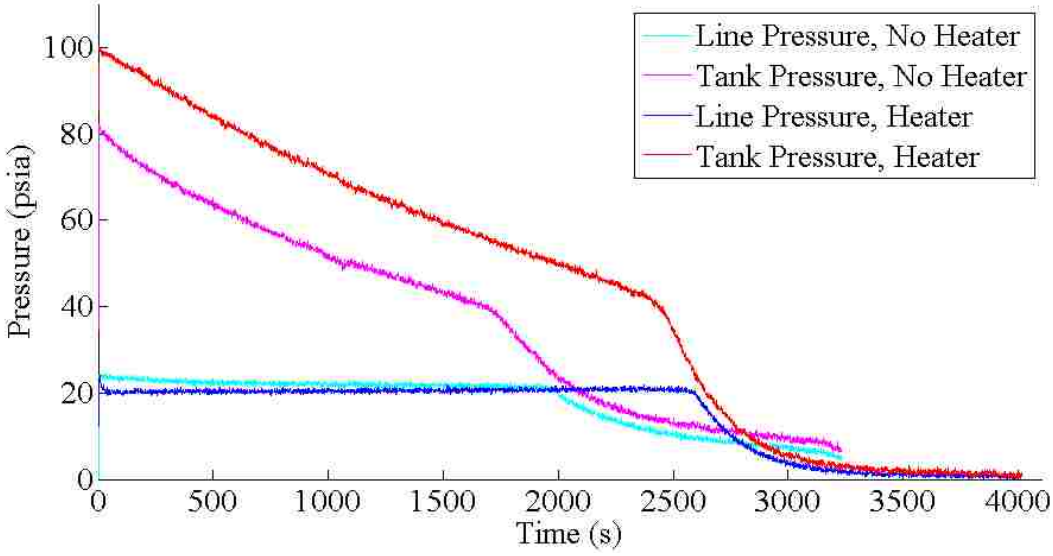

Figure B.3. Pressure vs. Time for 250 Grams of R-134a

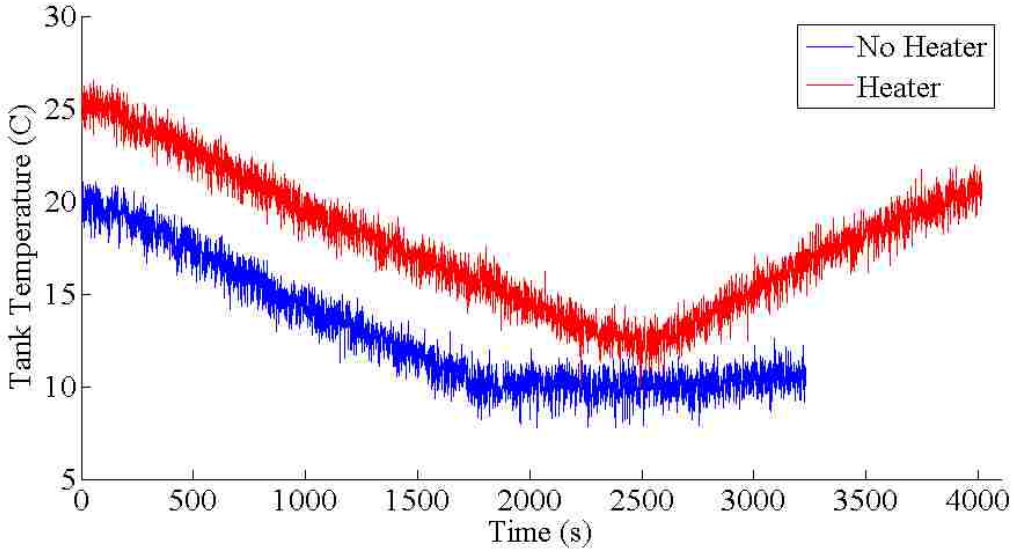

Figure B.4. Tank Temperature vs. Time for 250 Grams of R-134a

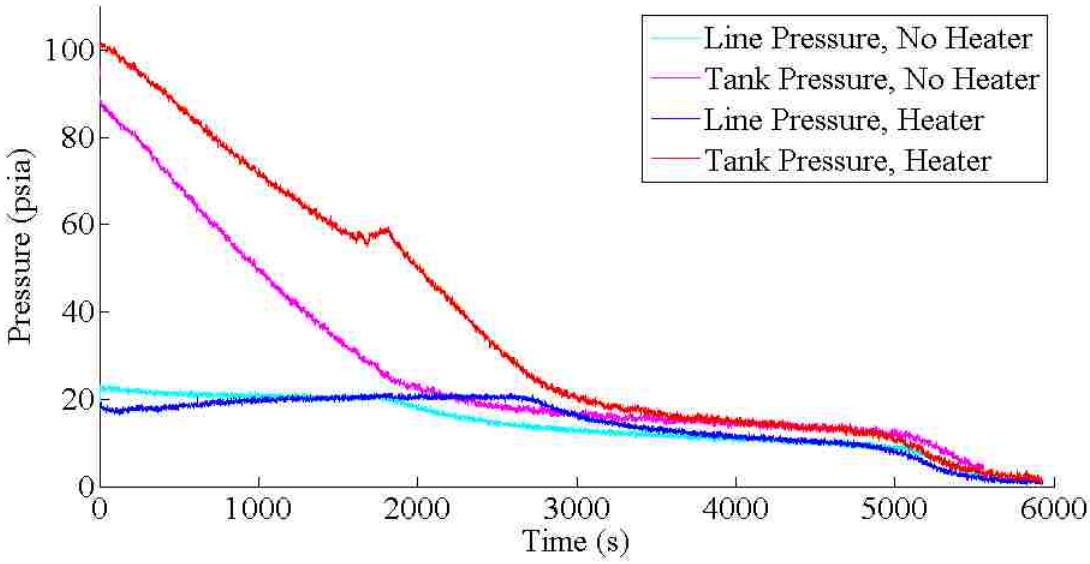

Figure B.5. Pressure vs. Time for 350 Grams of R-134a

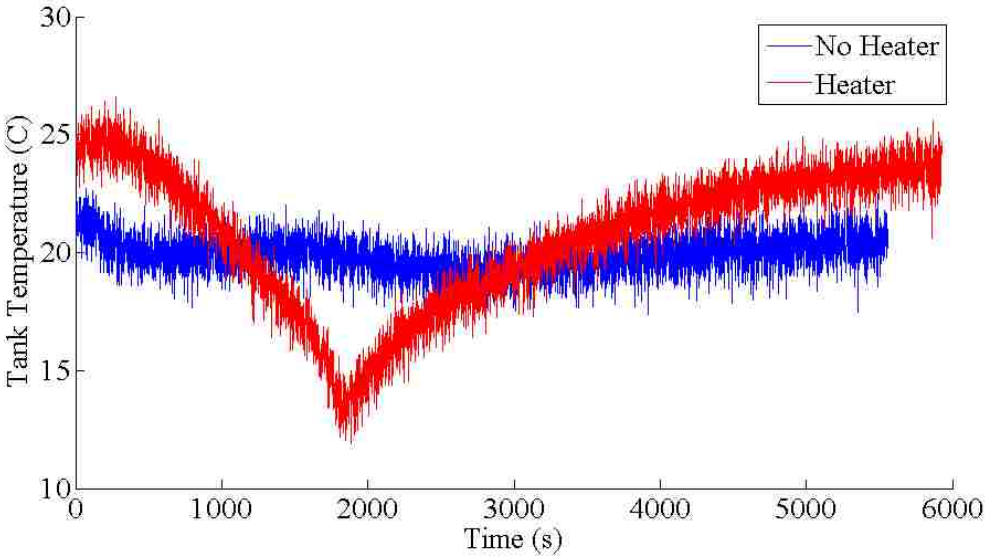

Figure B.6. Tank Temperature vs. Time for 350 Grams of R-134a

BIBLIOGRAPHY

[1] B, Lauren. "The First Satellites." 19 May 1997. 3 Sep 2009 <http://www.stmary.ws/highschool/Physics/97/LBOELS~1.HTM>.

[2] "Sputnik and The Dawn of the Space Age." *Sputnik: The Fiftieth Anniversary*. 10 Oct. 2007. NASA. 3 Sep 2009 <http://history.nasa.gov/sputnik/>.

[3] "First 50 years." *SPACE50*. 04 Jun. 2007. Web. 13 Sep 2009. <http://www.space50.net/sputnik.html>.

[4] Zak, Anatoly. "Sputnik-2." *RussianSpaceWeb*. 2007. Web. 13 Sep 2009. <http://www.russianspaceweb.com/sputnik2.html>.

[5] Bille, M., and E. Lishock. "EXPLORER I: A New Look at America's First Satellite." *Proceedings of the 40th AIAA Aerospace Science Meeting & Exhibit*. AIAA-2002-0313 (2002): Print.

[6] "Explorer I." *Space System Exploration*. 14 Mar 2009. National Aeronautical and Space Administration, Web. 13 Sep 2009. <http://solarsystem.nasa.gov/missions/profile.cfm?MCode=Explorer_01>.

[7] Bille, Matt, and Erika Lishock. "PROJECT VANGUARD: Setting the Record Straight." *Proceedings of the 41st AIAA Aerospace Sciences Meeting and Exhibit*. AIAA 2003-657 (2003): Print.

[8] Dr. Greyzeck, Ed. "Vanguard I." *National Space Science Data Center*. 26 Jun 2009. National Aeronautical and Space Administration, Web. 14 Sep 2009. <http://nssdc.gsfc.nasa.gov/nmc/spacecraftDisplay.do?id=1958-002B>.

[9] Dr. Greyzeck, Ed. "Pioneer I." *National Space Science Data Center*. 26 Jun 2009. National Aeronautical and Space Administration, Web. 14 Sep 2009. <http://nssdc.gsfc.nasa.gov/nmc/masterCatalog.do?sc=1958-007A>.

[10] Wertz, James R., and Wiley J. Larson. *Space Mission Analysis and Design*. 3rd ed. El Segundo, CA and Dordrecht, Netherlands: Microcosm Press and Kluwer Academic Publishers, 1999. Print.

[11] Mattingly, Jack D. *Elements of Propulsion: Gas Turbines and Rockets*. Illustrated Ed. Reston, VA: American Institute of Aeronautics and Astronautics, 2006. Print.

[12] Humble, Ronald W., Gary N. Henry, and Wiley J. Larson. Space Propulsion Analysis and Design. 1st ed. Rev. New York: McGraw-Hill Companies, 1995. Print.

[13] Sutton, George P., and Oscar Biblarz. *Rocket Propulsion Elements*. 7th ed. New York: John Wiley & Sons, inc., 2001. Print.

[14] Frisbee, Robert H. "Advanced Propulsion for the XXIst Century." *AIAA/ICAS*. AIAA 2003-2589 (2003): Print.

[15] Cassady, R. Joseph, W. Andrew Hoskins, Mark Campbell, and Christopher Rayburn. "A Micro Pulsed Plasma Thruster (PPT) for the 'Dawgstar' Spacecraft." *IEEE*. (2000): Print

[16] Çengel, Yunus A., and Michael A. Boles. *Thermodynamics: An Engineering Approach*. 4th ed. New York: McGraw-Hill Company, 2002. Print.

[17] Mauthe, Stephen, Freddy Pranajaya, and Dr. Robert E. Zee. "The Design and Test of a Compact Propulsion System for CanX Nanosatellite Formation Flying." *Proceedings of the 19th AIAA/USU Conference on Small Satellites*. SSC05-VI-5 (2005): Print.

[18] "Satellite Classification." *Small Satellite Home Page*. Surrey Satellite Technology Limited, Web. 22 Sep 2009. <http://centaur.sstl.co.uk/SSHP/sshp_classify.html>.

[19] Janson, Siegfried W. "Micro/Nanotechnology for Micro/Nano/Picosatellites." *AIAA*. AIAA 2003-6269 (2003): Print.

[20] Gibbon, D, Dr. J Ward, and N. Kay. "The Design, Development and Testing of a Propulsion System for the SNAP-1 Nanosatellite." *Proceedings of the 14th AIAA/USU Conference on Small Satellites*. SSC00-I-3 (August 2000): Print.

[21] Gibbon, D., Dr. C Underwood, Prof. M. Sweeting, and R. Amri. "Cost Effective Propulsion Systems for Small Satellites Using Butane Propellant." *Acta Astronautica*. 51.1-9 (2002): 145-152. Print.

[22] Swartout, Dr. Michael. "Bandit: A Platform for the Responsive Education and Research Activities." *Proceedings of the 4th AIAA Responsive Space Conference*. AIAA-RS4 2006-3004 (2006): Print.

[23] Futron Corporation, . "Space Transportation Costs: Trends in Price Per Pound to Orbit 1990-2000." (2002): Print.

[24] Salo, Timothy J. "The DoD Space Test Program: Free Launches for Amateur Satellites". *Proceedings of the AMSAT-NA 22nd Space Symposium, Arlington, VA, October 8-10, 2004.* Newington, CT: ARRL, 2004.

[25] AFRL/VS, University Nanosat-6 Program, 'Nanosat-6 Program User's Guide (Limited Release),' UN6-0001 – Rev A, University Nanosat Program Office, Kirtland AFB, NM, Jan 2009.

[26] Missouri University of Science and Technology – Missouri Satellite Team, "00-001 Executive Summary," Rev F, February, 2010.

[27] Dancer, M., Searcy, J., Walker, D., and Pernicka, H., "Attitude Determination And Control System For The University Of Missouri-Rolla Satellite Mission," AAS Guidance and Control Conference, Breckenridge, CO, February 3-7, 2007.

[28] C. R. Seubert, "Refrigerant-Based Propulsion System for Small Spacecraft," Master's Thesis. University of Missouri-Rolla. May 2007.

[29] Surrey Satellite Technology Limited, "Microsatellite Butane Propulsion System," Fact sheet, SSTL-9051-01, Surrey Space Centre, University of Surrey, Guildford Surrey GU2 7XH, United Kingdom, 26 April, 2006.

[30] S. J. Edwards, "End Item Data Package for Butane Storage Tank – BSS01-01," EI-BSS01-01-01 Issue 1, Marotta UK Ltd, Cheltenham Trade Park, Cheltenham, Gloucestershire GL51 8LZ, December 2006.

[31] J. R. Siebert, "Design, Hazard Analysis, And System Level Testing of a University Propulsion System for Spacecraft Application," Master's Thesis. Missouri University of Science & Technology. 2009.

[32] Missouri University of Science and Technology – Missouri Satellite Team, "04-010 Propulsion Maximum Tubing Length," Rev A, February, 2010.

[33] M. J. L. Turner, *Rocket and Spacecraft Propulsion, Principles, Practice and New Developments*, Praxis Publishing, UK 2000.

[34] G. P. Sutton, O. Biblarz, *Rocket Propulsion Elements*, Seventh Edition, John Wiley & Sons, Inc. U.S.A, 2001.

[35] Honeywell, . "Model AS17A/AS19G." Honeywell, Jun 2008. Web. 12 Mar 2010. <http://content.honeywell.com/sensing/sensotec/pdf_catalog08/008686-1-EN_Model_AS17A-AS19G.pdf>.

[36] "Micro Solenoid Valve." *The Lee Company*. Web. 22 Sep 2009. <http://www.theleeco.com/EFSWEB2.NSF/PDS52_CrossSec.jpg!OpenImageResource>.

[37] Beckwith, Thomas G., Roy D. Marangoni, and John H. Lienhard V. *Mechanical Measurements*. 6th ed. Upper Saddle River, NJ: Pearson, 2007. Print.

[38] "Lightband Release Mechanism." *Planetary Systems Corporation*. Web. 9 Mar 2010. <http://www.planetarysystemscorp.com/products.htm>.

[39] "NEA Release Mechanism." *NEA Products*. Web. 9 Mar 2010. <http://www.neaelectronics.net/>.

[40] Bhattacharjee, Subrata. "Evaluating Thermodynamic States: The R-134a State Daemon." N.p., 1999. Web. 11 Mar 2010. <http://flame.mech.gifu-u.ac.jp/TEST-j/testcenter/Test/solve/states/r134a/index.html>.

[41] *MatWeb*. 2010. MatWeb, Web. 9 Feb 2010. < http://www.matweb.com/>.

[42] Missouri S&T – Missouri Satellite Team, "04-016 Minimum Distributor Gasket Compression," February 10, 2010.

[43] Anderson, Rodger, A. *Fundamentals of Vibrations*. 1st ed. London: Collier-Macmillan, 1967. Print.

VITA

Ryan Alan Pahl was born on April 16, 1987 in Saint Louis, Missouri to Curtis and Pamela Pahl. He graduated fourth in his class at Eureka High School in May 2005 and went on to pursue a degree in Aerospace Engineering from Missouri University of Science and Technology, completing it in only three years in May 2008. After completing his Bachelor's degree, Ryan decided to continue his studies in pursuit of a Master's degree in Aerospace Engineering. In May of 2010, Ryan completed his studies and received a Master's degree with the intent of pursuing a Ph.D. in high density plasma and its application to spacecraft propulsion.

During his time at Missouri S&T, Ryan was a member of AIAA, the Advanced Aero Vehicle Group, and president of both the zero-gravity research team Miners In Space and the Aerospace honor society Sigma Gamma Tau. Additionally, Ryan participated in the Missouri Satellite Team in the Propulsion subsystem and eventually took over as lead in January 2008 and helped lead the team in their efforts in the Nanosat 6 competition.